THE EFFECTS OF CHROMIC ACID ANODIZING ON FATIGUE BEHAVIOR OF (AMS4050) 7050 T7451 ALUMINUM ALLOY

A THESIS SUBMITTED TO
THE GRADUATE SCHOOL OF NATURAL AND APPLIED SCIENCES
OF
MIDDLE EAST TECHNICAL UNIVERSITY

BY

ÇAĞRI İLHAN

IN PARTIAL FULFILLMENT OF THE REQUIREMENTS
FOR
THE DEGREE OF MASTER OF SCIENCE
IN
METALLURGICAL AND MATERIALS ENGINEERING

JANUARY 2019

Approval of the thesis:

THE EFFECTS OF CHROMIC ACID ANODIZING ON FATIGUE BEHAVIOR OF (AMS4050) 7050 T7451 ALUMINUM ALLOY

submitted by **ÇAĞRI İLHAN** in partial fulfillment of the requirements for the degree of **Master of Science in Metallurgical and Materials Engineering Department, Middle East Technical University** by,

Prof. Dr. Halil Kalıpçılar
Dean, Graduate School of **Natural and Applied Sciences** _____

Prof. Dr. Cemil Hakan Gür
Head of Department, **Met. and Mat. Eng.** _____

Prof. Dr. Rıza Gürbüz
Supervisor, **Met. and Mat. Eng., METU** _____

_____

Examining Committee Members:

Prof. Dr. Bilgehan Ögel
Met. and Mat. Eng.,METU _____

Prof. Dr. Rıza Gürbüz
Met. and Mat. Eng., METU _____

Prof. Dr. Cemil Hakan Gür
Met. and Mat. Eng.,METU _____

Prof. Dr. Vedat Akdeniz
Met. and Mat. Eng.,METU _____

Assoc. Prof. Dr. Ziya Esen
Material Science and Engineering,Çankaya University _____

Date: 08.01.2019

I hereby declare that all information in this document has been obtained and presented in accordance with academic rules and ethical conduct. I also declare that, as required by these rules and conduct, I have fully cited and referenced all material and results that are not original to this work.

Name, Surname: Çağrı İlhan

Signature:

ABSTRACT

THE EFFECTS OF CHROMIC ACID ANODIZING ON FATIGUE BEHAVIOR OF (AMS4050) 7050 T7451 ALUMINUM ALLOY

İlhan, Çağrı
Master of Science, Metallurgical and Materials Engineering
Supervisor: Prof. Dr. Rıza Gürbüz

January 2019, 87 pages

7050 T7451 is a solution heat treated, stress relieved, and overaged aluminum alloy which has extensively used in aerospace industry. Chromic Acid Anodizing (CAA) is a treatment against corrosion by producing aluminum oxide layer (Al_2O_3) at the surface. Although corrosion resistance is increased by CAA, fatigue life of the material is affected inversely due to CAA process. CAA process consists of pre-treatments (degrease, etching etc.) and anodizing steps which have different effects on fatigue life of the material. The effect of Chromic Acid Anodizing (CAA) surface treatment on 7050 T7451 aluminum alloy was presented in this study in terms of fatigue behavior.

In this study, eight different CAA processes were examined with regard to etching stage of pre-treatments by using an alkaline etchant and/or acid etchants during various immersion time. Optical microscopic examination was applied in order to measure pit depths, caused by pretreatments, and to determine pitting characteristics for selection of CAA process parameters before fatigue tests. After CAA process was selected among 8 processes in terms of pitting characteristics and conformity for ASM Volume 5 Anodizing, selected process was used as surface treatment of fatigue specimens.

Four groups were determined for fatigue tests which were as-machined, pre-treated, anodized and anodized with extended immersion time. These groups were to research bare condition of the material, only pretreated condition of CAA, standard CAA applied condition and effect of immersion time respectively. Constant amplitude axial fatigue tests, ASTM-E466, were conducted to specimens at 91 Hz with resonant test machine at stress ratio (R) of -1 until run-out criteria which was 10^6 cycles. Fatigue test results were evaluated according to AGARD-AG-292 for curve fitting in order to obtain S-N curve in which comparison of each fatigue groups was done. Fatigue limit reduction was detected due to pretreatments of CAA. While, fatigue limit reduction was not influenced by immersion time of CAA. Fracture surfaces of the specimens were examined by scanning electron microscope (SEM) to investigate morphology, crack initiation sites and striation counting. Crack propagation stage of fatigue failure was found to be independent from surface treatment by analyzing striation counting.

Keywords: Aluminum alloy, 7050 T7451, Chromic acid anodizing, Fatigue, S/N Curves, Fractographic analysis

ÖZ

KROMİK ASİTLE ANOTLAMANIN (AMS4050) 7050 T7451 ALUMİNYUM ALAŞIMININ YORULMA DAVRANIŞI ÜZERİNDEKİ ETKİLERİ

İlhan, Çağrı
Yüksek Lisans, Metalurji ve Malzeme Mühendisliği
Tez Danışmanı: Prof. Dr. Rıza Gürbüz

Ocak 2019, 87 sayfa

Bu çalışmada kromik asitle anotlama işleminin (AMS4050) 7050 T7451 Aluminyum alaşımı üzerindeki etkisi yorulma davranışı açısından incelenmiştir. Çözündürme ısıl işlemi sonrası gerilme giderme ve aşırı yaşlandırma işlemleri uygulanarak elde edilen 7050 T7451 alüminyum alaşımı havacılık endüstrisinde yaygın olarak kullanılmaktadır. Kromik asitle anotlama yöntemi, korozyona karşı yüzeyde alüminyum oksit (Al_2O_3) tabakası oluşturularak yapılan bir işlemdir. Malzemenin korozyon direnci bu işlemle arttırılmasına rağmen, yorulma ömrü azalmaktadır. Kromik asitle anotlama işlemi yorulma ömrüne farklı etkileri yağdan arındırma, dağlama önişlmeleri ile anotlama basamaklarından oluşur

Bu çalışmada, ön işlemlerden olan dağlama aşamasında alkali dağlayıcı ve/veya asit dağlayıcıların çeşitli sürelerde kullanıldığı sekiz farklı kromik asit anotlama işlemi incelenmiştir. Yorulma testleri öncesinde kromik asit anotlama parametrelerini belirlemek için ön işlemler sırasında oluşan çukurların aşınma özellikleri optik mikroskop incelemesi ile belirlenmiştir. Uygulanan sekiz farklı prosesten numune yüzeyini en çok aşındıran ve ASM Volume 5 Anodizing dökümanına uygunluk gösteren proses yüzey işlemi olarak yorulma numunelerine uygulanmıştır.

Yorulma testleri için dört farklı grup belirlenmiştir. Bu gruplar, malzemenin yüzey işlemsiz halini, sadece ön işlemlerin etkisini, standart kromik asitle anotlama ve kromik asit banyosunda geçirilen sürenin etkisini incelemek amacıyla seçilmiştir. ASTM E-466' ya uygun ve negatif gerilme oranı (R) -1 olan sabit genlikli tek eksenli yorulma testleri gerçekleştirilmiştir. Bu testler rezonans yorulma cihazlarında 91 Hz'lik frekans değerinde ve 10^6 çevrime kadar gerçekleştirilmiştir. Yorulma testleri sonuçları gerilim çevrim (S-N) grafiği oluşturmak için AGARD-AG-292'ye göre değerlendirilmiştir. Yorulma limitindeki azalma belirlenmiş, bununla birlikte kromik asitle anotlamanın uygulama süresinin etkisi de araştırılmıştır. Kırılma yüzeyleri, morfoloji, çatlak başlangıç bölgesi ve yorulma izi açısından taramalı elektron mikroskobuyla (SEM) incelenmiştir. Yorulma hasarında çatlak ilerleme aşamasının kromik asitle anotlama yüzey işleminden bağımsız olduğu fraktografik analiz verileri işlenerek bulunmuştur.

Anahtar Kelimeler: Aluminyum alaşım, 7050 T7451, Kromik asitle anotlama, Yorulma, Gerilme- Çevrim Eğrisi, Fraktografik analiz

To My Precious Family

ACKNOWLEDGMENTS

I cannot begin to express my thanks to my advisor who Prof. Dr. Rıza Gürbüz for his unwavering support and guidance throughout this study.

I'd also like to extend my gratitude to Turkish Aerospace Industry (TAI) for contributions and permission to perform tests in its premises and equipment.

I gratefully acknowledge the assistance of Özgün Köse and Anıl Yıldırım for their helpful advise and practical efforts for Scanning Electron Microscope (SEM) and Digital and Optical Microscopic analyses.

I'd like to recognize the help that I received from my collegues Salim Çalışkan, Şahin Gören and Mesut Güven. Thanks also to Aykut Kibar played a decisive role in my topic. I very much appreciate Ece Alpuğan provided me with encouragement and patience throughout the duration of this study.

Finally, I would also like to extend my deepest gratitude to my parents and my beloved Deniz whose love and guidance are with me in whatever ı pursue. They are the most important people in my life and this thesis is dedicated to them.

TABLE OF CONTENTS

LIST OF TABLES

TABLES

LIST OF FIGURES

FIGURES

CHAPTER 1

INTRODUCTION

Aluminum alloys have been widely used since first quarter of 20th century in aerospace industry to replace wood made parts [1]. Different aluminum alloys have been developed for aerospace applications until recent applications such as 7XXX series aluminum alloy. This type of alloy consists of zinc, magnesium and copper alloying elements in order to enhance mechanical properties of aluminum. 7050 T7451 which is one of the members of 7XXX series is called high strength aluminum alloy due to its alloying effect. The advantages of aluminum alloys are lightweight, high specific strength, easily manufacturing process and low production cost. However, low modulus elasticity, low elevated temperature capability and corrosion susceptibility are shortness of 7XXX aluminum alloys[2].

7050 T7451, which is a high strength type of aluminum alloy, is a candidate for anodizing due to its corrosion susceptibility. Therefore, anodizing is an effective protection way from corrosion by producing alumina layer at the surface of material [3]. Anodized components are widely used in aerospace industry ,for example, in root of helicopter blades, rotors, gear system, cabin trim, seating equipment and exterior panels of aircrafts.

Although anodized products have a resistance against corrosion, fatigue performance of these products are affected. Fatigue in metals, which occurs under cyclic or fluctuating load has been examined since 1830. Fatigue load is lower than a yield or fracture loading. Therefore, fatigue failures often could be observed during service period due to exposed load level. Importance of fatigue has been increased with technological developments and products such as automobiles, aircrafts, helicopters,

turbines [4]. So, importance of fatigue behavior of surface treated material reach critical level due to wide usage of them.

The aim of this study was to reveal fatigue limit reduction and to observe the effect of chromic acid anodizing of 7050 T7451 aluminum alloy on this reduction. For this purpose, the effect of various pre-treatments of chromic acid process on 7050 T7451 was examined depend on pitting formation with microscopic analysis in order to select proper CAA process. Fatigue behavior of this alloy was determined in different stages of the selected chromic acid anodizing (CAA) process. Material characterization such as X-Ray Fluorescence (XRF), tensile tests and fractographic analysis with scanning electron microscope (SEM) were applied for comprehensive understanding of the study. Finally, curve fitting were applied to test data which were obtained from different CAA conditions by the help of the least square method in order to construct S-N curve.

CHAPTER 2

LITERATURE REVIEW

2.1. Material

Aluminum alloys are classified depending on heat treatment applied to them. There are two types of aluminum alloys in this classification which are heat treatable and non-heat treatable. Heat treatable criteria is that whether capability of precipitation hardening exist or not [5]. Major alloying elements of aluminum are zinc, copper, magnesium and lithium [6]. Four digits numerical designation system are used to define aluminum alloys with respect to major alloying elements presented in Table 1.

Table 1. *Major Alloying Elements of Aluminum Alloys*

Alloy	Main alloying element
1*xxx*	Mostly pure aluminum; no major alloying additions
2*xxx*	Copper
3*xxx*	Manganese
4*xxx*	Silicon
5*xxx*	Magnesium
6*xxx*	Magnesium and silicon
7*xxx*	Zinc
8*xxx*	Other elements (e.g., iron and silicon)
9*xxx*	Unassigned

7050 T7451 is one of the members of 7XXX series aluminum alloy which is rich in Zn. It also contain Copper (Cu), Magnesium (Mg) and Zirconium (Zr) in considerable amount. Composition of 7050 is shown in Table 2 in detail[7] . Alloying with zinc and magnesium increases the strength potential of aluminum alloys by forming $MgZn_2$. However, it negatively affects the aluminum corrosion resistance. Furthermore, high

strength aluminum alloys are obtained by addition of copper to this Al-Zn-Mg system while corrosion resistance decreases due to copper addition. On the other hand, small amount of zirconium addition enhances the corrosion resistance of aluminum alloys [6].

Table 2. *Composition of 7050 T7451 [7]*

Element	min	max
Silicon	--	0.12
Iron	--	0.15
Copper	2.0	2.6
Manganese	--	0.10
Magnesium	1.9	2.6
Chromium	--	0.04
Zinc	5.7	6.7
Titanium	--	0.06
Zirconium	0.08	0.15
Other Elements, each	--	0.05
Other Elements, total	--	0.15
Aluminum	remainder	

7050 aluminum alloy can be obtained in bar or plate form in different nominal thicknesses. Plate form of 7050 aluminum alloy which is specified by AMS 4050 that is used in this study [7]. On the other hand, heat treatment of the 7050 is notified by T7451 that consist of solution heat treatment, stress relieving, and overaging [8].

Mechanical properties for 7050 T7451 is stated that tensile strength is 510 MPa while yield strength is 441 MPa for plate with nominal thickness up to 51mm [7].

Table 3. *Tensile properties of 7050 T7451[7]*

Nominal Thickness Millimeters	Specimen Orientation	Tensile Strength MPa	Yield Strength at 0.2% Offset MPa	Elongation in 50.8 mm or 4D %
Up to 51, incl	Longitudinal	510	441	10
	Long Trans.	510	441	9

2.2. Anodizing

Anodizing is a surface treatment conducted for multi-purposes. Anodizing term is used for electrolytic coating by making the specimen anode in a proper solution[9]. Anodizing process results in formation of oxide layer at the surface of substrate metal

which has porous structure. Porous oxide layer can be obtained by different acid solutions such as chromic, phosphoric and oxalic acid [10]. The oxide layer is formed in "hexagonal cell model structure" that is shown below in Figure 1. Hexagonal cells grow perpendicular to the base material with the pores at the center of the hexagonal cells [11]. The name of the anodizing process is directly related with type of acid in the anodizing bath. Chromic acid, sulfuric acid and hard anodizing are common types in industrial applications and research studies.

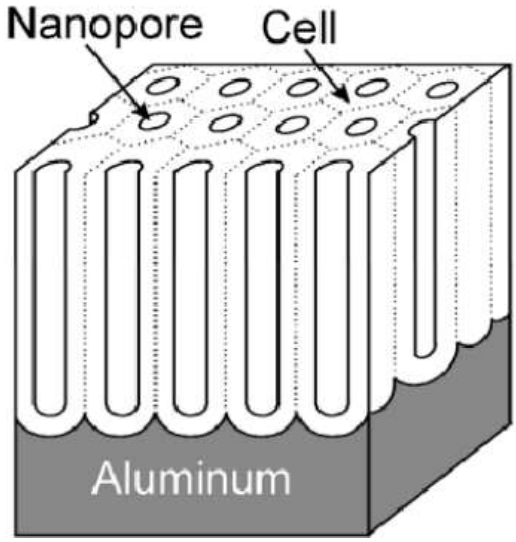

Figure 1. Formation of porous oxide layer on aluminum[11]

Many types of anodizing could be applied for various purposes that are indicated below[12]:

- Corrosion Resistance
- Electrical Insulation
- Decorative Appearances
- Improve Lubricity
- Abrasion Resistance

2.2.1. Chromic Acid Anodizing (CAA)Process

Chromic acid anodizing is a type of anodizing method which is generally preferred for increasing the corrosion resistance of the applied metal(s). This process also includes pretreatment steps. Pretreatments are compulsory before CAA to form porous oxide layer that enhances corrosion resistance. Typical CAA procedure can be seen in Table 4. Vapor degrease and alkaline cleaning are preparation operations of the CAA process. Etching with alkaline and/or acid solutions is the main pretreatments for application of CAA successfully. After etching, specimens with oxide free surface are dipped into CAA bath. Rinse operations are applied among pre-treatment steps for not only cleaning of the specimens but also for protection from contamination of the baths.

Table 4. *Stages of CAA process[11]*

Operation	Solution	Solution temperature		Treatment time, min
		°C	°F	
Vapor degrease	Suitable solvent	. . .	. . .	. . .
Alkaline clean	Alkaline cleaner	(a)	(a)	(a)
Rinse[(b)]	Water	Ambient	Ambient	1
Desmut[(c)]	HNO_3, 10-25 vol%	Ambient	Ambient	As required
Rinse[(b)]	Water	Ambient	Ambient	1
Anodize	CrO_3, 46 g/L ($5\frac{1}{4}$ oz/gal)[(d)]	32-35	90-95	30[(e)]
Rinse[(b)]	Water	Ambient	Ambient	1
Seal[(f)]	Water[(g)]	90-100	190-210	10-15
Air dry	. . .	105 max[(h)]	225 max[(h)]	As required

(a) According to individual specifications.

2.2.1.1. Pretreatmens

The first requirement for CAA is the cleaning of the surface from organic and inorganic residuals. Cleaning method should be chosen depending on contaminations and the dimensional tolerances due to abrasive nature of the cleaning. Vapor degrease is the commonly used cleaning method for organic residuals compared to solvent wiping and alkaline soak cleaning [12].

When the organic free surface is obtained, etching process is carried out to eliminate inorganic contaminations at the surface and to obtain an uniform irregular surface. Both or either alkaline and acid solutions can be used during this etching process. Major parameters for this etching process are time, temperature and concentration of the etchant [10]. Etched surfaces should be cleaned from all residuals either organic such as hydrocarbons and inorganics such as oxides. HNO_3 is a conventional acid for etching operation [12].

2.2.1.2. Chromic Acid Anodizing (CAA)

Pretreated parts are immersed into aqueous chromic acid anodizing bath which has a concentration in the range of 3 to 10 wt % CrO_3. Moreover, pH value of the bath shall be between 0.5-1. Relationship between chromic acid concentration and pH of the solution is shown in Fig.2.

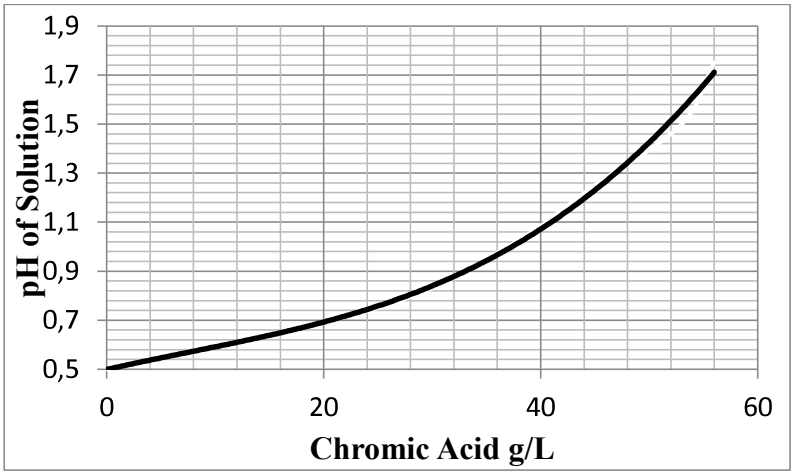

Figure 2. pH vs Chromic acid solution curve [12]

Generally voltage is gradually increased until 40V in 5-8 min with 0.1 A/dm^2 current density at least. Anodizing are applied minimum 30 minutes after voltage reaches required value such as 40V [12]. On the other hand, CAA application at 22V cause preferable results rather than 40V for 7XXX series aluminum alloys. However, application time should be lengthened to 40-60 minutes, when voltage is decreased to 22V [13]. After switching off the current, rinsing and sealing should be employed to the parts.

2.3. Fatigue Mechanism

Fatigue failures that occur under dynamic loading was recognized firstly in 1830. There has been widespread with technologically developed devices and vehicles such as train, automobile and helicopters that are working under fluctuating and/or vibratory stresses. 90% fatigue failures are observed after certain service life of these products [4]. Fatigue mechanism is valid when fluctuating stress at lower level than stress causing fracture in singular type of loading .

Main factors causing fatigue failures are:

1. Sufficient applied stress in tensile direction,
2. Large enough dynamic amplitude in cyclic stress,
3. Sufficient number of cycles [14].

Fluctuating stresses can be varied as reversed stress, repeated stress and irregular or random stress cycle which is indicated in Fig.3. The mean stress on reversed stress cycles equals to zero and maximum and minimum stresses are compression and tension direction are the same. On the other hand, the mean stress on repeated stress cycles are tensile stress, besides maximum and minimum stresses are in tensile direction. However, there is no constant mean stress on random stress cycles because of unsteady load spectrum.

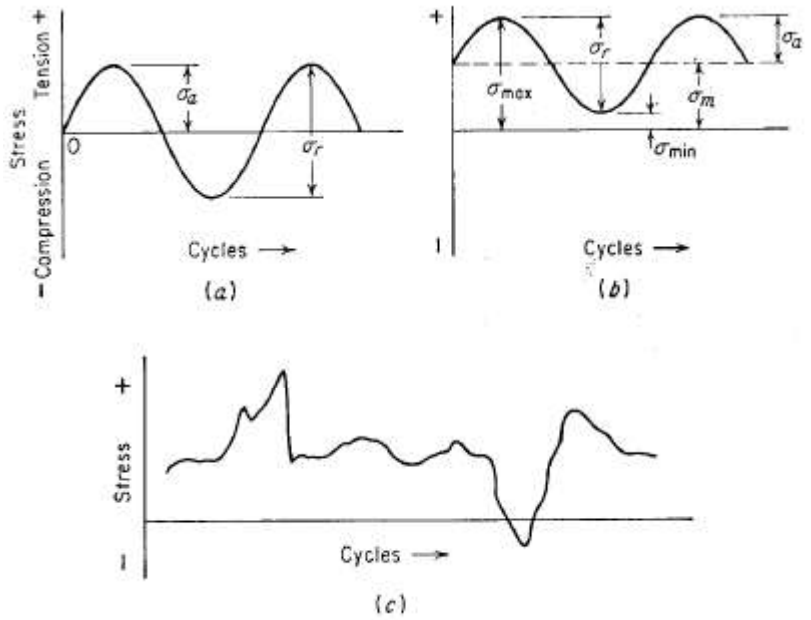

Figure 3. Types of fatigue load spectrum[4]

(a) Reversed stress,(b) Repeated stress and (c) Random stress.

Mean stress, stress amplitude and stress ratio are the terms in order to describe fluctuating stress types. The mean stress is the average of the sum of the minimum and maximum stress:

$$\sigma_m = \frac{\sigma_{max}+\sigma_{min}}{2} \qquad \textit{Eqn 1}$$

Stress amplitude is the half of the stress range:

$$\sigma_a = \frac{\sigma_{max}-\sigma_{min}}{2} \qquad \textit{Eqn 2}$$

$$\Delta\sigma = \sigma_{max} - \sigma_{min} \qquad \textit{Eqn 3}$$

Stress ratio (R) is the ratio of the minimum and maximum stresses:

$$R = \frac{\sigma_{min}}{\sigma_{max}} \qquad \textit{Eqn 4}$$

Fatigue could be explained by dividing into 4 different steps each having their mechanisms. These steps affect a material respectively under dynamic loading.[4]

1. *Crack initiation stage* – premature duration of fatigue damage that could be taken away thermally.
2. *Slip-band crack growth* – advancement of initial crack on planes having high shear stress. This is called *stage I crack growth.*
3. *Crack growth on planes of high tensile stress stage* – growth of advanced crack in normal direction according to maximum tensile stress direction. This is called *stage II crack growth.*
4. *Ultimate ductile failure stage* – critical crack length is satisfied. Therefore, catastrophic failure occur. This is the final stage of the fatigue failure.

Fatigue mechanism starts when crack nucleation and propagation occur as buildup of slip movements in nanoscale under dynamic loading. Some grains at the surface have more tendency to slip movement since their one side is open to environmental conditions such as gaseous (oxygen) or liquid (water). Therefore, these grains are become favorable to plastic deformation. Slip movements occur on surface grains through inner or outer side of the material. These movements are called slip-band extrusions and slip-band intrusions [15].

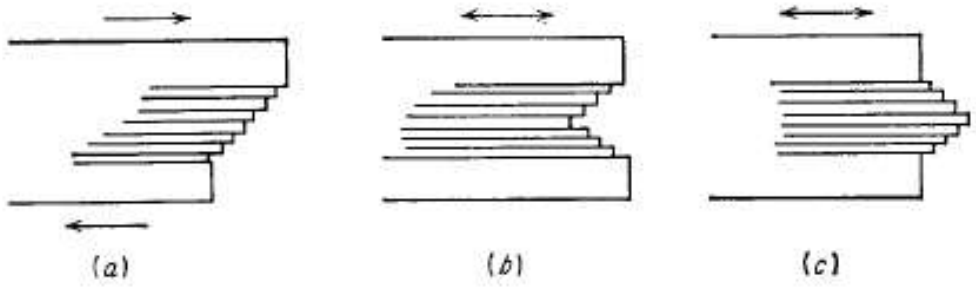

Figure 4. Slip band movements under dynamic loading[4]

Slip band movements under dynamic loading build up stress concentration points which are micro notches (Fig.4 a) and ridges (Fig.4 b) by moving forward and backward unlike slip sliding by producing contours under static loading.[4] Two

major effects can be observed during slip band accumulation. Firstly, oxide layer are formed on new fresh surfaces due to slip movement. Second effect is strain hardening on material. These two effects increase shear load acting on slip bands during unloading. So, slip movements continue with next parallel slip planes[16]. Slip movements can be seen in Fig.4.

Crack initiation along slip bands have maximum stress concentration by localizing at the first stage. Crack propagation during this stage is very short and nanoscale which means generally its size equals to a few grains. On the other hand, micron scale fatigue striations can be observed during crack propagation in Stage II. These are proof of fatigue failure which can be find out from fracture surface. However, fatigue striations couldn't be observed throughout crack propagation region. This is resulting from insufficient resolution of scanning method and incapable ductility at crack tip for fatigue striation formation. Crack propagation in Stage II can be explained by a plastic crack blunting which is shown Fig.5. Firstly, load concentrates slip at the sharp crack tip (Fig.5 a) to form twin notch at 45^{o} to crack front under tensile loading (Fig.5b). Not only crack elongate by shear loading but also its tip becomes blunt when crack mouth reach the maximum extension (Fig.5c). When loading direction turn to reverse side that is compression, slip movement change reverse direction at end of crack but not at the crack tip (Fig.5d). Fresh crack surfaces are formed under compressive loading due to crash of crack faces (Fig.5e). This loop is repeated until dynamic loading stops or final fracture occurs.

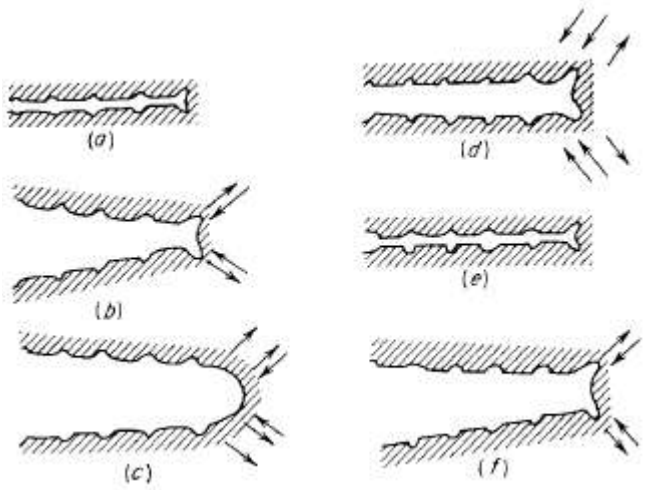

Figure 5. Crack initiation and propogation[4]

2.3.1. Effect of Stress Concentration on Fatigue

Stress concentration points cause reduction of the fatigue strength when certain material has a stress raiser such as irregularities on the surface of the material. These geometrical stress raisers are threads, fillets, hole and other geometrical features in practical cases. The most suspicious regions are these machine elements in terms of crack initiation and propagation due to stress concentration. On the other hand, discontinuities such as surface roughness, porosity or inclusions are the stress concentration points which are formed during the manufacturing process of raw material or product. Parameters causing stress concentration should be minimized in design phase, in order to avoid reduction of fatigue strength. Furthermore, precautions must be taken to prevent formation of stress raisers during manufacturing [4].

2.3.2. Specimen Size Effect

Specimen size affects fatigue limit of the unnotched, smooth specimen negatively. Fatigue limit of certain material decreases with the increase in specimen size [4]. Fatigue limit reduction factor resulting from size effect is indicated in Fig.6 . Although the general consideration is that fatigue limit and size of the specimen are inversely proportional, the effect of specimen size is not observed in some research [17]. Schjive et al.[16] researched the fatigue limit change of 1.05Cr-Steel depending on specimen

size. It is found that fatigue limit decreases with increasing specimen size for both type of tests which are axial tension/compression and rotating bending fatigue tests. Moreover, fatigue limit decreases dramatically in rotating bending tests; whereas, a linear relationship exists in axial tension/compression fatigue test in terms of fatigue limit reduction[16].

Table 5.*Coefficients of size effects depend on diameters*

Diameter, mm	Cs
D≤10	1
10≤D≤50	0.9
50≤D≤230	1-(D-0.76/380)

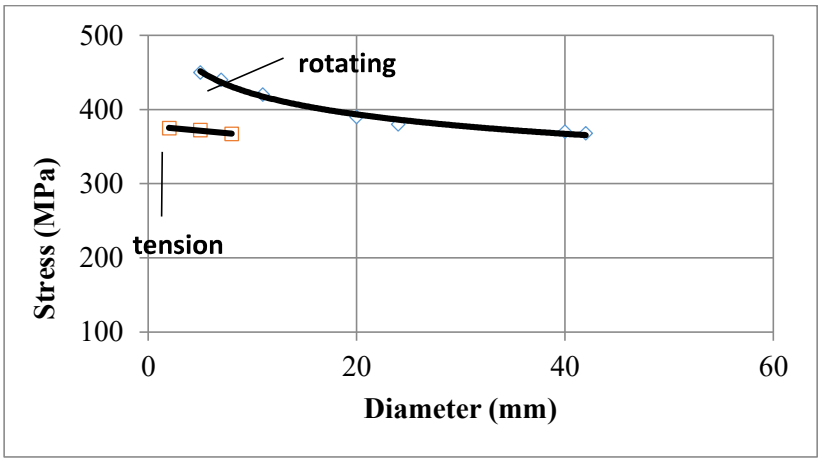

Figure 6. Fatigue limit reduction factor due to size effect [16]

2.3.3. Surface Effect on Fatigue

Crack initiation is always a surface phenomenon theoretically; besides, the condition of the surface is directly related with fatigue life. Crack initiation stage is the dominant part of the fatigue life in high cycle fatigue (HCF) which is higher than 10^4 cycles. Surface condition can be affected from various variables that are shown in Fig. 7.

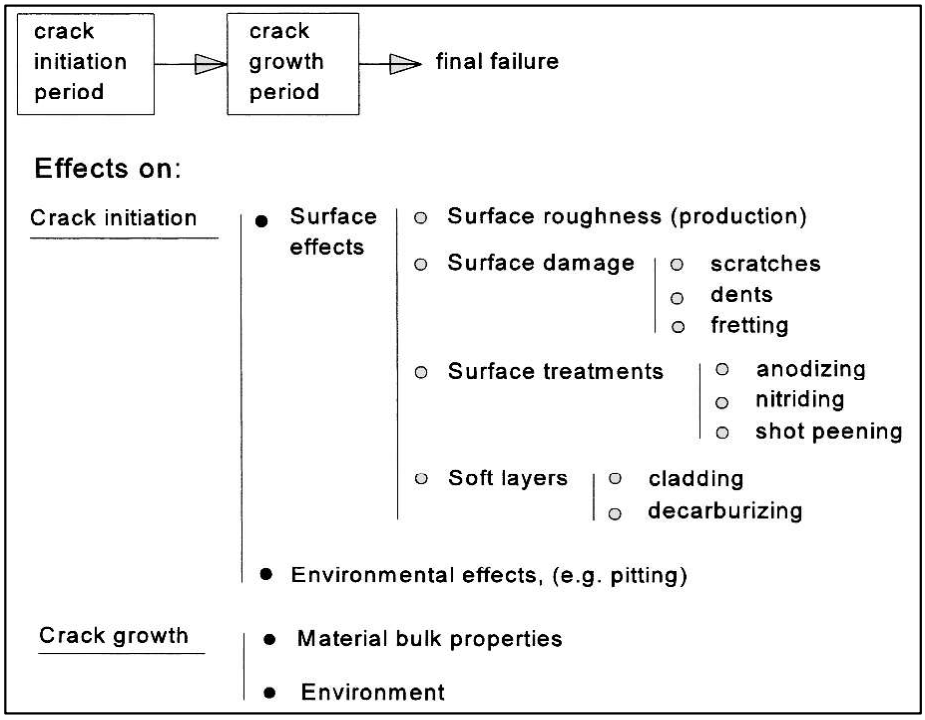

Figure 7. Effect of surface condition on crack periods.[16]

Although surface effects can be formed from different sources such as roughness and treatments, same effect such as stress raisers is observed on a material in terms of fatigue. These non-uniformities are stress concentration points so they decrease crack initiation period and lead to fatigue limit reduction [16]. Comparison of surface effect between with/without S/N curve for certain material is indicated in Fig8. Higher stress amplitude which is low cycle fatigue (LCF) region is less affected from fatigue limit reduction because crack initiation is minority stage for fatigue life. However, low stress amplitude region shows that fatigue limit can be highly affected from surface effect since crack initiation stage is dominant for high cycle fatigue (HCF) region.

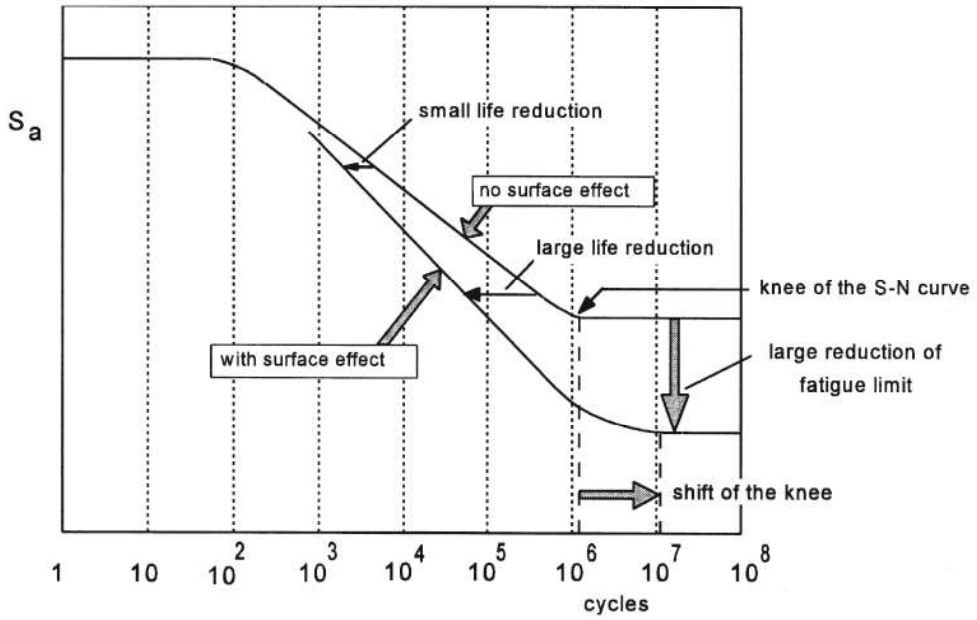

Figure 8. Surface effect on S/N curve[16]

2.3.4. Residual Stress

Residual stress is a very complex phenomena, but it can be explained with a simple model. Bending movement produces tension and compression stresses on a material. These stresses can plastically deform material`s surface even if bulk material is elastically deformed. These permanent shape change causes residual stress that is shown in Fig.9.

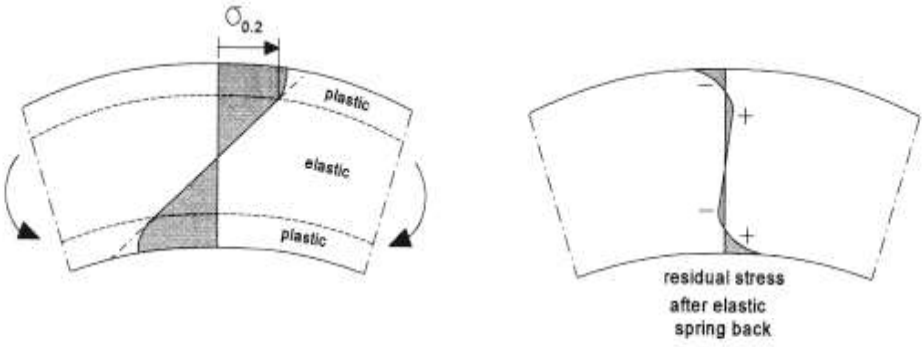

Figure 9. Residual stress under bending loading[4]

Residual stress can be produced in a material because of several processes. These processes are listed below;

1. Inhomogeneous plastic deformation,

2. Manufacturing processes,

3. Shot peening,

4. Plastic hole expansion,

5. Heat treatment,

6. Assembly of the products [16].

On the other hand, residual stress can be useful depending on purposes. For example, shot peening process consists of compressive stress layer on material's surface. It enhances fatigue life of the material by retarding the crack initiation. Stress distribution of the shot peened material during fatigue test is indicated in Fig10. However, tensile stress on the surface can be very dangerous in terms of fatigue limit since premature crack initiation can result in catastrophic failure of the material.

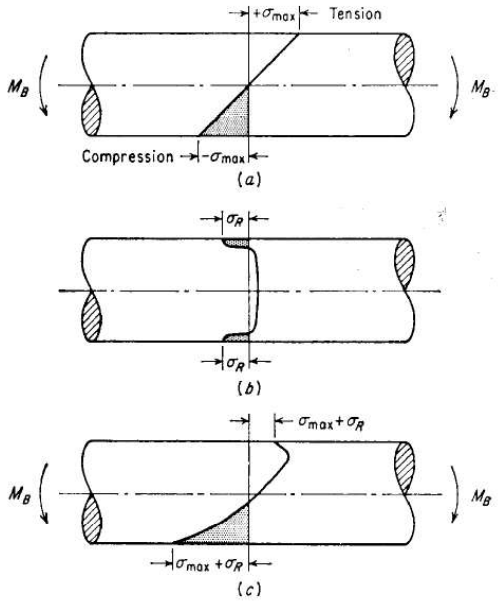

Figure 10. Residual stress at various stress and surface conditions[4]

(a) Bear material under bending, (b) shot peened (compressive stress layer), (c) shot peened material under bending [4].

2.4. Fatigue Tests

Fatigue tests can be conducted for various purposes in order to clarify issues; however, issues and required data should be well defined before fatigue tests. Ambiguous issues could be ended up unrequired results, waste of time and work. Fatigue tests are categorized below to explain different problems in literature of fatigue problems.

- Material fatigue properties
- Effect of surface treatments and production techniques
- Joint and structural elements
- Environmental effects
- Crack growth (crack nucleation & propagation)
- Verification of fatigue model

Although variables could be increased depend on type of investigation which are stated above list, general variables are (i) specimen, (ii) test loads and (iii) test procedures. Specimen types have to be compatible with purpose of the fatigue tests. For example, the un-notched specimen should be chosen to compare surface treatment but pin loaded hole joint is suitable for jointed element tests [16]. Several specimen types are shown in Fig.11.

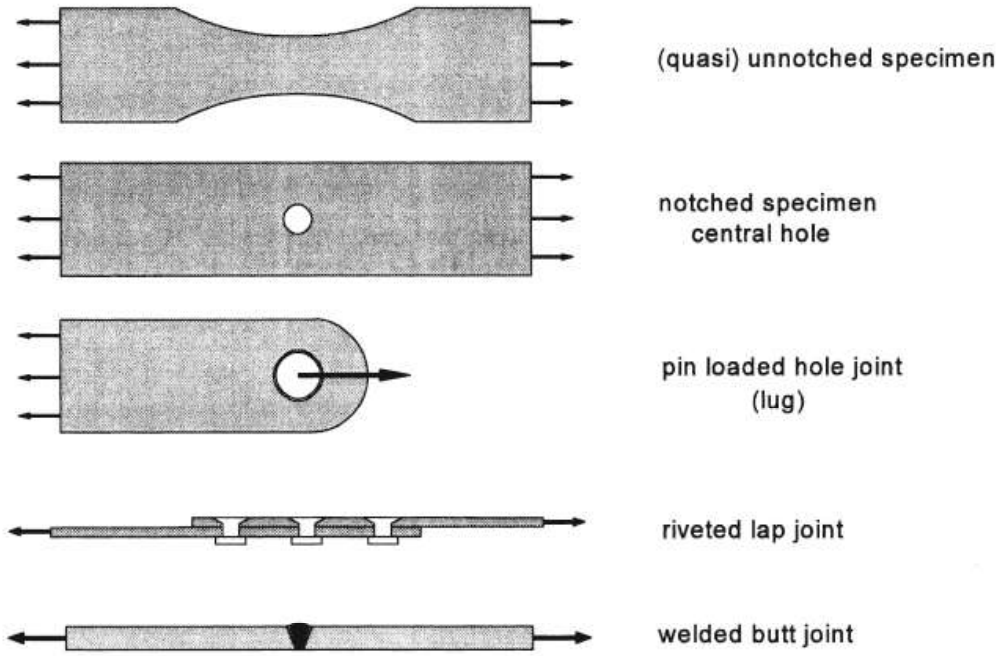

Figure 11. Types of specimens[16]

The second major variable for fatigue tests is the test load which is determined during test due to noteworthy aspects such as scatter and coefficient of determination (R^2) etc. when S/N curve construction. Test loads are firstly chosen at high stress level which is low number of cycles in general approach in order to avoid non-failure test which is called run-out. Another advantageous of this approach are short test time and test setup confirmation[18].

Test procedure for fatigue tests can be composed as custom depend on requirements for a certain test. On the other hand, international standards state detail of the fatigue test procedures with respect to type of the test such as ASTM E466[19] and ASTM E647[20]. ASTM E466[19] describes force controlled constant amplitude fatigue test for metallic materials while ASTM E647[20] defines crack growth test. ASTM E466 includes not only procedure but also test data calculation and specimen preparation which is consist of specimen type and manufacturing process. In this thesis, fatigue tests were conducted based on ASTM E466[19] which is constant amplitude axial fatigue tests.

Type of fatigue testing machine is not restricted by ASTM E466 such as servohydraulic or resonant type of testing machines. Resonant testing machine was used for fatigue tests in this research. It runs by oscillation at natural resonance of the material. Specimen is statically loaded to the mean load of the fatigue test by the help of ball spindle that is controlled by a gearbox and servomotor before dynamic loading. Dynamic loading is applied by oscillating system which is driven by mass and elasticity of specimen. Electromagnets are located upper side of the testing machine and oscillating system is activated by electromagnetic interaction. Oscillating system can partially be controlled by changing mass of the system. Test frequency can be decreased by activating masses at the upper part of the testing machines or vice versa. Components of the resonant testing machines is shown in Fig. 12.

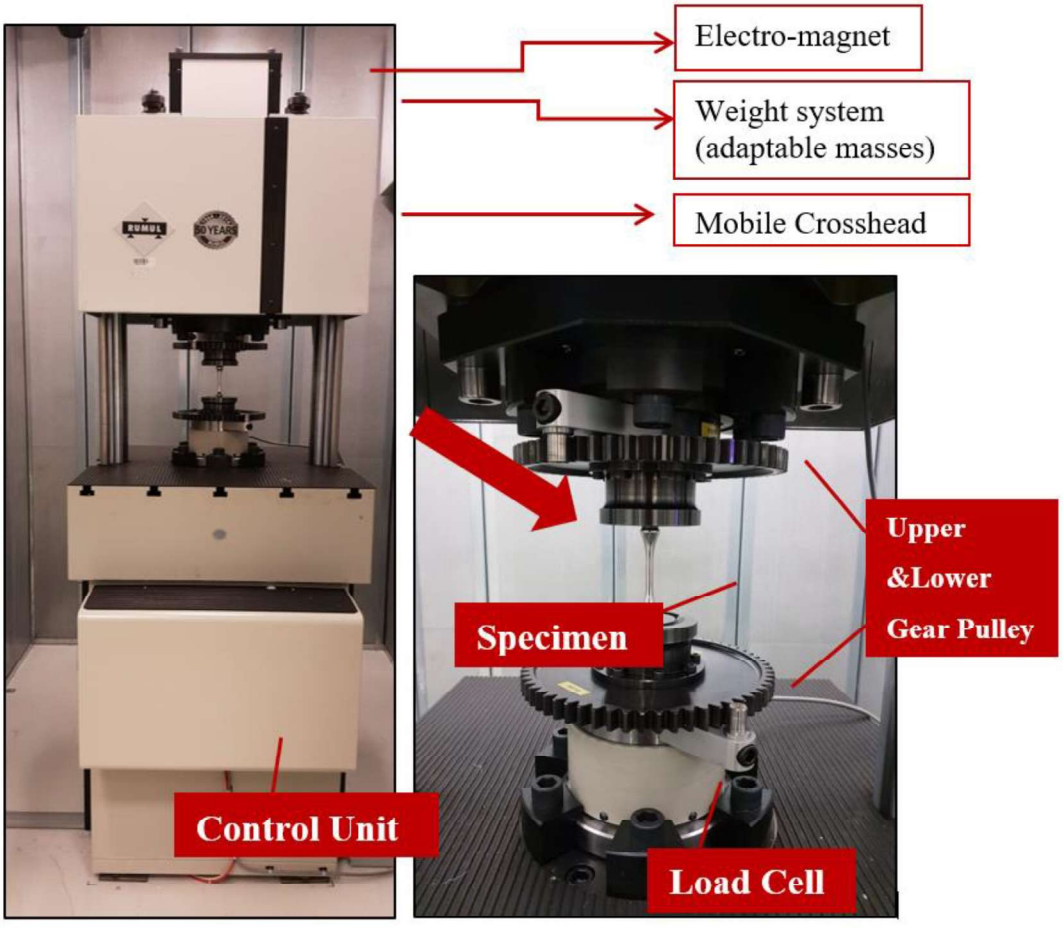

Figure 12. Resonant testing machine

2.5. S-N Curve

Stress vs number of cycles curve (S-N Curve) is the basic technique to represent the fatigue data. Number of cycles axis is commonly represented in log scale but both of the axis could be shown in log scale on S-N curve. Three different regions are used for S-N curve label. Low cycles region is until 10^4 cycles, while high cycles region is higher than 10^5 cycles. Region between low and high cycles regions is called transition region. S-N curves have different characteristic shape with respect to material type. S-N curve of ferrous materials generally have horizontal limit stress after certain cycles, such as steel. On the other hand, the curve slopes continuously downwards for nonferrous materials such as aluminum. The S-N curve can be constructed by 8 to 12 specimen`s fatigue test results [4]. Representative S-N curves are shown in Fig13.

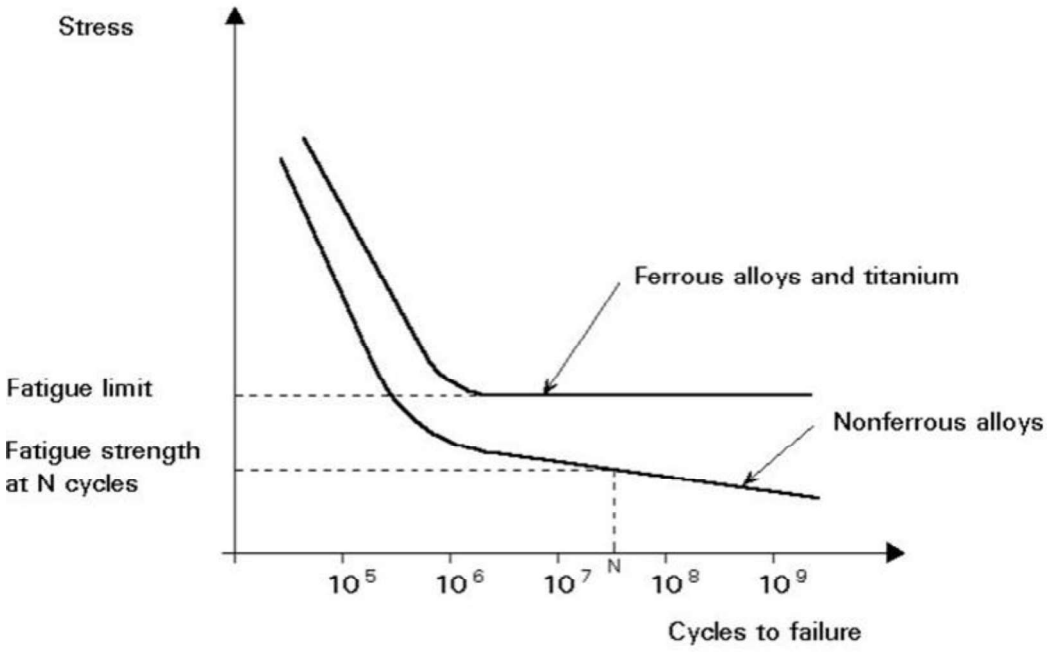

Figure 13. S/N curve with/without horizontal endurance limit

Scatter of fatigue test data is natural phenomena because of parameters that affects fatigue mechanism such as stress concentration or residual stress which were explained in section 2.3. Scatter is less at low cycle region while it is much higher at high cycle region which is low stress state. Scatter band progressively expands by

decreasing stress state. This is resulting from difference between crack nucleation and propagation stages for high and low stress states. Crack nucleation is major stage at low stress state since stress is not high enough for microcrack formation. Microcrack formation occur due to surface inhomogeneities or irregularities at low stress state. These surface conditions that reduce crack initiation time can vary for each specimen. Therefore, scatter band reach maximum value at low stress state. On the other hand, crack propagation stage is dominant at high stress state. So different surface conditions are not much effective, however, intrinsic properties of materials have significant role at high stress state[16]. Scatter levels are shown in Fig.14.

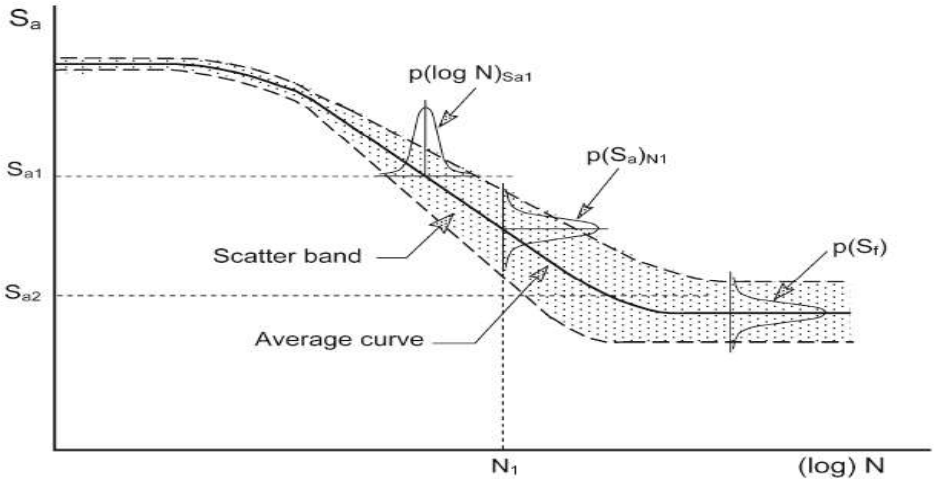

Figure 14. Scatter band of S/N curve[16]

2.5.1. Statistical Approach

Many types of statistical approach can be applied to convert test data points into S/N curve after fatigue tests. The most common equation is 4 parameters proposed by Weibull which is stated as Eqn.5 [21].

$$S - S_e = b(N + B)^{-a} \qquad \textit{Eqn 5}$$

Where;

S= Stress,

Se=Endurance Stress,

N= Number of Cycles,

B= Time Scale Parameter,

a= Shape Parameter,

b= material constant

Unknown parameters in the equation are estimated by the least square method. For curve fitting, nonlinear regression of S on Log N is carried out by minimizing sum of squared deviations in stress states. On the other hand, ultimate strength value (UTS) of the testing material is used as N=1 stress value unless S/N curve is obtained infinitely at very low cycles. Therefore, UTS value as N=1 is practical solution to evaluate fatigue curve at very low cycles. Comparison between S/N curve for same data with and without UTS value as N=1 is shown in Fig15 [18].

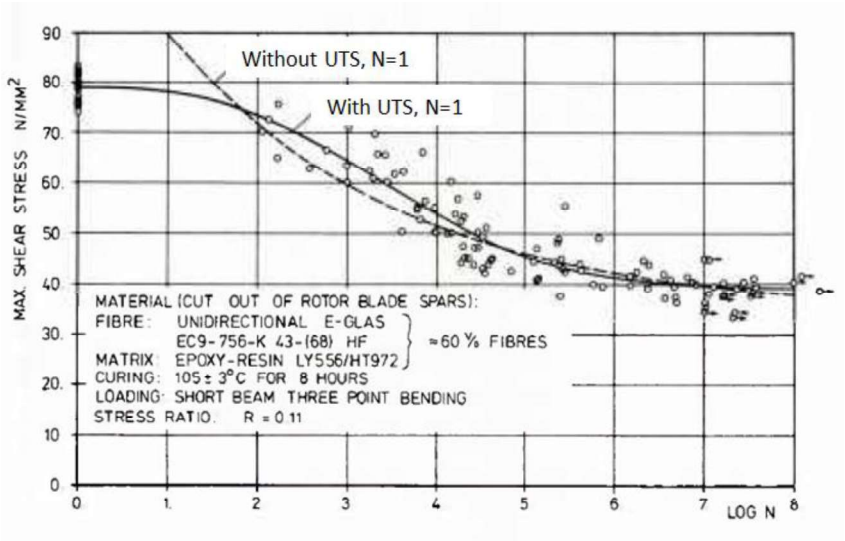

Figure 15. S/N curve shape comparison for using UTS as N=1 [18]

Fatigue data can be present in three different ways with respect to their coordinates system. These are (i) linear coordinates, (ii) semi-logarithmic coordinates and (iii) logarithmic coordinates. Linear coordinates are dangerous because the tendency of the curve at endurance limit is higher than semi-logarithmic coordinates. This comparison is shown in Fig16. This could cause catastrophic results in service of the product. On the other hand, there is no big difference between semi-logarithmic and logarithmic coordinates. Semi-logarithmic coordinates are more practical with regards to understanding of stress value. Therefore, semi-logarithmic coordinates are widely used way for presentation of the fatigue results [21].

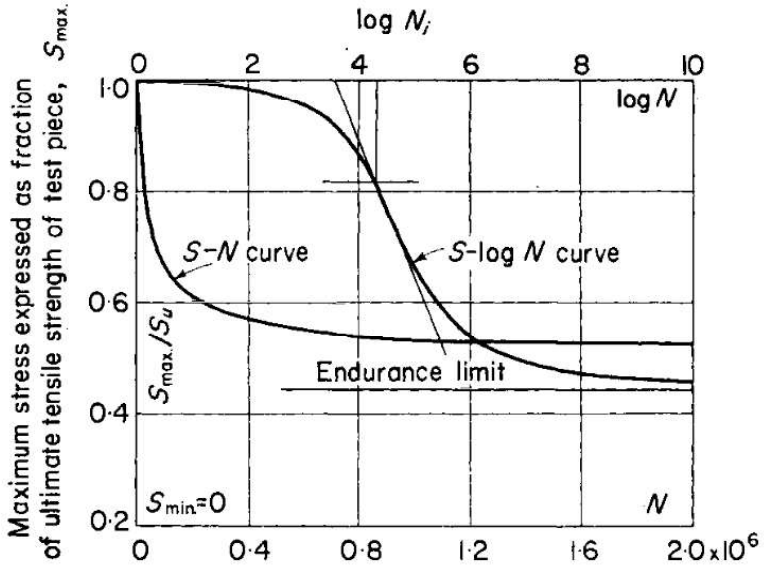

Figure 16. Logarithmic and Semi-logarithmic S/N curve[4]

2.6. Effect of Chromic Acid Anodizing (CAA) on Cyclic Load

Chromic acid anodizing changes the surface characteristic of the material, therefore, fatigue behavior is directly affected since crack initiation stage is influenced due to CAA. Roughness is one of the major surface parameters. Fatigue strength is inversely proportional with surface roughness along S/N curve. Reduction amount in stress based is about 10% at high stress region and 32% at low stress region [22].

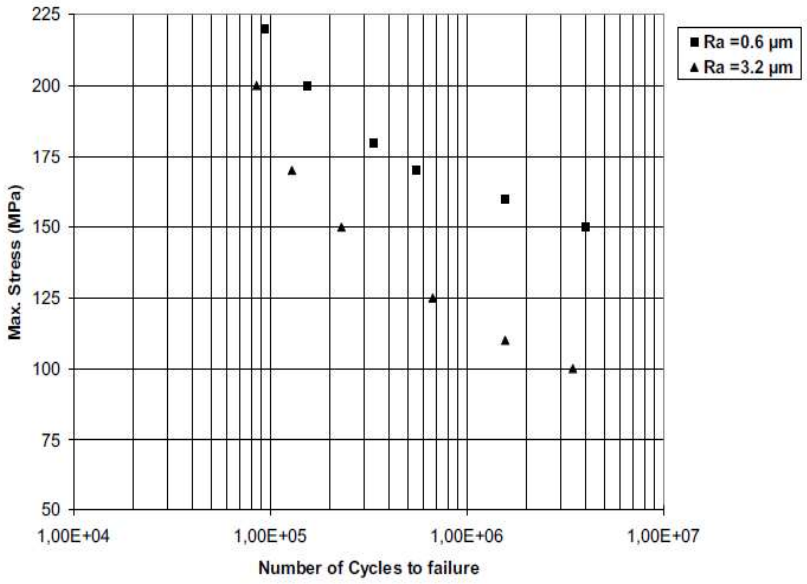

Figure 17. Roughness effect on fatigue [22]

Otherwise, the surface condition is affected by different levels in the CAA stages such as pretreatment and anodizing. Pretreatments are degreasing and etching that they were explained in section 2.2.1.1. They clean the material surface and create a smooth surface without any organic and inorganic residuals. Surface is not impaired due to degreasing [23]. However, etching stage is the predominant process in terms of fatigue life reduction [1]. Barter, et.al[24] examined pitting shape, size and morphology caused by pickling for 7050 T7451 aluminum alloy before CAA. It is found that pitting having 15µm depth is maximum frequency and range of pitting is 5-37µm [24]. Pitting size distribution is indicated Fig18.

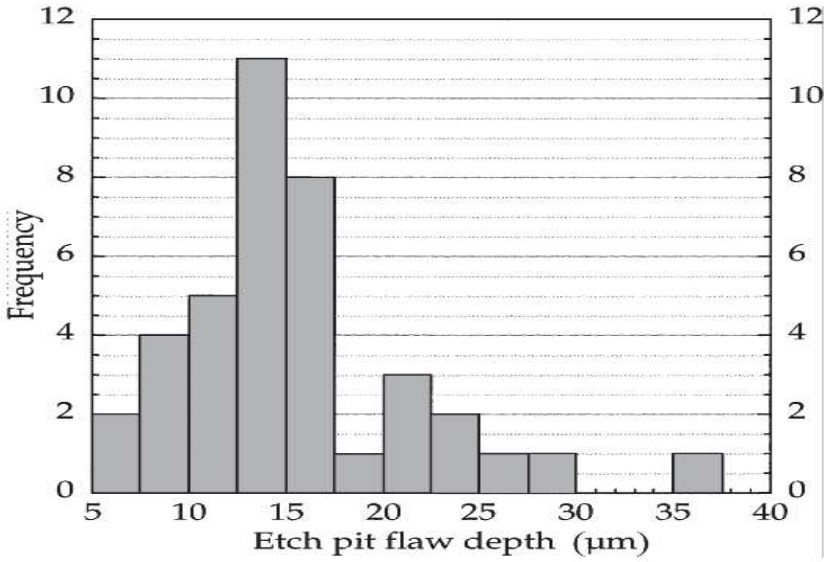

Figure 18. Pitting depths after pickling [24]

Pitting generally occurred in "V" shape since etching solution is localized on material surface. These pits are suspected to crack initiation sites due the stress concentration effect [24]. Crack growth paths from a stress concentrated pit is demonstrated in Fig19. Pitting shape images taken by optical microscope and scanning electron microscope (SEM) are shown in Fig.20.

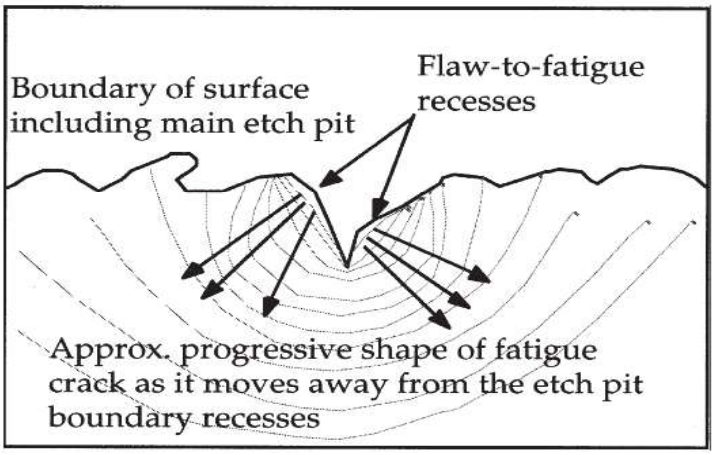

Figure 19. Crack growth sketch from the pit[24]

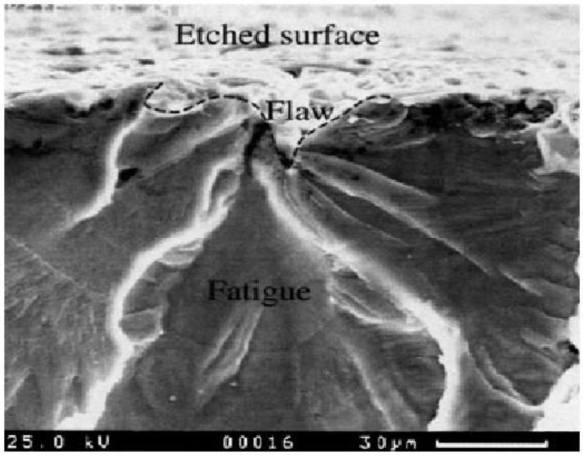

(a)

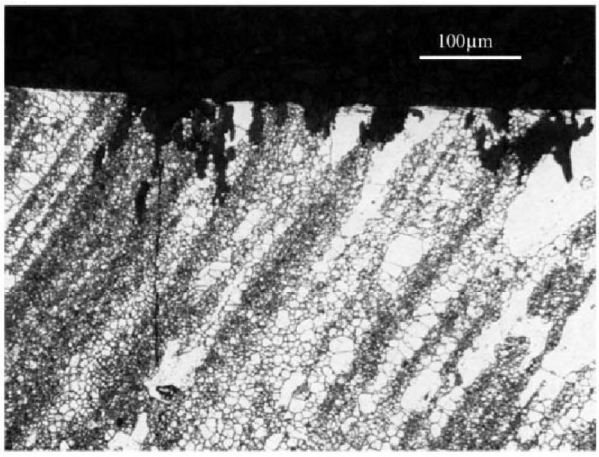

(b)

Figure 20. Pitting images after CAA taken by SEM(a) and Optical Microscope(b)[24]

7050 T7451 alloy is immerged into anodizing a bath, after pretreatments are done. Average and maximum pitting depths after pretreatments which are coherent with that of after anodizing [1]. Therefore, fatigue limit reduction is affected slightly after anodizing which is 9% with respect to pickled condition while it is affected dramatically after pickling that is 32% with respect to as machined condition[1]. Total fatigue limit reduction was found to be 41%. S/N data of these conditions are shown in Fig.21. This slight decrease between pretreatments and anodizing is caused by brittle oxide layer formed during anodizing[1].

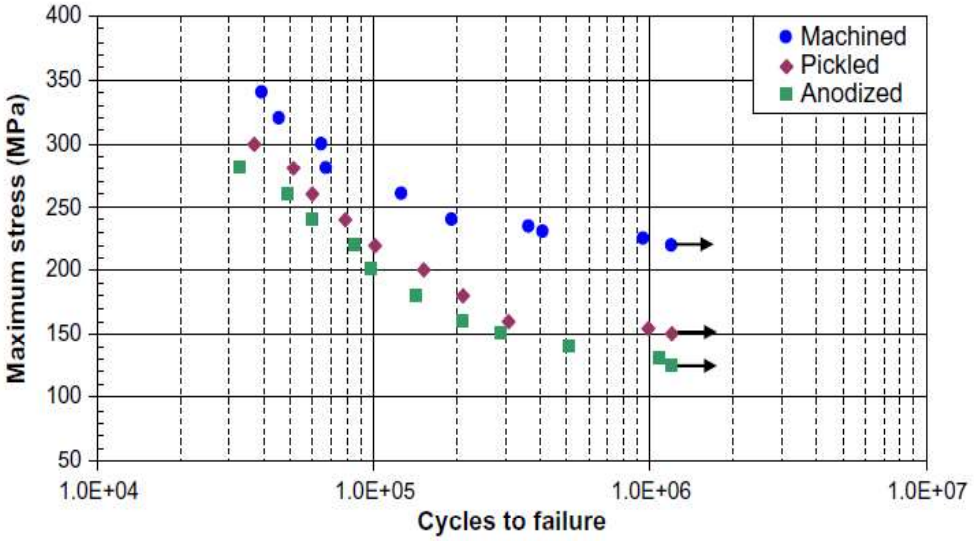

Figure 21. Effect of CAA stages on fatigue life[1]

Aluminum oxide layer is formed by anodizing thickness does not affect the fatigue life of the material. S/N curve of 7075 T73 aluminum alloy is shown in Fig22. It presents similar results for both 10 and 20 μm[25]. SEM images of pitting[23] and coating layer [1] are shown in Fig23.

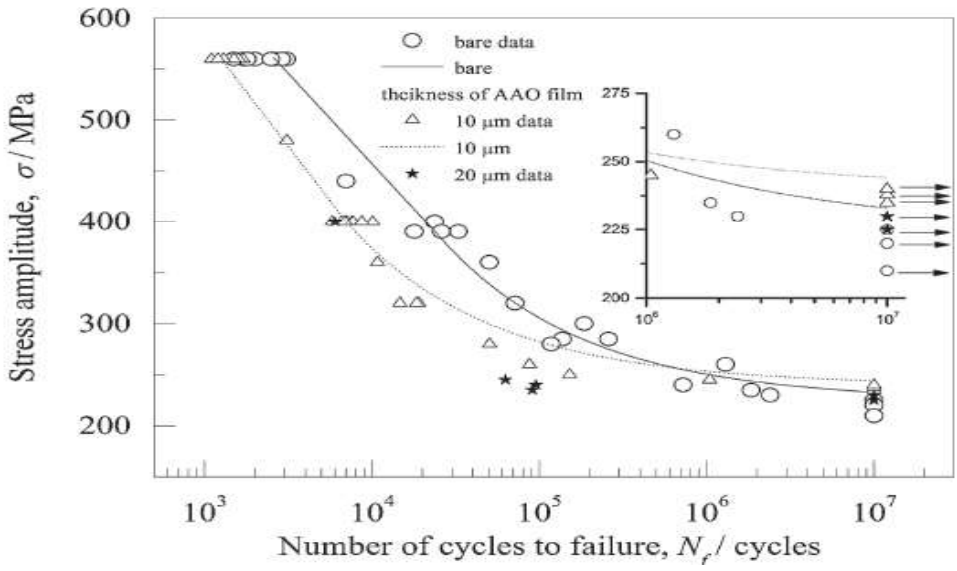

Figure 22. Anodizing thickness effect on S/N curve[25]

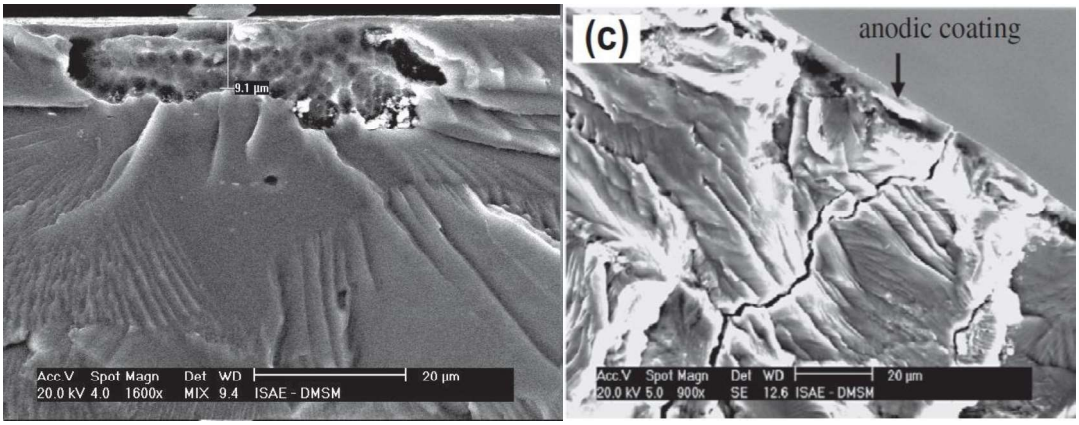

Figure 23. SEM images of pitting and CAA layer[23]

CHAPTER 3

EXPERIMENTAL PROCEDURE

3.1. Material Characterization

First of all, 7050 T7451 was characterized by applying x-ray fluorescence (XRF) microscopic examination, hardness measurements and tensile test. These techniques were executed to confirm AMS4050 specified 7050 T7451 raw material. Composition of the raw material was found by XRF. Grain direction, grain size and aspect ratio were determined by microscopic analysis. Hardness of 7050 T7451 was measured in Brinell Scale. Tensile properties were determined with respect to ASTM E8[26]. This standard describes the application of tensile test for metallic materials. Tensile test was performed per ASTM E8 [26] with crosshead speed 0.5 mm/min. Specimen geometry was the same with specimens using during fatigue tests. This geometry was chosen to use static test result as the first cycle data during curve fitting [18] and reduce manufacturing time and cost. The specimen geometry was presented in Fig.27 at Section 3.3.

3.2. Chromic Acid Anodizing (CAA) Process Selection

Eight different processes were followed to select the most suitable CAA process by changing type of etchant and etching time such as alkaline etching and acid etching. Process1 to Process 4 were followed Path1 in Fig.24 that have included both alkaline and acid etch stages in pretreatments before CAA bath. The rest of the processes included only acid etching in pretreatments before CAA bath. Concentration of the baths for etchings and anodizing was indicated in Table 5.

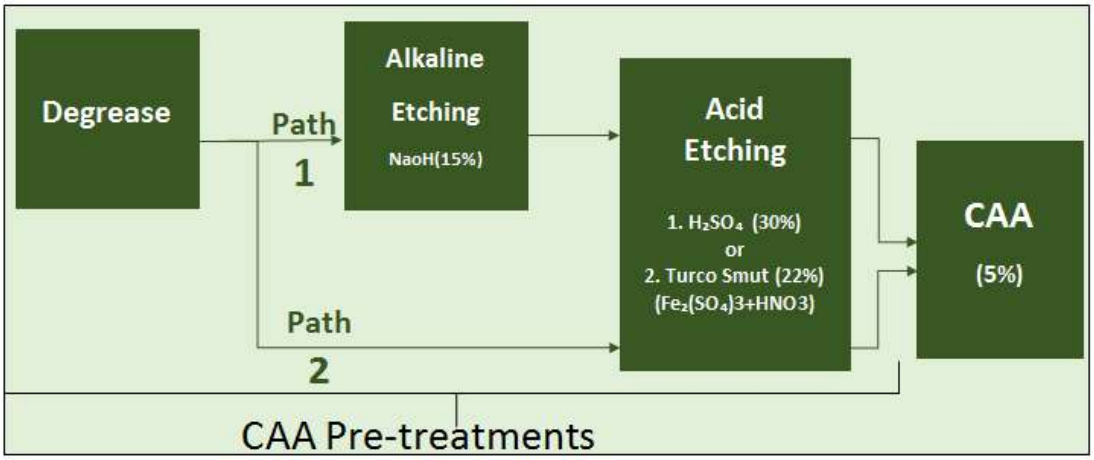

Figure 24. CAA process paths

Table 6. *Concentration of the baths*

Stage	Tank Chemicals	Tank Concentrations (g/L)	Temperature (°C)
Alkaline Etching	NaOH	150	23-29
Acid Etching	H_2SO_4	300	Ambient
Acid Etching	TURCO SMUT	220	Ambient
Anodizing	Chromic Acid	50	32-37

Holding time in alkaline etch and acid etch tanks were variable for Process 1 to Process 4. In order to select CAA process for surface treatment of fatigue tests, applied pretreatments and immersion time of them with respect to processes were indicated in Table 7. Detail flow chart of the applied CAA processes were shown in Fig.25.

Table 7. *CAA process selection specimen matrix*

Process #	PRE-TREATMENTS						CAA
	Path#	Degrease	PICKLING				
			Alkaline Etching (NaOH)	Alkaline Etching Time (min)	Acid Etching	Acid Etching Time (min)	
Process 1	1	√	√	7	Smut	1	√
Process 2	1	√	√	7	Smut	5	√
Process 3	1	√	√	7	H2SO4	1	√
Process 4	1	√	√	7	H2SO4	5	√
Process 5	2	√	X	N/A	Smut	1	√
Process 6	2	√	X	N/A	Smut	5	√
Process 7	2	√	X	N/A	H2SO4	1	√
Process 8	2	√	X	N/A	H2SO4	5	√
√: applied, X: not applied, N/A: not applicable							

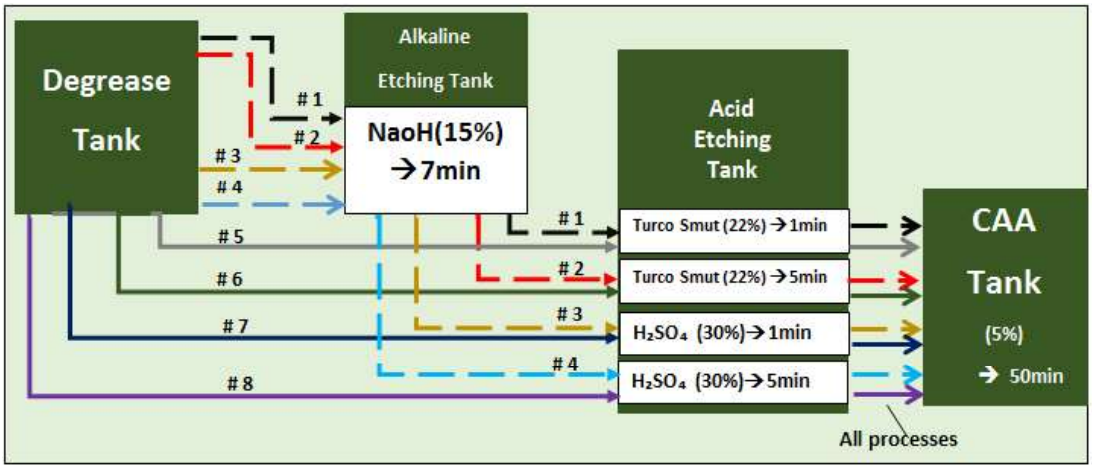

Figure 25. CAA process paths depend on process number

Geometry of the specimens for all processes was chosen as rectangular bar in order to examine in optical microscope easily, which was shown in Fig.26. After specimens were anodized in chromic acid according to their individual process, they were grinded with 200, 600, 1000, 1600 and 2000 grid emery papers respectively during three minutes for each. Polishing was applied with 0.1µm alumina paste after grinding for optical microscopic examination. Grinding and polishing were applied to

perpendicular to longitudinal (L) direction because fatigue tests were executed in longitudinal (L) direction.

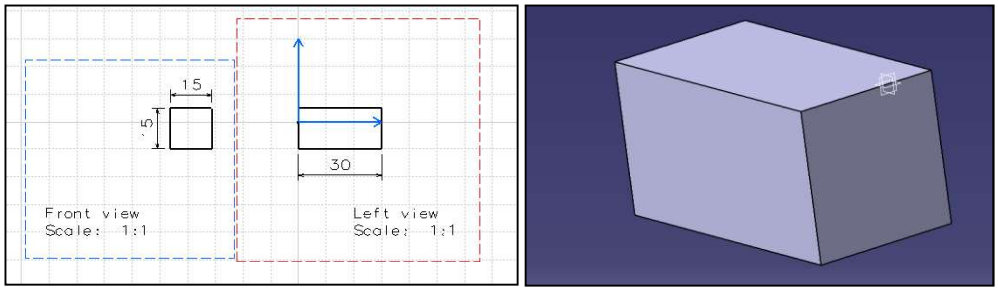

Figure 26. Rectangular bar specimen

Pits at transverse direction caused by CAA was measured with the optical microscope from metallographic prepared specimens. In addition to this, coated layer of the specimens was measured by eddy current method according to ASTM-B244[27]. Results of the pits depth and coating layer for each specimens were tabulated. CAA process resulting with the deepest pit and the highest average pit depths with appropriate coating thickness was selected to apply fatigue specimens since major effect on fatigue life was caused by pit formation during CAA[1]. Moreover, Pitting path depend on grains were examined from metalurgically prepared rectangular specimen by optical microscope. This specimen prepared by using Keller`s etchant for 40 seconds after grinding and polishing. Pit formation and how to affect fatigue life of the material is explained in the section 2.6 in detail.

3.3. Fatigue Tests

7050 T7451 aluminum alloy was obtained according to AMS4050 aeronautical grade bulk material. Furthermore, all specimens without noticing ,whether they were coated or not, were manufactured from same batch for fatigue test in order to eliminate bulk material differences resulting from batch differences. All specimens were manufactured by machining at a very slow rate to decrease residual stress due to manufacturing. Machining parameters for fatigue specimens were given in Table 8.

Table 8. *Machining parameters for fatigue specimens*

Spindle Speed (RPM)	Cutting speed (m/min)	Feeding rate (mm/RPM)	Depth of Cut (mm)
200	50	0.02	0.1

Specimen`s threads (M22x1) were compatible with test machines which was shown in Fig.27. Roughness of the specimens were measured as bare condition after machining. Average roughness value (Ra) was taken by repeating at least three times according to ISO EN4287. All specimens had to satisfy 0.4µm Ra value depends on technical drawing seen on Figure 27.

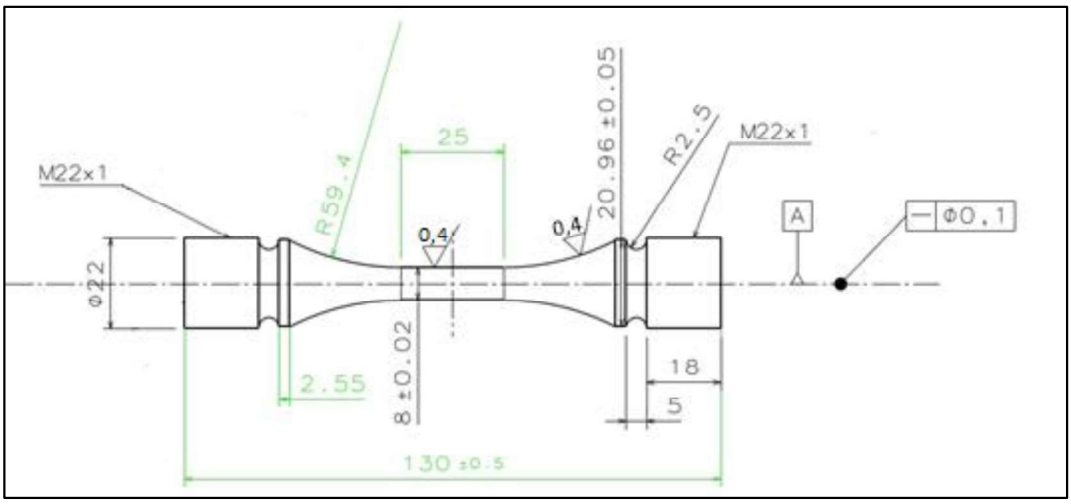

Figure 27. Fatigue Specimen Geometry

Sinusoidal loading was applied to the specimens with stress ratio (R) equals to -1. This stress ratio represents the most crucial situation in terms of crack initiation and propagation. Force controlled axial fatigue tests under constant amplitude were conducted according to ASTM E-466 [19]. Fatigue tests were conducted at 91Hz with resonant type test machine. This type of machines are capable of testing at very high frequency until 270 Hz depending on the specimen stiffness. Groups of specimens for fatigue test are indicated at Table 9 with respect to applied process and time.

Table 9. *Groups of fatigue specimens*

Group	Surface Condition	Degrease	Pickling	Anodizing	Anodizing immersion time(min)
ASM	As-machined	x	x	x	N/A
PRET	Pretreated	√	√	x	N/A
CAA	Chromic Acid Anodized	√	√	√	50
CAAT	Extended Chromic Acid Anodized	√	√	√	100
√: applied, x: not applied, N/A: not applicable					

Group ASM was as-machined stated without any surface treatment in which no additional process was applied after machining. However, only acid and alkaline pickling stages of chromic acid anodizing were done for group PRET . Chromic acid anodizing was completely applied for group CAA and CAAT. Difference between two groups was only holding time in chromic acid anodizing bath. Immersion time of chromic acid anodizing for group CAA was twice of group CAA which were 50 and 100 minutes respectively. All groups were determined to investigate effects of different stages of chromic acid anodizing process on fatigue behavior. Group ASM was reference group for fatigue tests. Although, Group PRET showed pretreatment effect of this process, group CAA was a standard complete process. Group CAAT was to compare effect of immersion time of chromic acid anodizing while it have exactly same pretreatments with group CAA.

Stress levels for each specimen which were entitled depend on their group was indicated in Table 10. Fatigue tests were conducted with respect to stress levels that was stated below at R=-1 on resonant test machine.

Table 10. *Stress levels of specimens for fatigue test*

Fatigue Test Groups & Stress levels							
ASM		**PRET**		**CAA**		**CAAT**	
Specimen	**Stress**	**Specimen**	**Stress**	**Specimen**	**Stress**	**Specimen**	**Stress**
ASM-1	220	PRET-1	180	CAA-1	180	CAAT-1	180
ASM-2	240	PRET-2	200	CAA-2	165	CAAT-2	165
ASM-3	260	PRET-3	165	CAA-3	150	CAAT-3	210
ASM-4	280	PRET-4	170	CAA-4	210	CAAT-4	230
ASM-5	210	PRET-5	150	CAA-5	220	CAAT-5	150
ASM-6	300	PRET-6	140	CAA-6	160	CAAT-6	150
ASM-7	200	PRET-7	140	CAA-7	150	CAAT-7	140
		PRET-8	230	CAA-8	140		

After fatigue tests, results were obtained as a pair of values, one of which was related to the applied stress and the other to the number of cycles. The trend of test data was interpreted by the relationship S = f (N) with S = maximum stress and N = number of cycles to failure. The type of the equation f (N) was established by a numerical analysis of test data. For this kind of curve, the modified Weibull equation for four parameters was used[18].

$$S = S_{\infty} + b(N + B)^{a} \qquad \textit{Eqn 6}$$

Where;

S: Applied maximum stress level

S_{∞}: Stress level at infinity

N: Number of cycles for a certain stress level

a, b, B: Variables for construction of best fit

The S-N curves according to Eqn.6 were derived from test data and exhibits the mean curves with %50 probability. After evenly distributed seven or eight data which were the high enough for curve construction[18] between N = 1 and 1,0E+06 cycles was obtained. The best fit curves based on Eqn.6 were drawn through the test points. The

advantage of this approach was that it treats the test data from a purely statistical aspect and hence results in a mean curve with the lowest data scatter. Best estimates of the unknown constants S_∞, a, b and B were obtained in fitting the Eqn.6 of the S-N curve to the fatigue life data by applying the method of the least squares with non-linear regression. The regression of stress on life was performed by given formula;

$$Sum\ of\ the\ Least\ Square = \sqrt{\frac{\sum_{i=1}^{n}(logS - logS_i)^2}{n}} \qquad Eqn\ 7$$

where:

S: Estimated stress from Eqn6.

Si: Maximum stress of individual specimen

n: number of specimens

The representative sum of squared deviations in the vertical direction between the test data points and the best fitting curve was least that is shown in Fig28. Complete S-N curves were found by using the static strength and the high-cycle data points. Least square was performed on data points between N = 1 and N = ∞; eventually, the complete S-N curve matches as close as possible to the simplified S-N curve. Logarithmic based stress difference is described for least square method in AGARD-AG-292 helicopter design guide[18]. Therefore, Eqn.7 was applied with respect to this description. Constraints of modified Weibull equation to calculate all unknowns i.e. S_∞, a, b and B were given in Table11.

Table 11. *Constraints for unknown parameters of modified Weibull equation*

$b \geq 0$	$a \leq 0$	$B \geq 0$	$S\infty \geq 0$

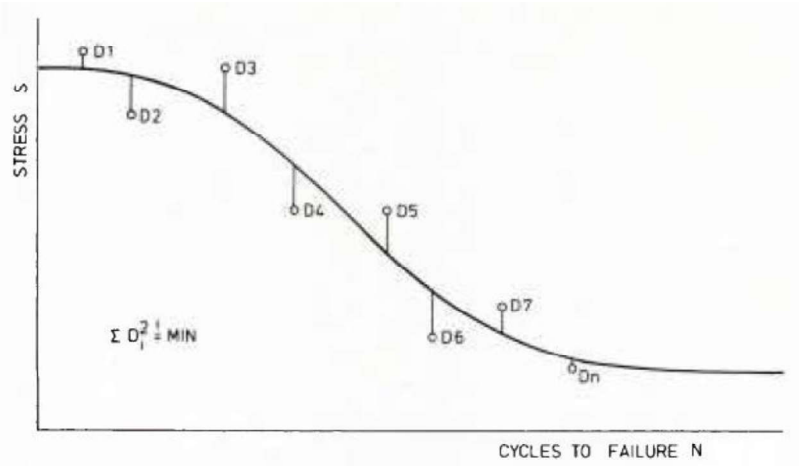

Figure 28. Fatigue test data deviation from mean curve[18]

Degree of the curve fittings were checked by standard deviation and R^2 . Standard deviations were calculated at the run-out cycle (1E+06 cycles). To determine standard deviation at the run-out cycle, S_∞ values for each data point was calculated per Eqn.6. Hereby, maximum stress and life data come from test results and rest of the fitting parameters i.e. a, b and B are already known; so, S_∞ for each data point was easily found. Then, extrapolation was carried out to the run-out criterion for each data point. Standard deviation at normal scale was calculated based on maximum stress at 1E+06 cycles. Extrapolation of fatigue test data for standard deviation was presented in Fig29. Run-out results were included curve fitting if they were inside of the standard deviation or just below standard deviation[18].

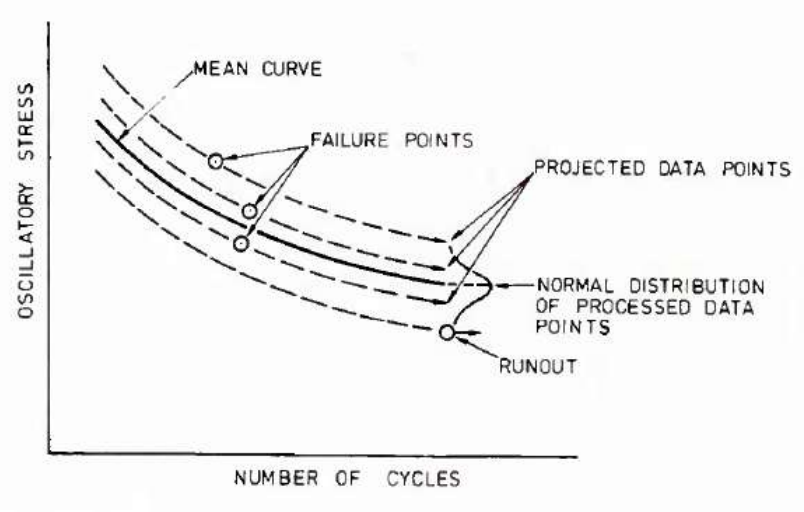

Figure 29. Extrapolation of fatigue test data for standard deviation[18]

3.4. Fractographic Analysis

Fractographic analysis of fatigue specimens were carried out by digital microscope and scanning electron microscopy (SEM). Morphology examination, crack initiation region determination and striation counting were done during this analysis. Morphological features and crack initiation region were compared to the specimen`s surface condition i.e. as-machined, anodized or pretreated.

Striation counting was performed from fracture surfaces by measuring striation width at certain distance away from crack initiation point. Striation widths were measured at least two different regions from each examined specimen. Striation width data were taken at 19 different regions from 7 specimen`s fracture surfaces. Stress intensity factors (ΔK) were calculated for each striation width according to Eqn 8. After striation counting, stress intensity factor (ΔK) vs da/dN was plotted in order to examine crack growth behavior of surface treated and as-machined conditions for 7050 T7451 aluminum alloy.

$$\Delta K = K_{\max} - K_{\min}$$

$$\Delta K = \sigma_{\max}\sqrt{\pi a} - \sigma_{\min}\sqrt{\pi a} = \sigma_r\sqrt{\pi a}$$

Eqn 8

d: crack length

i: Striation width

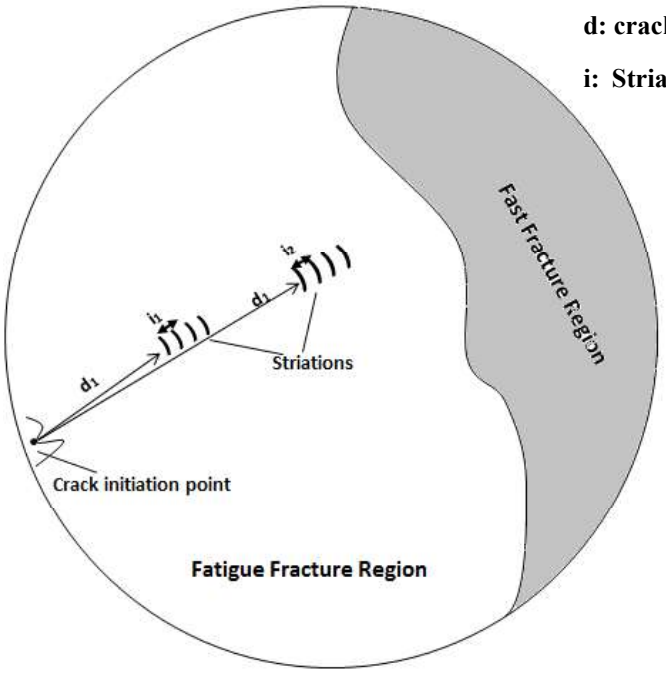

Figure 30. Striation width measurement method

CHAPTER 4

RESULTS AND DISCUSSION

4.1. Material Characterization

X-Ray Fluorescence (XRF) measurements were conducted so as to confirm composition of the raw material which was 7050 T7451 aluminum alloy. Results of compositional measurements by XRF was exactly compatible with AMS4050 which was material specification of aeronautical grade 7050 T7451 aluminum alloy. Besides, raw material was examined by optical microscope in order to find out grain direction, grain size and aspect ratio. Recrystallized equiaxed and large grains were observed in microstructure of the 7050 T7451. Average grain size and aspect ratio were determined as 10.7 μm and 2.14 μm respectively. Longitudinal direction which was the fatigue test direction was shown on microscopic images in Fig.31. Grain size distribution was shown in Fig.32 and Table 13.

Table 12. *XRF results of the raw material*

Element	Measured (%)	AMS 4050 Specification Min. (%)	AMS 4050 Specification Max. (%)
Al	89.11	84.00	93.00
Mg	2.66	1.90	2.70
Zn	5.86	5.70	6.90
Si	0.01	0.00	0.12
Cu	2.10	1.90	2.60
Fe	0.09	0.00	0.15
Mn	0.02	0.00	0.10
Ti	0.01	0.00	0.06
Zr	0.11	0.08	0.15

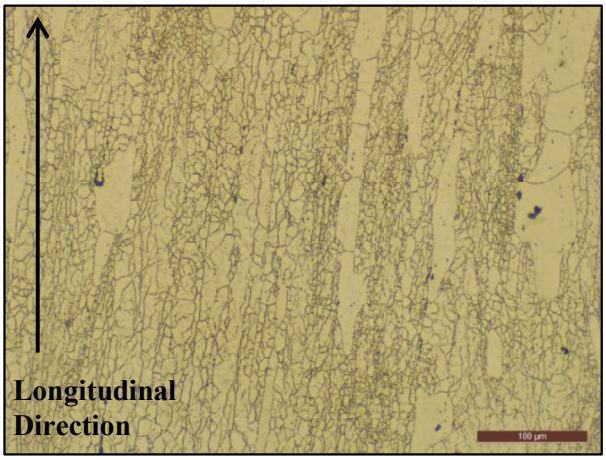

Figure 31. Microscopic images of 7050 T7451 Raw material

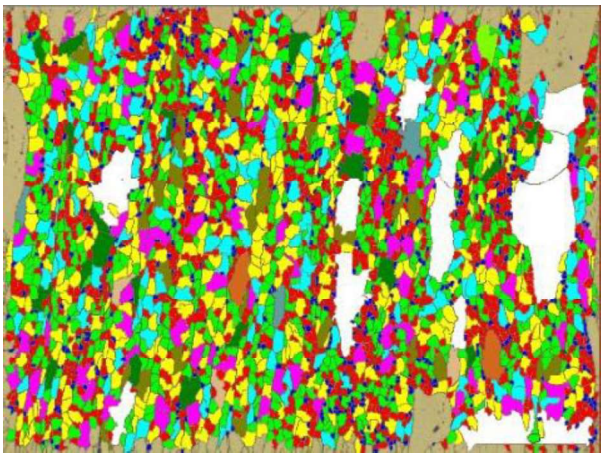

Figure 32. Grain size distribution of 7050 T7451 Raw material

Table 13. Grain size distribution histogram of 7050 T7451 Raw material

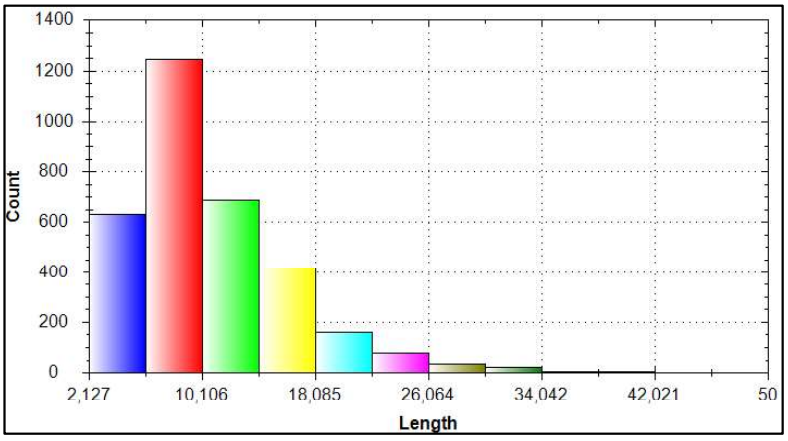

Microstructure of the 7050 T741 was examined by SEM. Grains and intermetallics were oriented in rolling direction which was longitudional direction. They were consistent with optical microscopic images. Intermetallics were viewed and analyzed by SEM and EDS. They were consisted of Al-Cu-Fe (Al_7Cu_2Fe).Moreover, uniform and homogeneous precipitates were observed in grains. Intermetallics and precipitates were shown in Fig.34.

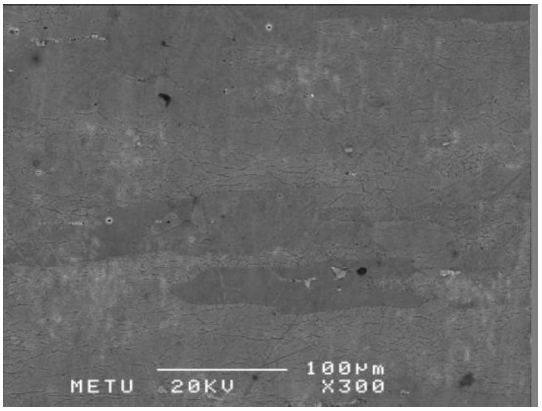

Figure 33. SEM images of 7050 T7451 microsturcture

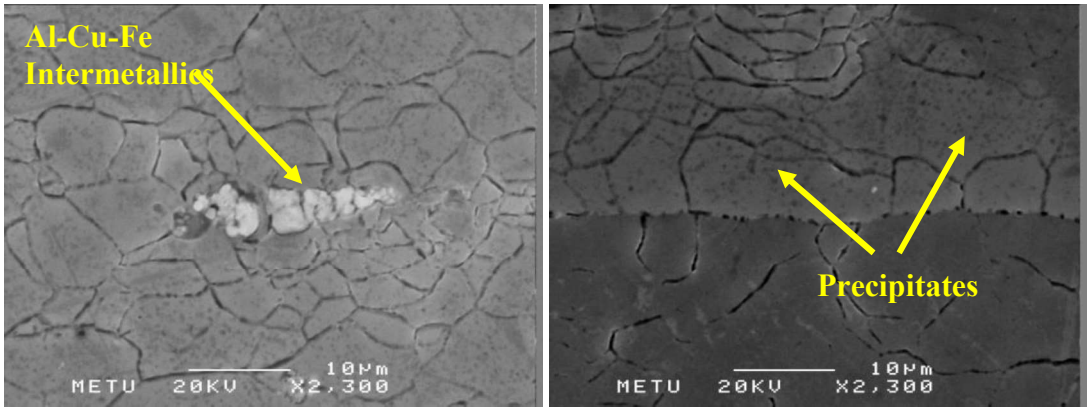

Figure 34. Intermetallics and precipitates of 7050 T7451

Brinell hardness(HRB) of 7050 T7451raw material was measured under 500kg with 10mm ball before tensile tests. Average hardness was found 142.3 HRB which was indicated in Table 14. AMS4050 specification require minimum 510 MPa ultimate tensile strength (UTS) for plate thickness until 51mm on longitudinal direction. Tensile test results satisfied the minimum requirement of the material specification.

On the other hand, UTS for as-machined specimens was found 541 MPa while it was 527 MPa for chromic acid anodized specimen. UTS difference between as-machined and chromic acid anodized specimens was 2.6%. It shows that tensile test results was not affected by chromic acid anodizing.

Table 14. *Hardness of 7050 T7451 Raw material*

	Measurement (HRB)			
Group	1	2	3	Average
ASM	141	143	143	142.3

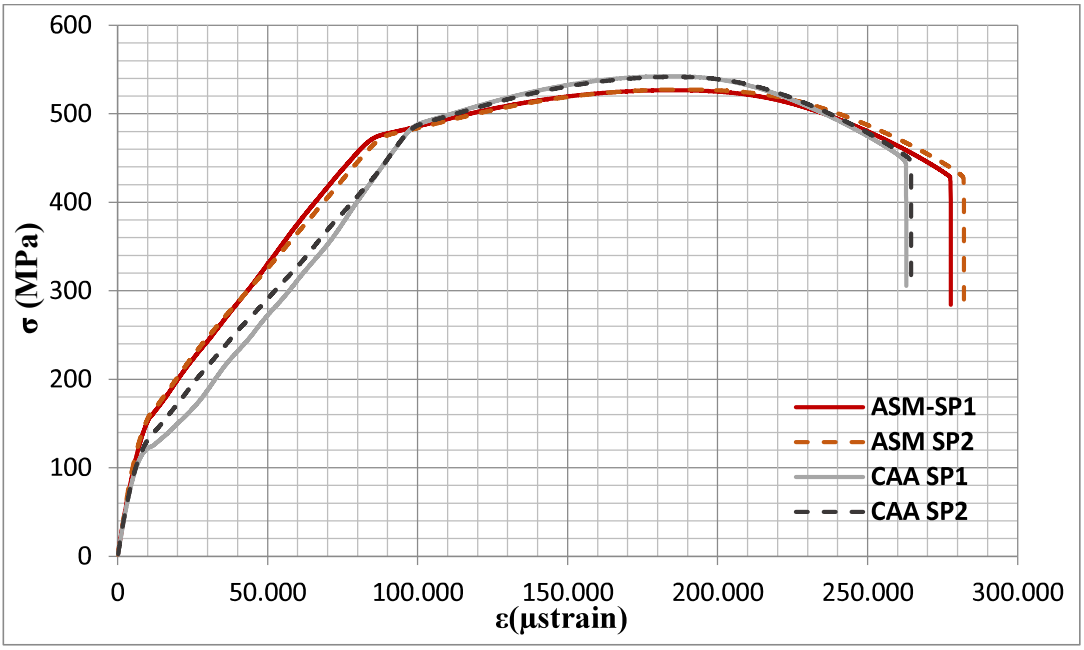

Figure 35. Tensile test results

Table 15. *Tensile test results of the as-machined and CAA specimens*

Specimen	Diameter (mm)	σ_y (MPa)	Ultimate Tensile Strength (UTS)	%Elongation
ASM SP1	8.0	469.2	526.7	19.9
ASM SP2	8.0	468.7	527.5	20.2
CAA SP1	8.0	479.8	542.5	17.4
CAA SP2	8.0	477.6	541.8	17.5

4.2. Chromic Acid Anodizing (CAA) Process

After material compatibility with AMS 4050 and tensile properties of 7050 T7451 were supplied by XRF and tensile tests respectively, eight different chromic acid anodizing processes that were indicated in Table 7 were applied to rectangular specimen. All specimens were examined and compared by optical microscope in terms of pit depths. These specimens were grinded with 200, 600, 1000, 1600 and 2000 grid emery papers respectively during three minutes for each before optical microscopic examination. All pits were determined and their depths were measured by taking images with the optical microscope at 500x magnification. Images of the maximum pit depths for all process were given in Fig.38 to Fig.45.

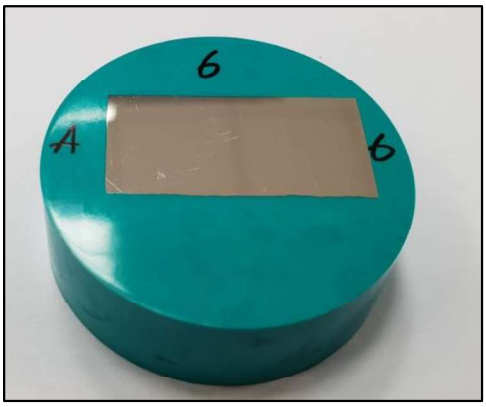

Figure 36. Prepared rectangular specimen for microscopic examination

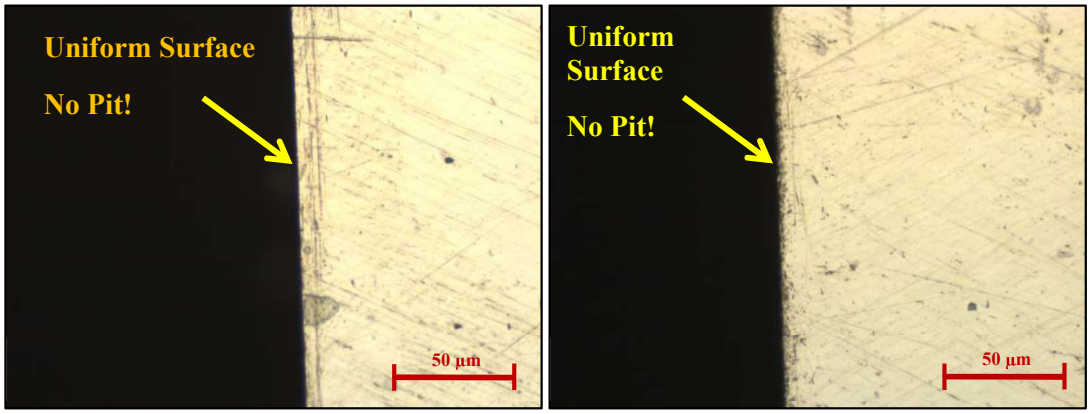

Figure 37. Surface of rectangular specimen surface before CAA

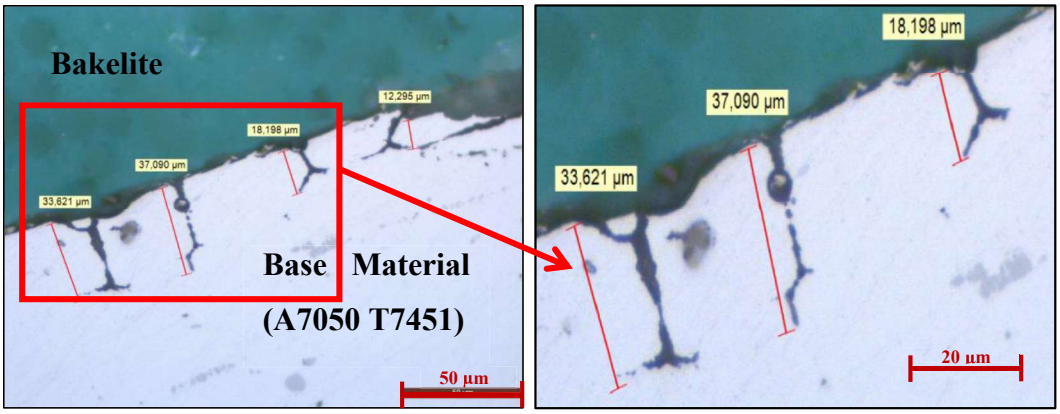

Figure 38. Maximum pit depth for Process 1

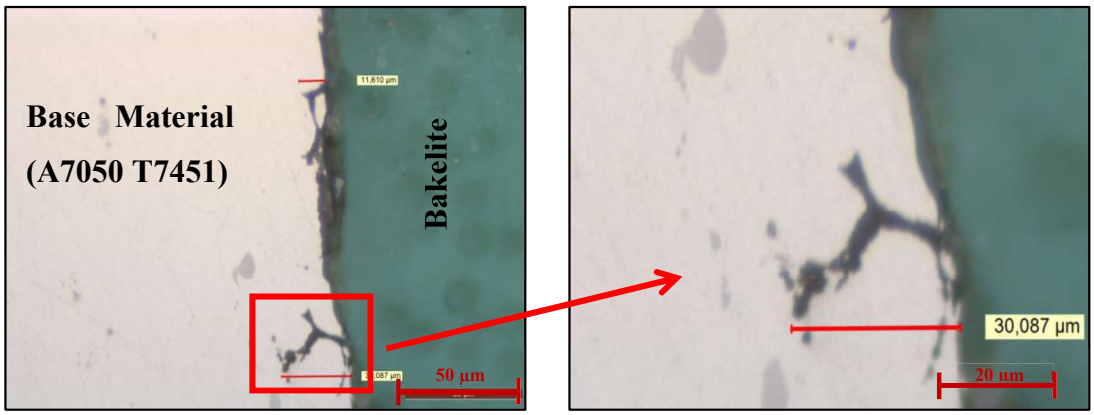

Figure 39. Maximum pit depth for Process 2

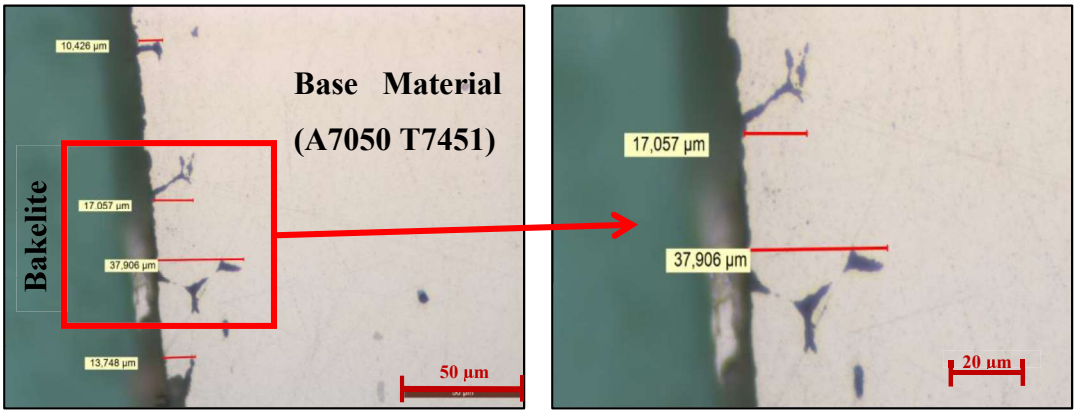

Figure 40. Maximum pit depth for Process 3

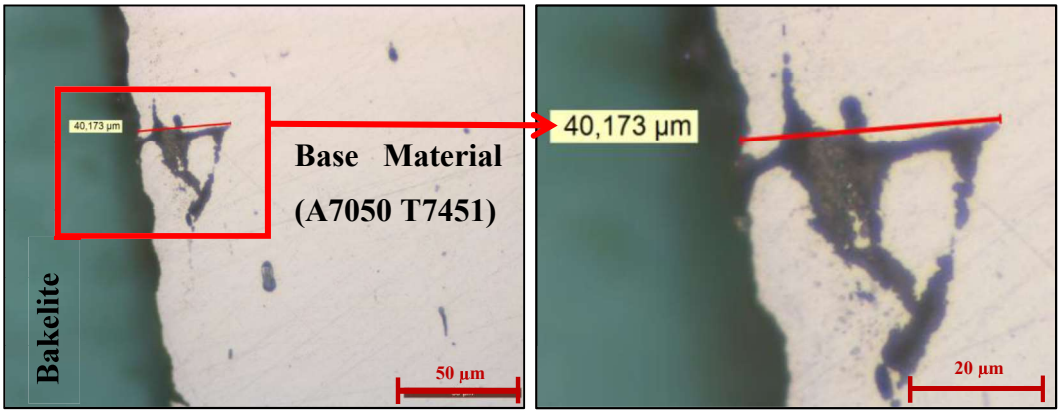

Figure 41. Maximum pit depth for Process 4

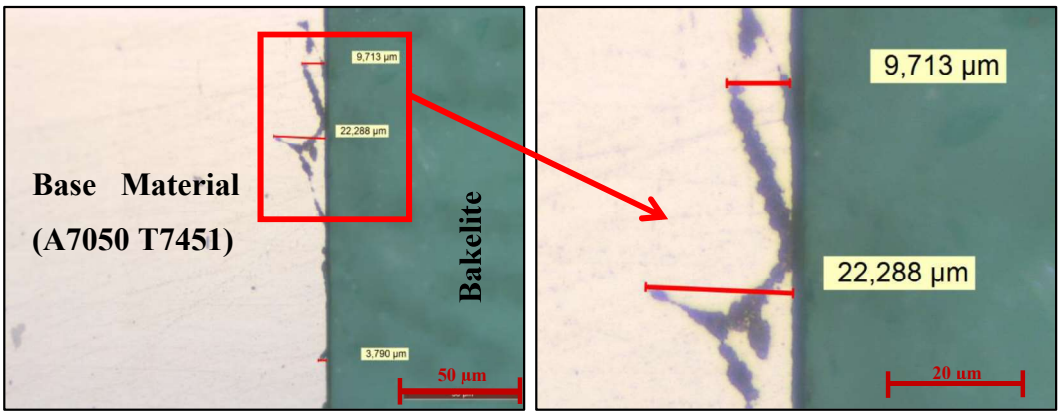

Figure 42. Maximum pit depth for Process 5

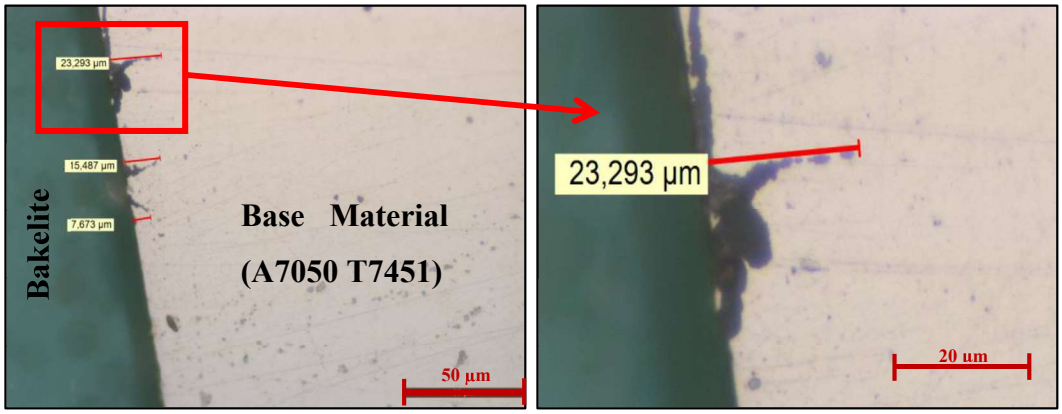

Figure 43. Maximum pit depth for Process 6

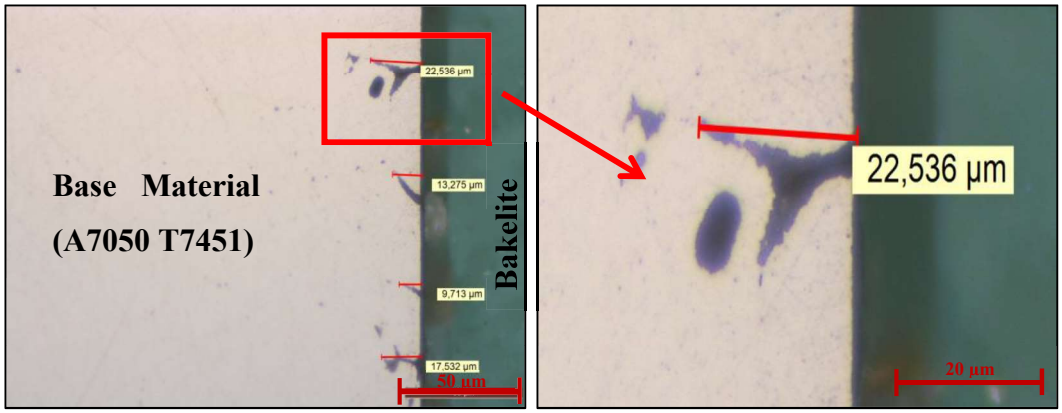

Figure 44. Maximum pit depth for Process 7

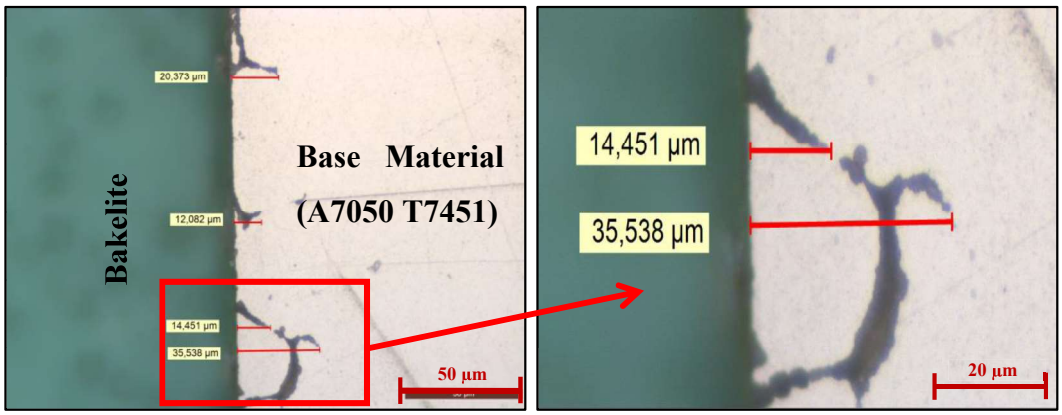

Figure 45. Maximum pit depth for Process 8

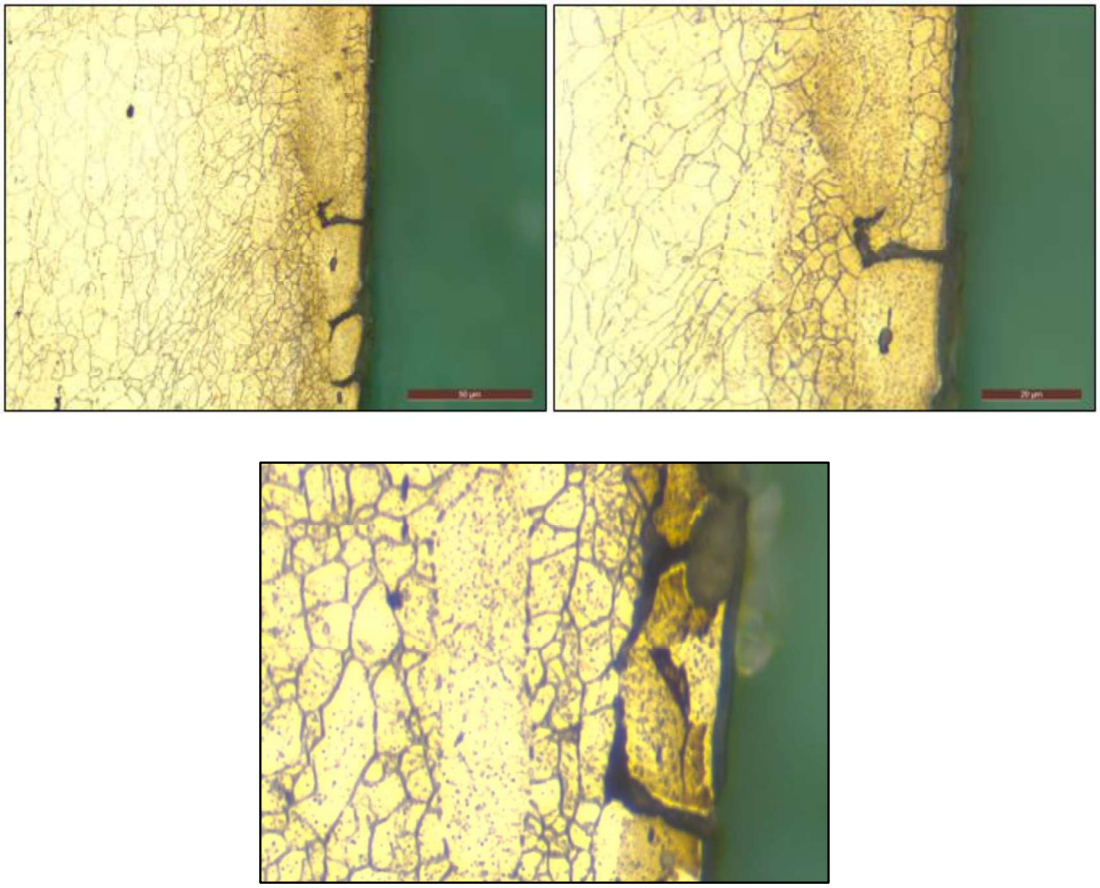

Figure 46. Pits following grain boundaries

Depth of all pits were measured from each specimen which were exposed to 8 CAA processes separately. Distribution of pit depths that was obtained from 8 specimens were given from Fig.47 to Fig54. Fatigue tests were applied at longitudinal direction. Hence, pit depths were measured transverse direction since the most favorable direction for crack enhancement is the perpendicular to loading direction. Anodic coating layer of the rectangular specimens were measured by the help of eddy current method per ASTM B244 [27]. Although thickness of the layer was restricted between 4 to 7 μm by ASM Anodizing chapter for chromic acid anodizing, insufficient anodic layer thickness was obtained by processes 1,5,6,7and 8[12]. Therefore, these were eliminated for fatigue test specimens due to an inadequate coating. Maximum pit depths and average pit depths were considered in order to select among processes 2,3 and 4. Because pit depths are directly proportional to fatigue life reduction by

decreasing crack initiation[1]. Process 4 was come to the forefront in terms of maximum and average pith depths with proper anodic layer thickness, as 18.49 µm average pit depth,40.17 µm maximum pit depth and 5.5 µm CAA layer thickness were obtained. Average and maximum depths of pits were stated in Table 16 in order to select CAA process for fatigue tests. In addition, pits were followed grain boundaries on 7050 T7451. Therefore, pit depths could be characterized by controlling manufacturing process such as forging or heat treatment of 7050 T7451. Pits following grain boundaries were shown in Fig.46.

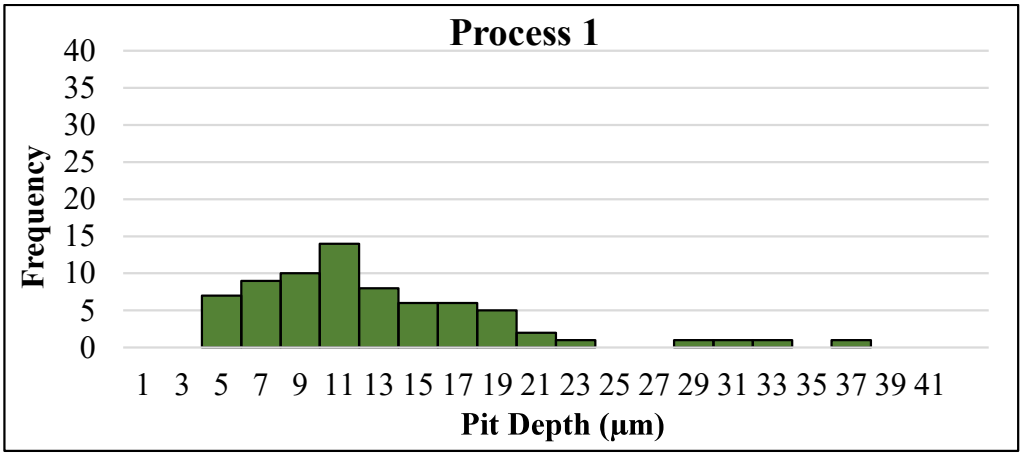

Figure 47. Distribution of pit depths for Process 1

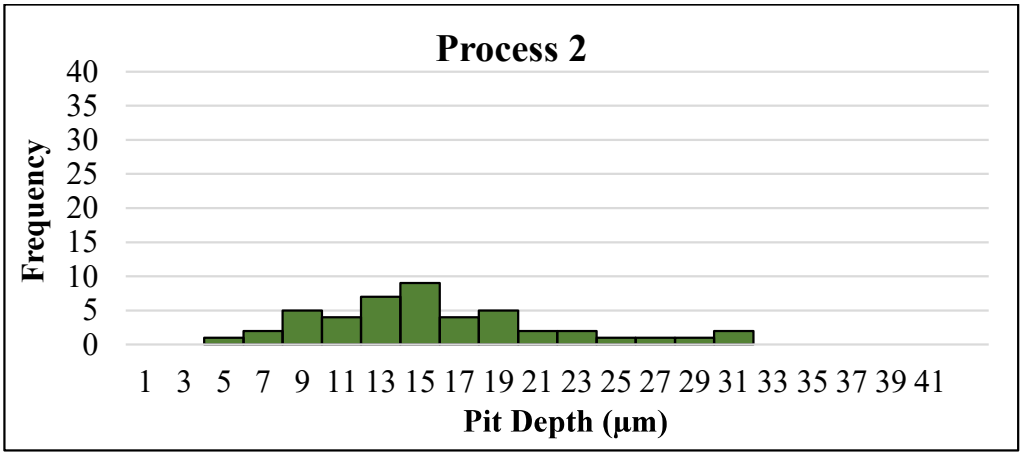

Figure 48. Distribution of pit depths for Process 2

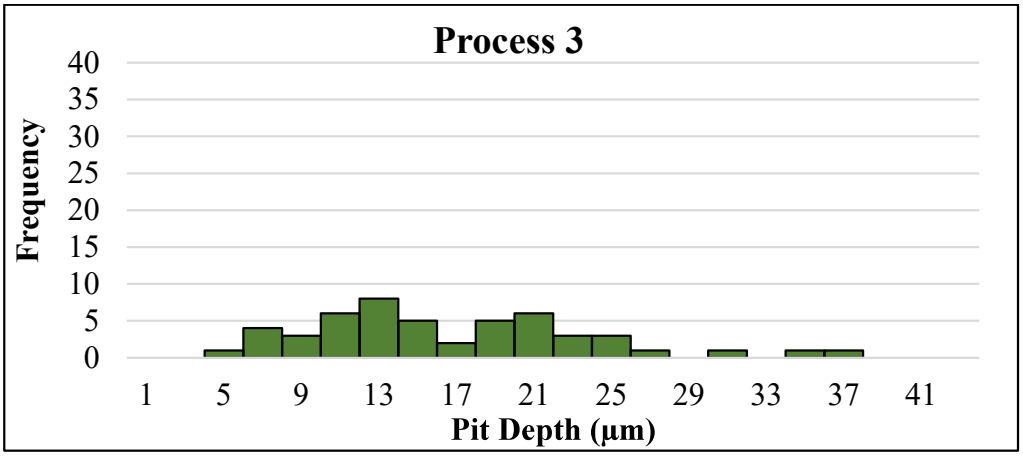

Figure 49. Distribution of pit depths for Process 3

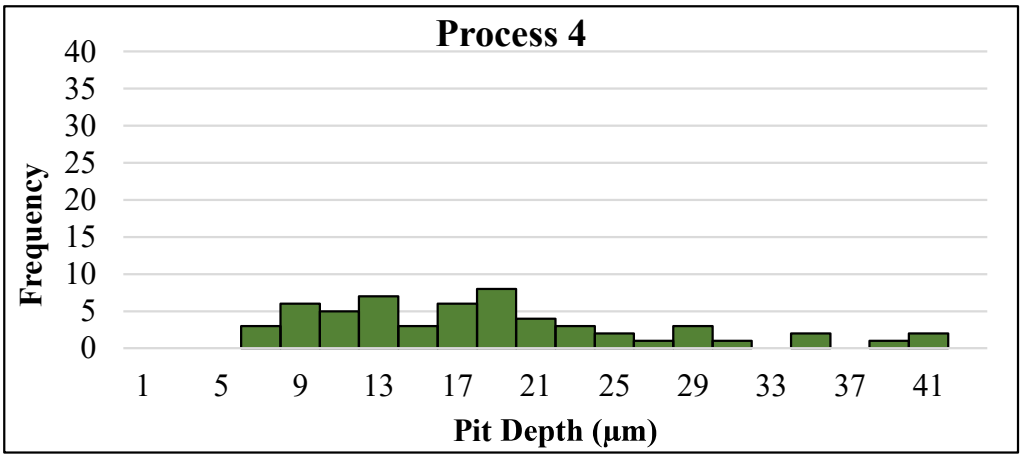

Figure 50. Distribution of pit depths for Process 4

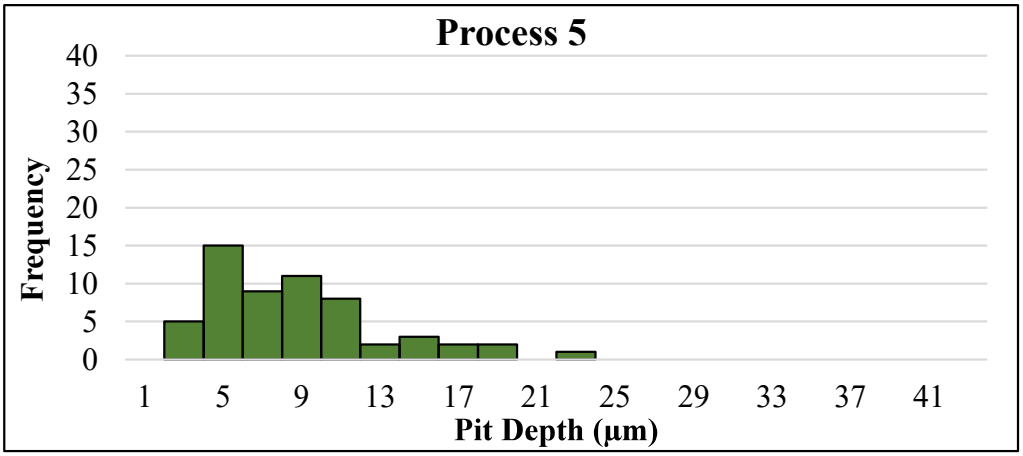

Figure 51. Distribution of pit depths for Process 5

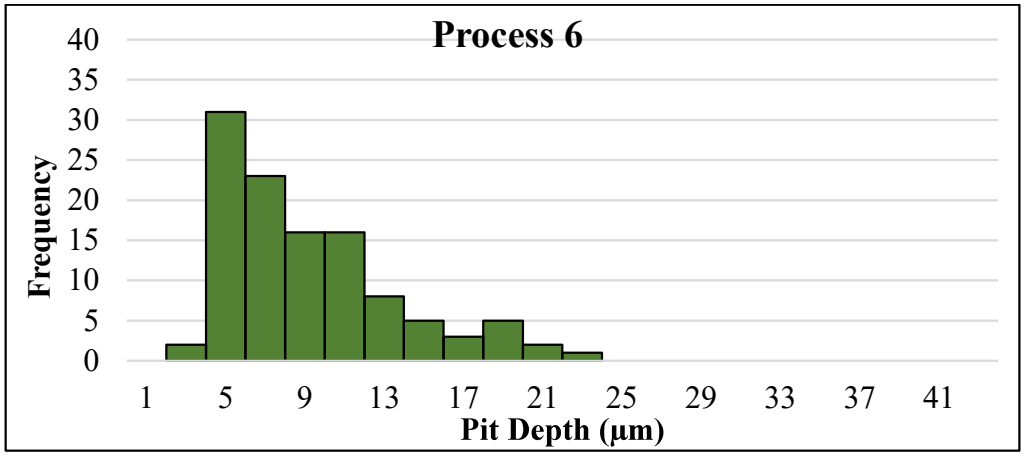

Figure 52. Distribution of pit depths for Process 6

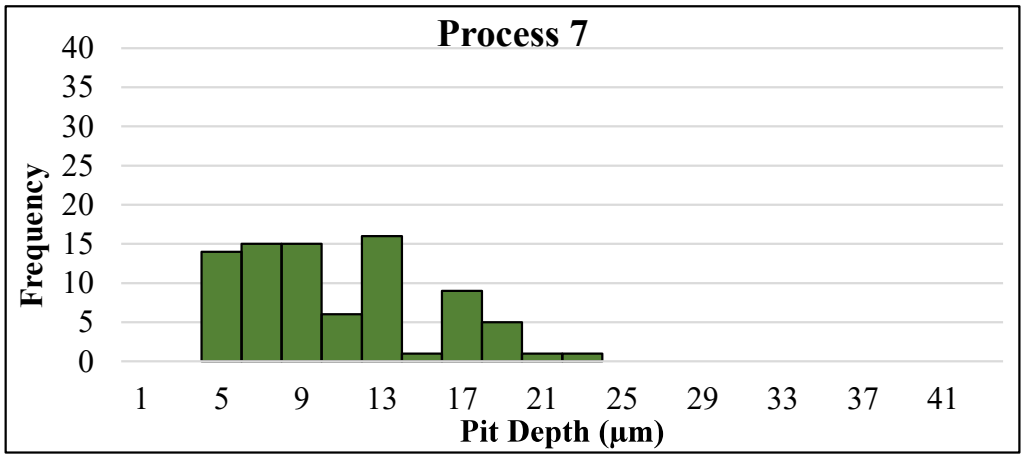

Figure 53. Distribution of pit depths for Process 7

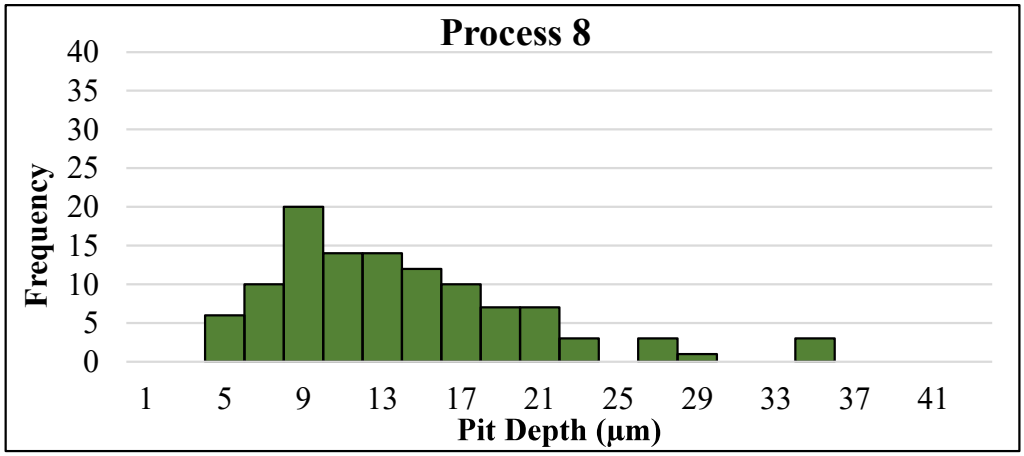

Figure 54. Distribution of pit depths for Process 8

Table 16. *Average and maximum pith depths for CAA process selection*

Process #	Average Pit Depth (μm)	Max. Pit Depth(μm)	CAA Layer Thickness (μm)
Process 1	12.77	37.09	3.00
Process 2	15.98	30.09	5.50
Process 3	16.65	37.91	5.00
Process 4	18.49	40.17	5.50
Process 5	8.76	22.28	0.50
Process 6	9.25	23.29	2.00
Process 7	10.82	22.536	2.00
Process 8	13.93	35.54	2.00

Process 4 was consisted of degrease, alkaline etching, acid etching, anodizing stages and rinsing before each stage. Firstly, degreasing was applied during 5 minutes at 85 ºC. Then, etching with 15% NaOH based solution was executed during 7 minutes at 25 ºC. It was continued with acid etch of 35% H_2SO_4 which was done during 5 minutes at ambient temperature. The major stage of anodizing was applied during 50 minutes at 35 ºC by using 21 V. Rinsing was done before each stage during 2 to 5 minutes at ambient temperature. Process 4 was chosen as the most suitable chromic acid anodizing process for fatigue tests which was tabulated below. CAA was exposed to fatigue test specimens by using this process which was shown in Table 17.

Table 17. *Chromic acid anodizing process for fatigue test group CAA*

TANK NAME	IMMERSION TIME (min)		TEMPERATURE (ºC)		VOLTAGE (V)	
	RANGE	RESULT	RANGE	RESULT	RANGE	RESULT
Degrease	1-15 min.	5	83-86 C	85	-	-
Rinse	2-5 min.	3	AMBIENT	AMB	-	-
Caustic etch (NaOH)	7-8 min.	7	23.8-29.4	25	-	-
Rinse	2-5 min.	4	AMBIENT	AMB	-	-
Acid etch (H_2SO_4)	5-15 min.	5	AMBIENT	AMB	-	-
Rinse	2-5 min.	3	AMBIENT	AMB	-	-
Anodize	30-60 min	50	32.8-37.2	35	20-24	21
Rinse	0.5-15min	4	35 C Max	AMB	-	-

On the other hand, only some part of chromic acid anodizing process was applied to fatigue test group PRET in order to evaluate pretreatment stages effect on fatigue life. In pretreatment, degreasing had no effect on fatigue life of 7050 T7451 [23]. However, fatigue life reduction was expected due to pickling, which was etching with acid and alkaline. So part of chromic acid anodizing process was applied to fatigue test group PRET until pretreatment was completed.

Table 18. Surface treatment process for fatigue test group PRET

TANK NAME	IMMERSION TIME (min)		TEMPERATURE (°C)		VOLTAGE (V)	
	RANGE	RESULT	RANGE	RESULT	RANGE	RESULT
Degrease	1-15 min.	5	83-86 C	85	-	-
Rinse	2-5 min.	3	AMBIENT	AMB	-	-
Caustic etch (NaOH)	7-8 min.	7	23.8-29.4	25	-	-
Rinse	2-5 min.	4	AMBIENT	AMB	-	-
Acid etch (H_2SO_4)	5-15 min.	5	AMBIENT	AMB	-	-
Rinse	2-5 min.	3	AMBIENT	AMB	-	-

Final surface treated fatigue test group was CAAT. Chromic acid process for group CAAT was the same with group CAA except immersion time at anodizing bath. Pretreatments for these two groups were completely identical. However, immersion time of anodizing for fatigue test group CAAT was twice of fatigue test group CAA. In order to evaluate the effect of anodizing time on fatigue life. Immersion time for two groups were 50 minutes and 100 minutes respectively.

Table 19. *Chromic acid anodizing process for fatigue test group CAAT*

TANK NAME	IMMERSION TIME (min)		TEMPERATURE (°C)		VOLTAGE (V)	
	RANGE	RESULT	RANGE	RESULT	RANGE	RESULT
Degrease	1-15 min.	5	83-86 C	85	-	-
Rinse	2-5 min.	3	AMBIENT	AMB	-	-
Caustic etch (NaOH)	7-8 min.	7	23.8-29.4	25	-	-
Rinse	2-5 min.	4	AMBIENT	AMB	-	-
Acid etch (H_2SO_4)	5-15 min.	5	AMBIENT	AMB	-	-
Rinse	2-5 min.	3	AMBIENT	AMB	-	-
Anodize	30-60 min	**100**	32.8-37.2	35	20-24	21
Rinse	0.5-15min	4	35 C Max	AMB	-	-

Different surface treatments for fatigue test groups PRET, CAA and CAAT were noticeable by visual inspection (Figure 55). Color of the specimens became dull after pretreatments. However, it was gray after anodizing completion. If immersion time of anodizing was increased, color of the specimens turned yellow.

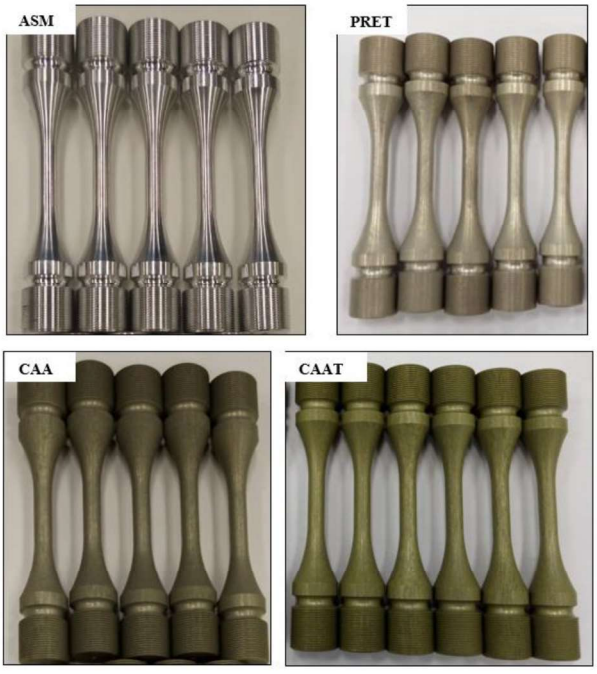

Figure 55. Picture of fatigue test groups

4.3. Fatigue Tests Results

After specimens were manufactured according to technical drawing (Fig.27) and machining parameters (Table8) with/without surface treatments, roughness of the specimens were measured from three specimens in each group before fatigue tests. Thus, roughness values were compared among as machined, pretreated and anodized surface conditions. Roughness of the as machined specimens which was 0.23 μm that was directly result of the machining, but all other groups of specimens had 0.1 μm rougher surface than because of surface treatments. Average roughness values of group PRET, CAA and CAAT were very close and their standard deviation comprised each other`s roughness. Therefore, surface treated groups were considered equal in terms of roughness effect on fatigue. Roughness measurements were tabulated in Table 20.

Table 20. *Roughness measurements*

Measurement #		1	2	3	Average
Group	ASM	0.24	0.22	0.23	0.23±0.01
	PRET	0.33	0.30	0.33	0.32±0.01
	CAA	0.32	0.30	0.36	0.33±0.02
	CAAT	0.40	0.34	0.31	0.35±0.04

When fatigue tests were conducted at stress levels that were stated at Table 10, results of as machined specimens were considered as reference to compare surface treatment of other groups. Results of pretreated specimens were in order to examine effect of degreasing and etching stages without any organic or inorganic residuals at the surface before anodizing. Although results of anodized specimens revealed the whole CAA effect, results of group CAAT were to find out impact of only anodizing immersion time. Specimens of group CAAT were hold at anodizing tank during 100 minutes rather than 50 minutes which is standard immersion time, however, whole pretreatment stages were identical for group CAA and group CAAT.

Results of group ASM, PRET, CAA, CAAT were given in Table 21 to 24. Curve fitting was applied to all groups by including UTS as the first cycle. S/N curve of all groups were shown in Fig.56 to 59.

Table 21. *Fatigue test results of Group ASM*

Specimen	Stress (MPa)	Cycles(N)	Frequency (Hz)	Standard Deviation at 10^6 cycles
ASM-1	220	474,542	91	4.43
ASM-2	240	310,137		
ASM-3	260	133,413		
ASM-4	280	62,432		
ASM-5	210	744,717		
ASM-6	300	41,484		**Coefficient of Variance**
ASM-7	200	1,000,000		2.41%
ASM-8	300	33,342		
ASM-9	210	1,000,000		
UTS	541	1		

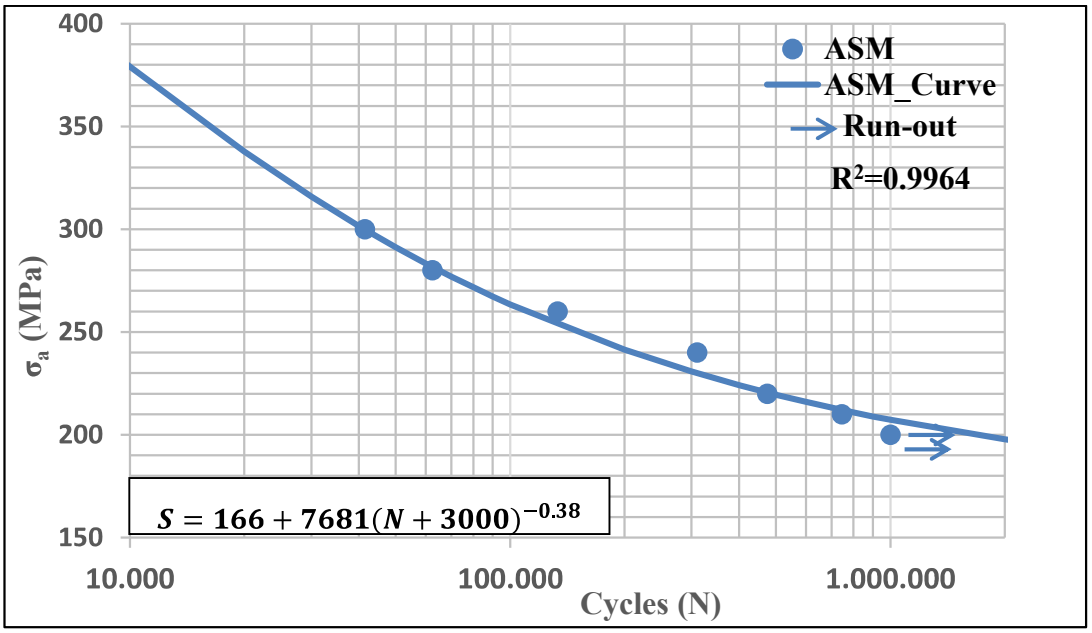

Figure 56. S-N Curve of Group ASM

Table 22. *Fatigue test results of Group PRET*

Specimen	Stress (MPa)	Cycles(N)	Frequency (Hz)	Standard Deviation at 10^6 cycles
PRET-1	180	186,273	91	6.70
PRET-2	200	105,273		
PRET-3	165	195,805		
PRET-4	170	309,549		
PRET-5	150	330,704		
PRET-6	150	302,495		**Coefficient of Variance**
PRET-7	140	850,093		5.54%
PRET-8	230	65,777		
UTS	527	1		

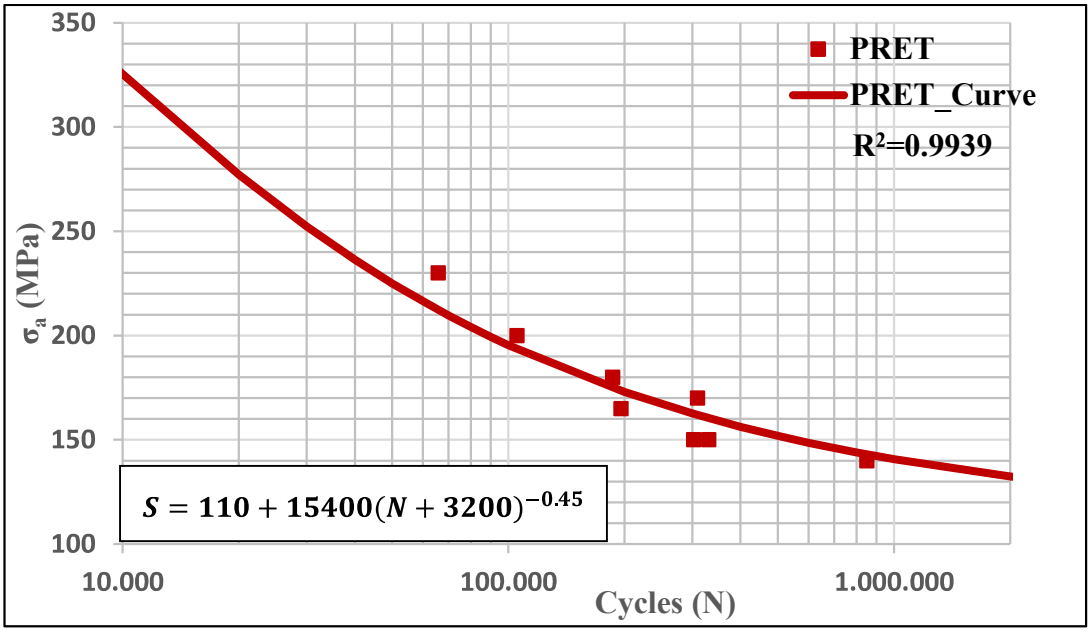

Figure 57. S-N Curve of Group PRET

Table 23. *Fatigue test results of Group CAA*

Specimen	Stress (MPa)	Cycles(N)	Frequency (Hz)	Standard Deviation at 10^6 cycles
CAA-1	180	114,331	91	4.39
CAA-2	165	142,464		
CAA-3	220	47,703		
CAA-4	220	35,875		
CAA-5	210	64,915		
CAA-6	160	237,206		**Coefficient of Variance**
CAA-7	150	328,279		3.39%
CAA-8	145	1,000,000		
CAA-9	145	1,000,000		
UTS	527	1		

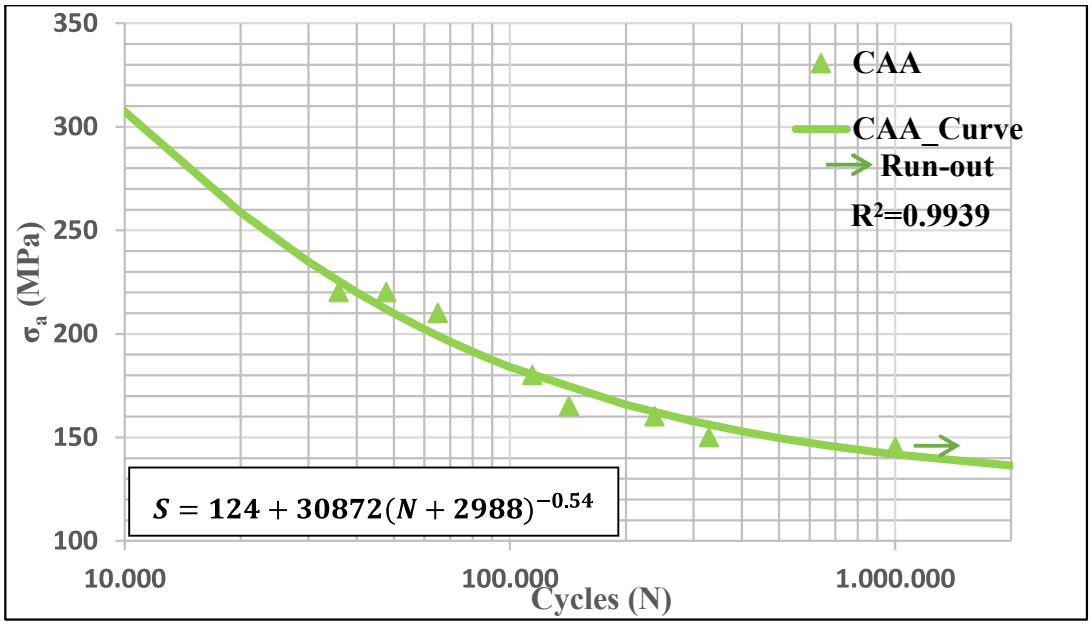

Figure 58. S-N Curve of Group CAA

Table 24. *Fatigue test results of Group CAAT*

Specimen	Stress (MPa)	Cycles(N)	Frequency (Hz)	Standard Deviation at 10^6 cycles
CAAT-1	180	132,088	91	7.23
CAAT-2	165	159,093		
CAAT-3	210	73,726		
CAAT-4	230	48,510		
CAAT-5	150	1,000,000		
CAAT-6	150	180,442		**Coefficient of Variance**
CAAT-7	145	1,000,000		5.81%
CAAT-8	230	45,623		
UTS	527	1		

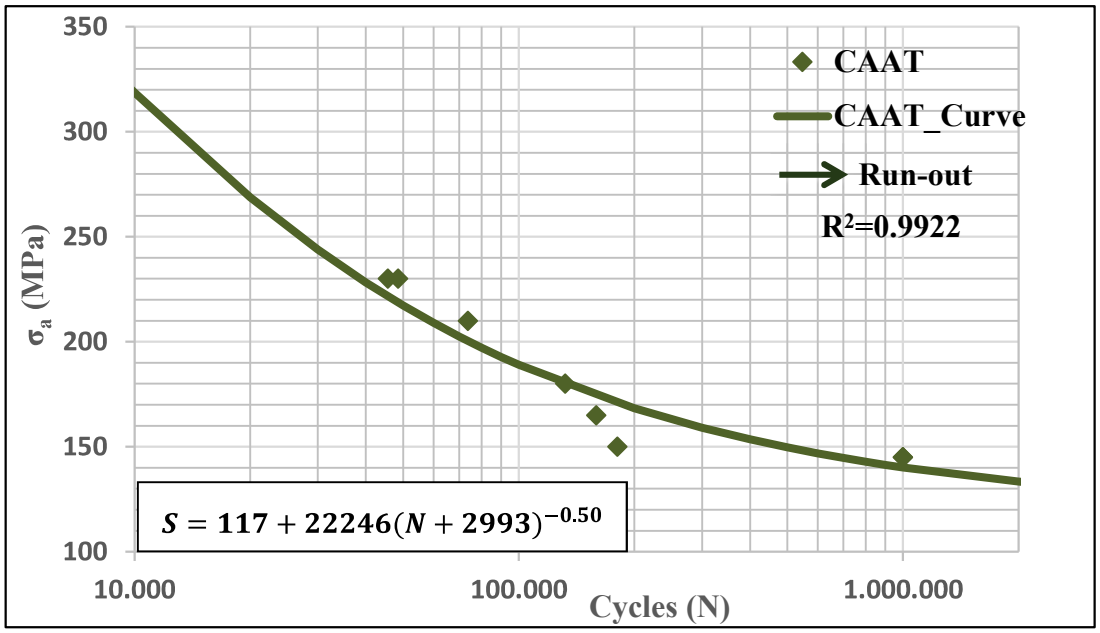

Figure 59. S-N Curve of Group CAAT

All fatigue tests were executed as constant amplitude axial loading at 91 Hz frequency with resonance fatigue machine. ASTM E466 states that frequency does not affect cycles for constant amplitude axial fatigue tests until 10^2 Hz. Therefore, deviation due to frequency was not exist for fatigue test results.

Coefficient of determination (R^2) value for all fatigue test groups were calculated. R^2 values were higher than 0.99 for all data after curve fitting. Therefore, reliability of the fitting was solid. Besides, a coefficient of variation was determined for all groups. This coefficient was lower than 6% for all groups. Coefficient of variation values were stated on S/N curves for each fatigue test groups.

All fatigue test data were shown Fig.60. It was clearly recognized that fatigue stress of surface treated specimens were dramatically lower than as machined specimens. However, it was not noticeable difference between fatigue stress of surface treated specimens i.e. pretreated, chromic acid anodized. This was the proof that same crack initiation mechanism was valid for group PRET, CAA and CAAT. The most important outcome from Fig.60 was that pretreatments before anodizing affect fatigue life dramatically while anodizing had no extra effect on fatigue life. Furthermore, comparison between fatigue data of group CAA and CAAT shows that immersion time of anodizing was ineffective on fatigue life even if it was increased twice.

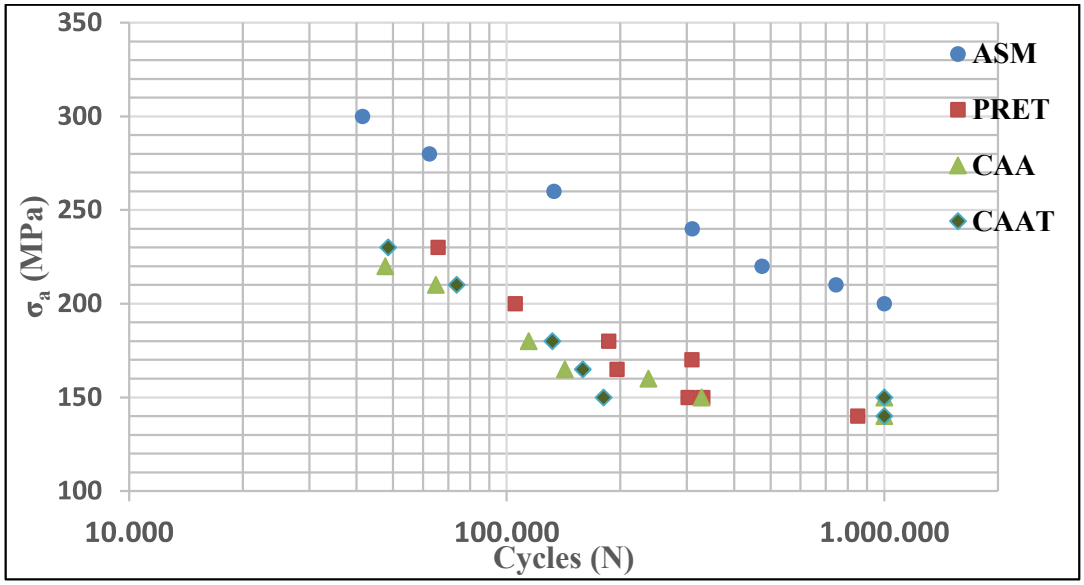

Figure 60. Fatigue test data for all test groups

After curve fitting, small reduction of the fatigue curves was observed at low cycles region which is lower than 10.000 cycles. Furthermore, there were no meaningful reductions of the curves that was 1.4% reduction at the first cycle when cycles were lower than 1000 cycles because crack initiation was not dominant at low cycles region. Crack propagation dominated fatigue failure at low cycles region.

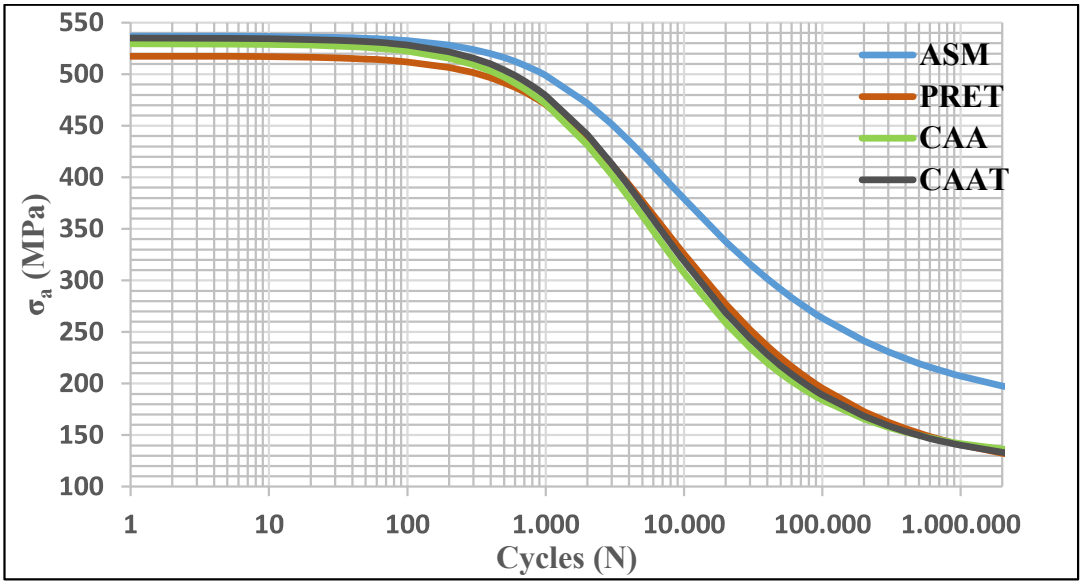

Figure 61. S-N curves for all test groups after curve fitting (N=1 to 10^6)

On the other hand, curves of surface treated groups were followed similar trend after curve fitting. All three curves which were belong to groups PRE, CAA and CAAT comprised their standard deviation at 1.000.000 cycles. Because variation among stresses of three groups at run-out (1.000.000 cycles) was lower than 2 MPa which was shown in Fig.63.

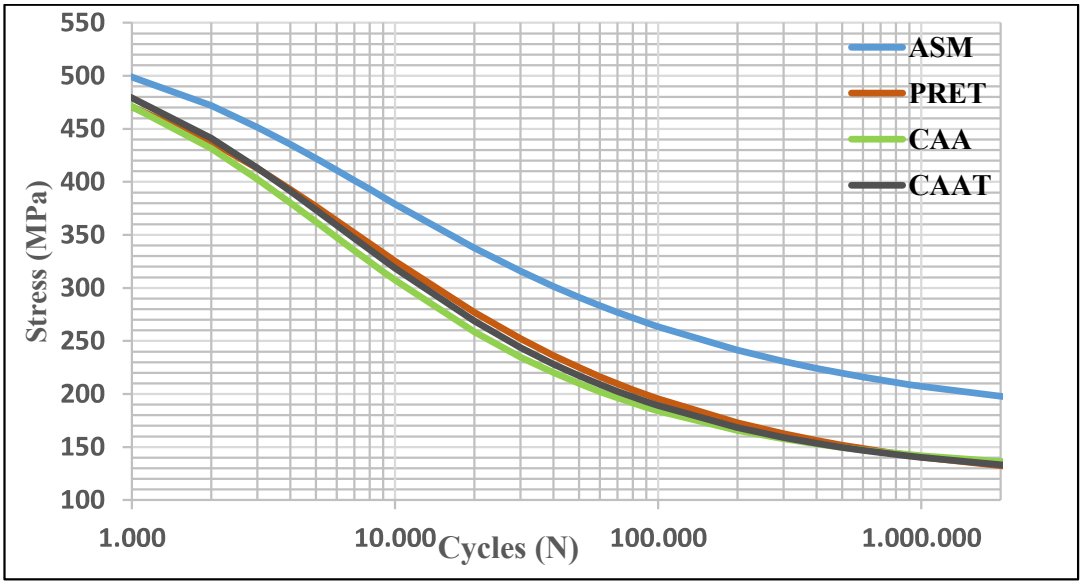

Figure 62. S-N curves for all test groups after curve fitting (N=1000 to 10^6)

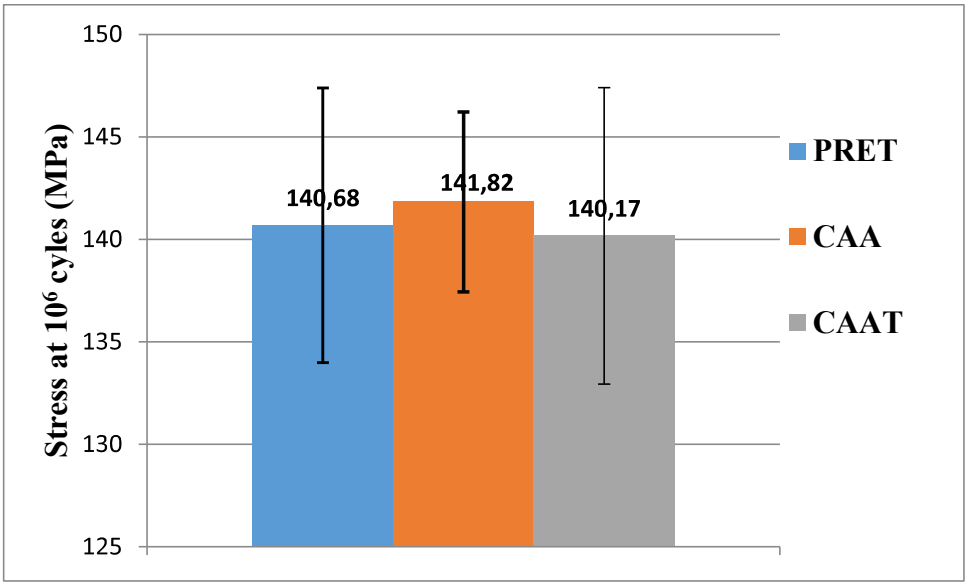

Figure 63. Stress at Run-out cycles for surface treated groups

Reduction due to chromic acid anodized 7050 T7451 was stated as 41% in literature. Furthermore, it was also indicated that fatigue limit was reduced 32% after the pickling stage[1]. However, maximum reduction was obtained 31.8% after chromic acid anodizing was exposed to 7050 T7451 in this research. Moreover, the same decrease (31.8%) was observed on fatigue limit of the material after pretreatment which is equal to pickling stage in the literature. It is due to the fact that similar fatigue test results were obtained from chromic acid anodized and pretreated specimens unlike the literature. Additionally, fatigue test results of group CAAT was the proof that fatigue life was not affected by immersion in the chromic acid anodizing tank. Therefore, consistency was supplied by observing no difference between S/N curves of pretreated and chromic acid anodized specimens. Stress based reduction due to chromic acid anodizing with respect to cycles can be seen in Fig. 64.

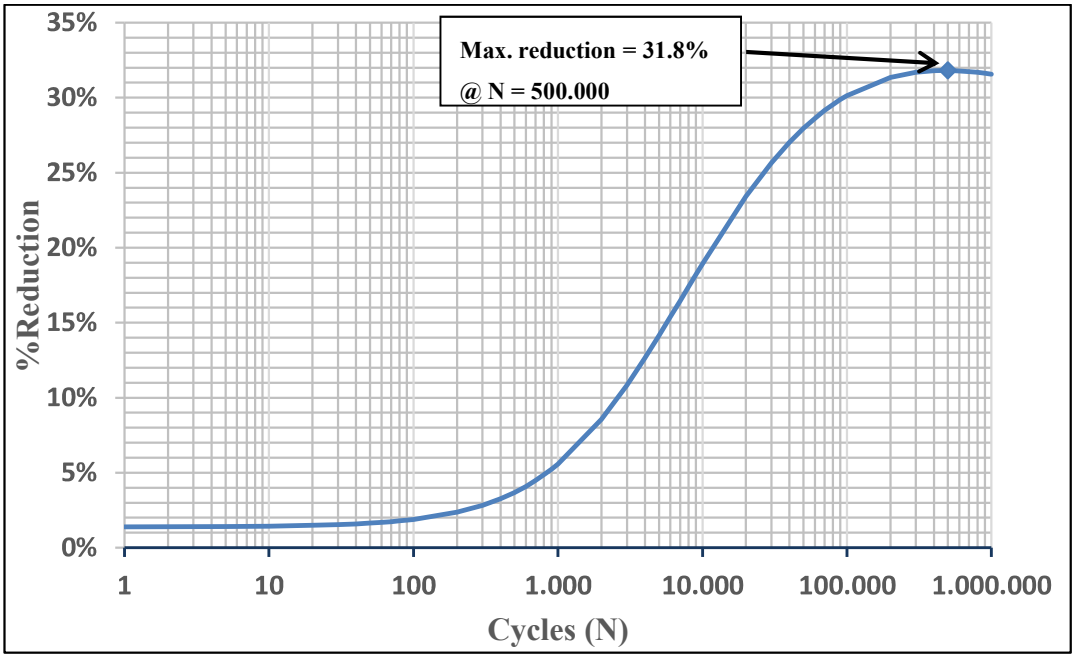

Figure 64. %Reduction vs cycles curve

4.4. Fractographic Analysis

Fracture surface of the specimens were examined following the fatigue tests by digital microscope and scanning electron microscope (SEM) in order to distinguish the effect of chromic acid anodizing (CAA) from as-machined state. Digital microscope images were shown in Fig.65 to Fig.68. SEM images of fracture surface were shown in Fig.69 to Fig72. Crack initiation region and crack direction were shown on each figure with yellow arrows. Cracks were initiated and propagated at transverse direction which is perpendicular to loading direction , as fatigue tests were applied at longitudinal direction of the specimens. Ductile fracture was occurred at fast fracture region and dimples were determined during the fast fracture at the end of fatigue tests due to high

ductility of 7050 T7451 aluminum alloy. Dimples at fast fracture region was given at Fig.73.

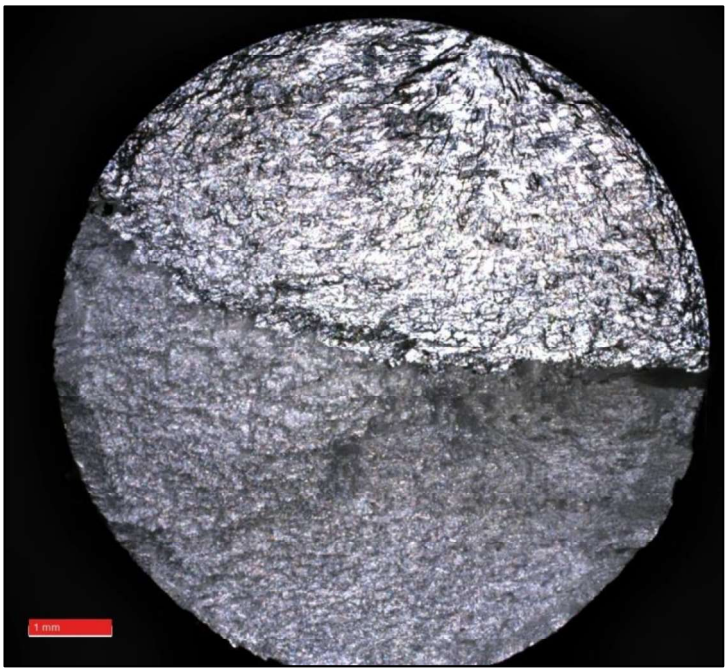

Figure 65. Digital microscope image of ASM-2 fracture surface

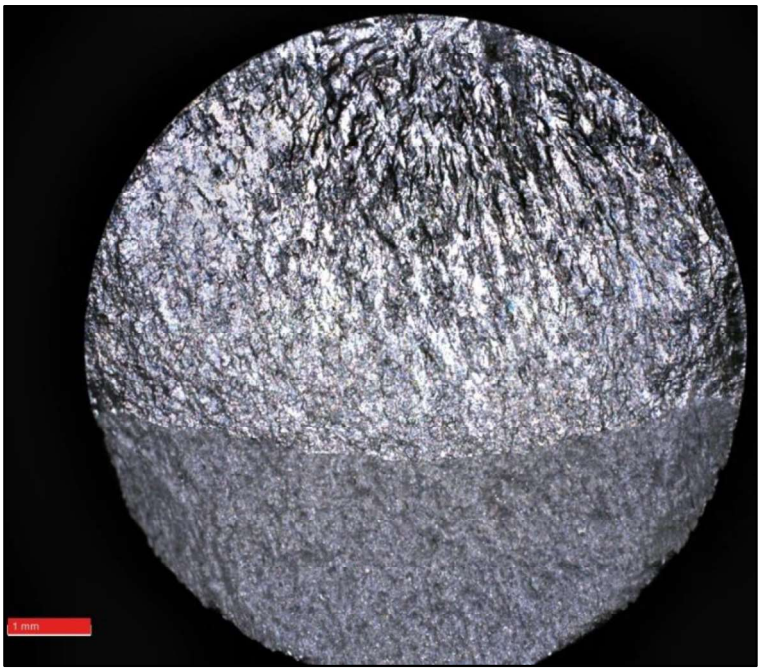

Figure 66. Digital microscope image of PRET-5 fracture surface

*Figure 67.*Digital microscope image of CAA-7 fracture surface

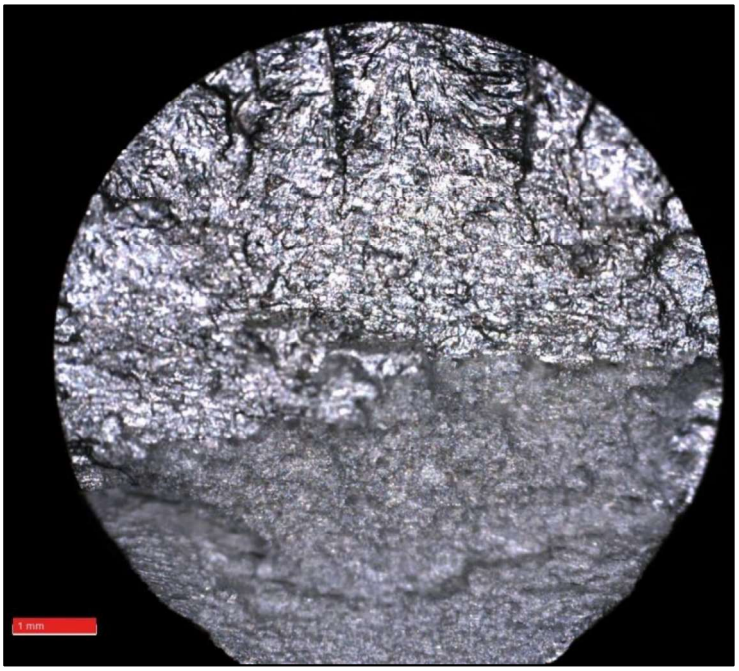

Figure 68. Digital microscope image of CAAT-3 fracture surface

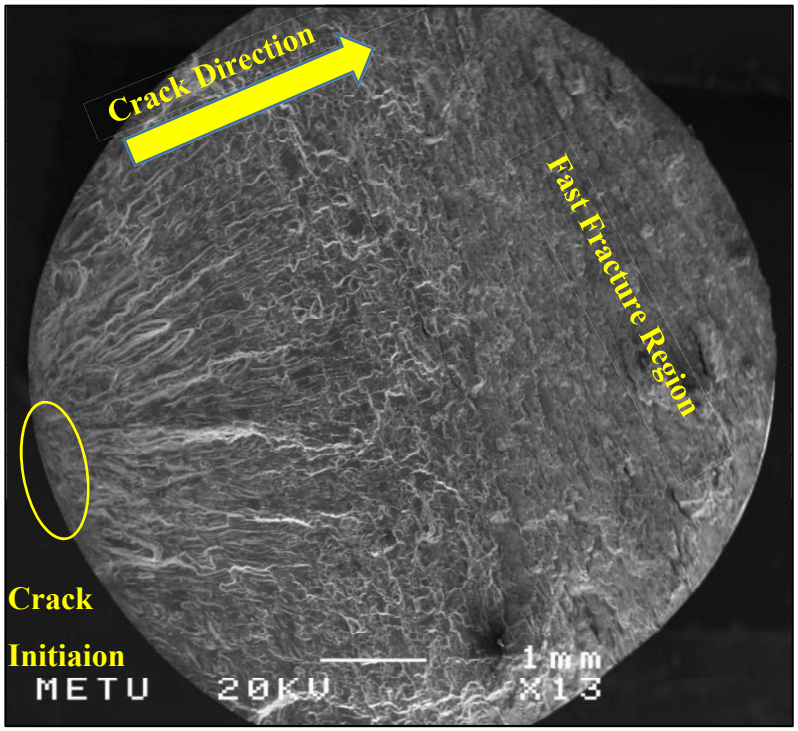

Figure 69. SEM image of CAA-6 fracture surface

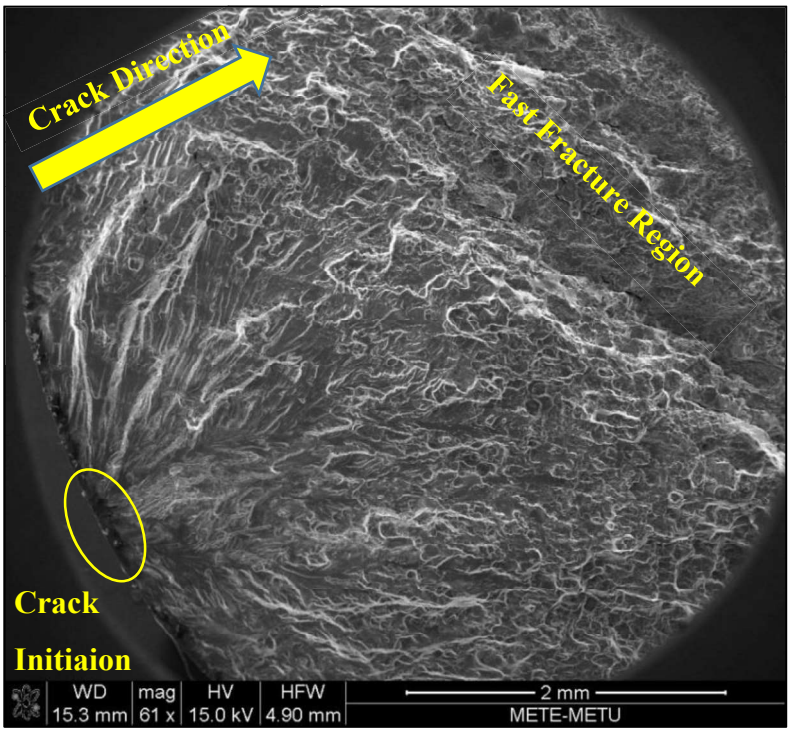

Figure 70. SEM image of ASM-6 fracture surface

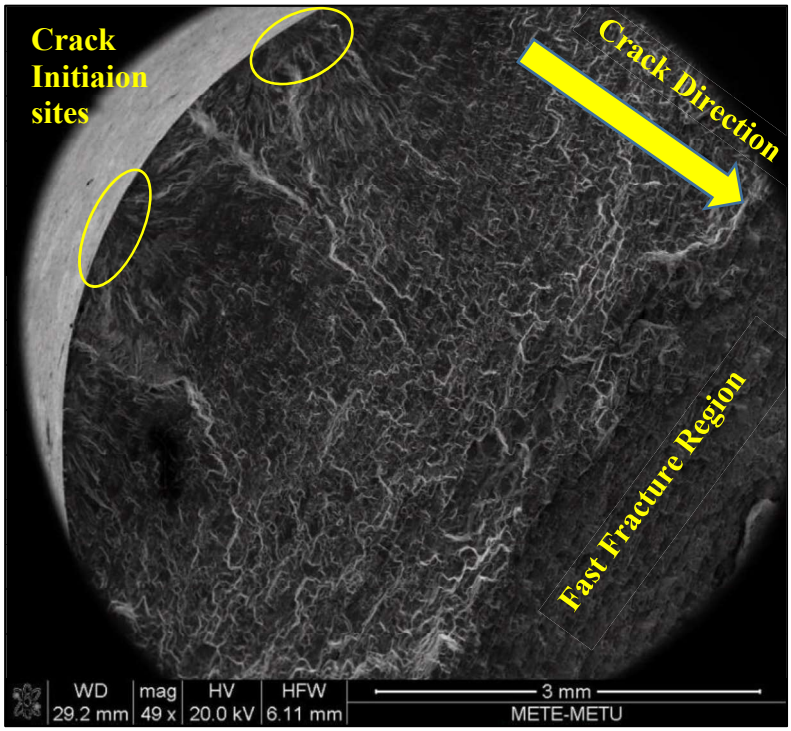

Figure 71. SEM image of CAA-3 fracture surface

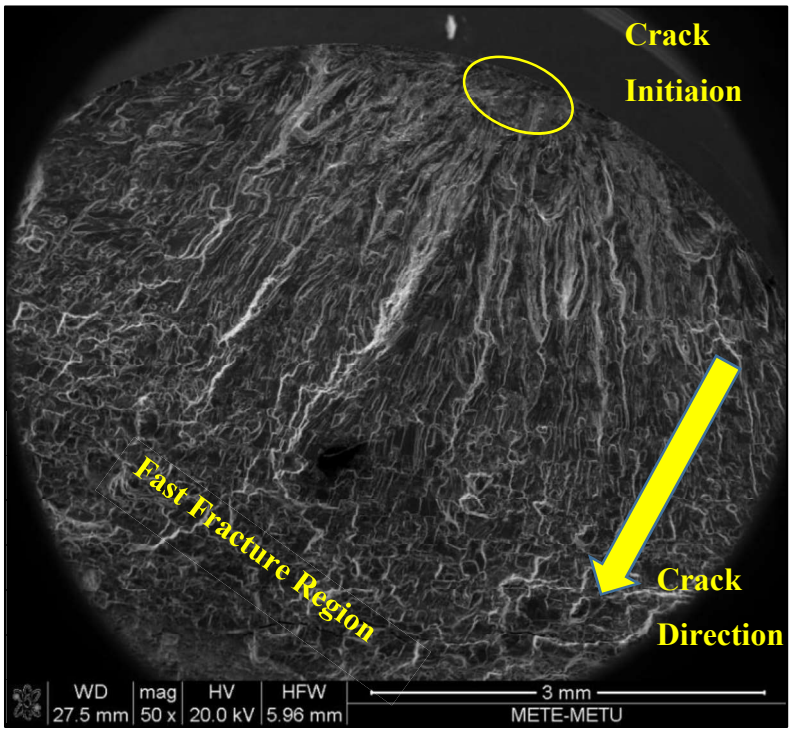

Figure 72. SEM image of CAA-1 fracture surface

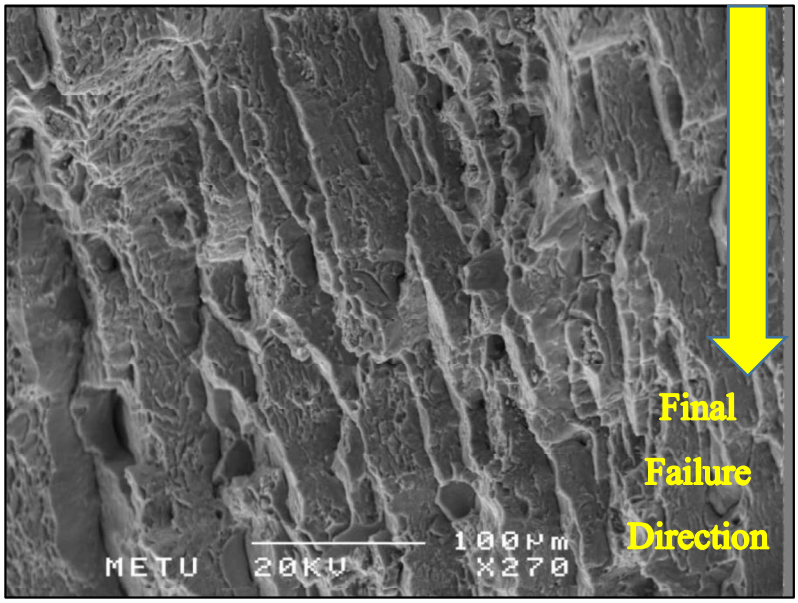

Figure 73. Dimples at final failure region

Chromic acid anodized layer was observed and its thickness was measured by SEM. The thickness of the porous alumina growth over 7050 T7451 was 4.96 µm which was shown in Fig.74. Thickness of the CAA layer was compatible with the measurement during CAA process selection and the layer size in ASM volume 5 [5].

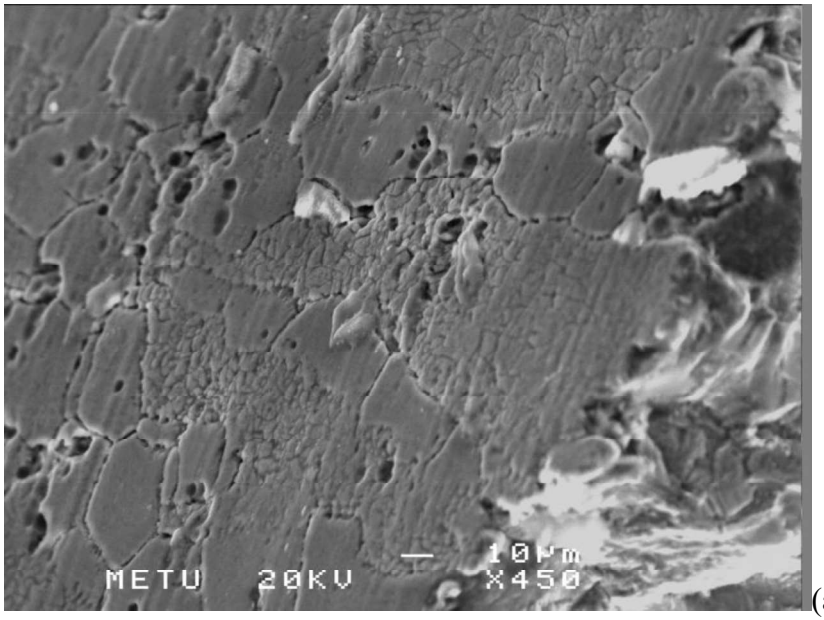

(a)

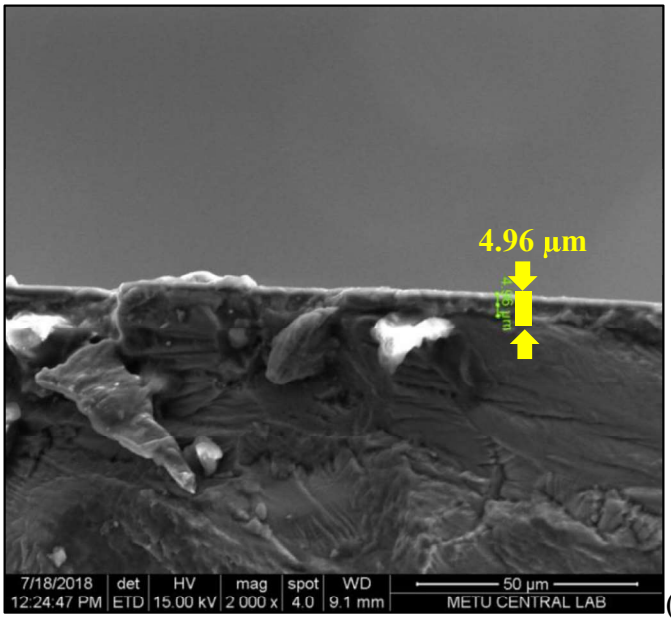

(b)

Figure 74. SEM image of Anodized layer from (a) side view and (b) fracture surface

Although, cracks were initiated at exactly surface for as-machined specimens, cracks were initiated from pits which were formed during surface treatment for all of surface treated specimens that were belongs to group PRET, CAA and CAAT. Pit depths were measured from fracture surfaces by SEM. Average pit depths were 23.46 µm, 26.67 µm and 30.75 µm for group PRET, CAA and CAAT respectively. Although differences were determined on pit depths for surface treated groups, fatigue test results showed that this difference were ineffective in terms of fatigue behavior since S/N curves of surface treated groups were overlapped each other while as-machined group had diversified curve. On the other hand, some of surface treated specimens were failed from multiple crack such as CAA-1 and CAA-3 Multiple crack formation was favorable due to existence of pits on surface under loading. SEM images of crack initiation points and pits were shown in Fig.75 to 80.

Table 25. *Pit depths from fracture surfaces*

	PRET	CAA	CAAT
Pit Depths from fracture surfaces (μm)	17.92	10.93	36.29
		48.23	
		39.06	
	29.00	13.13	25.20
		21.99	
Average (μm)	23.46 ± 5.54	26.67 ± 14.64	30.75 ± 5.55

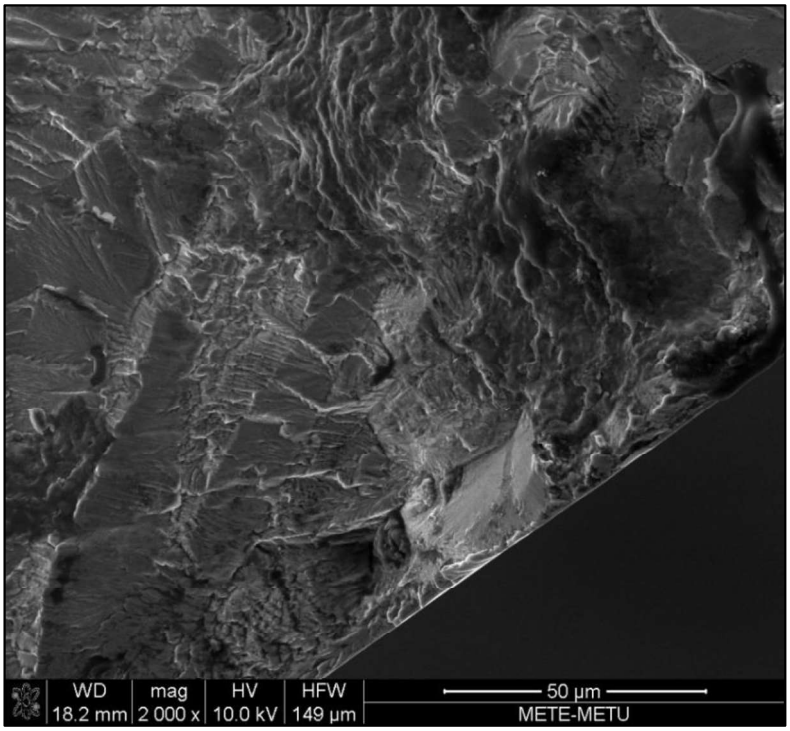

Figure 75. SEM image of ASM-5 crack initiation site

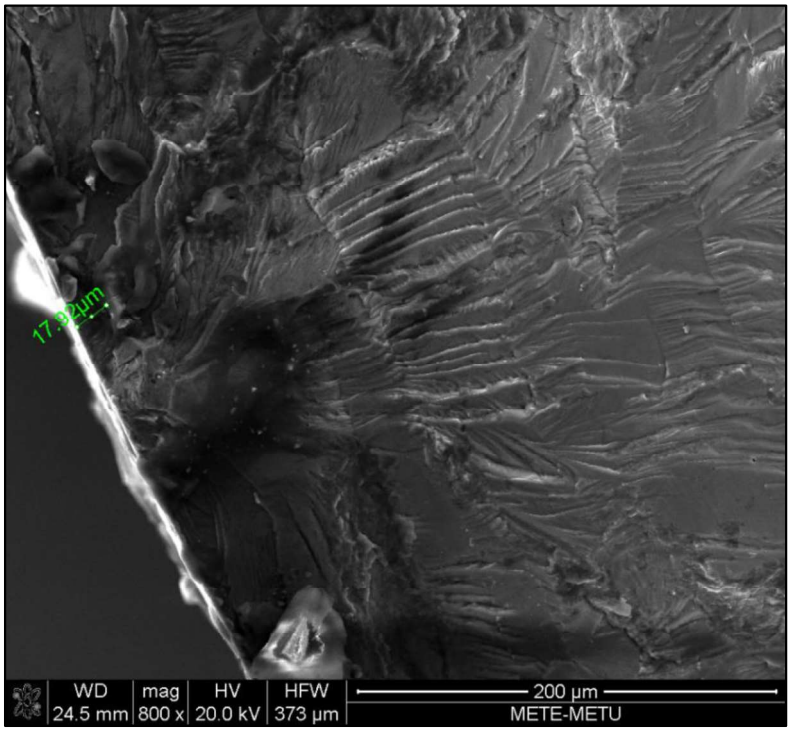

Figure 76. SEM image of PRET-1 crack initiation site

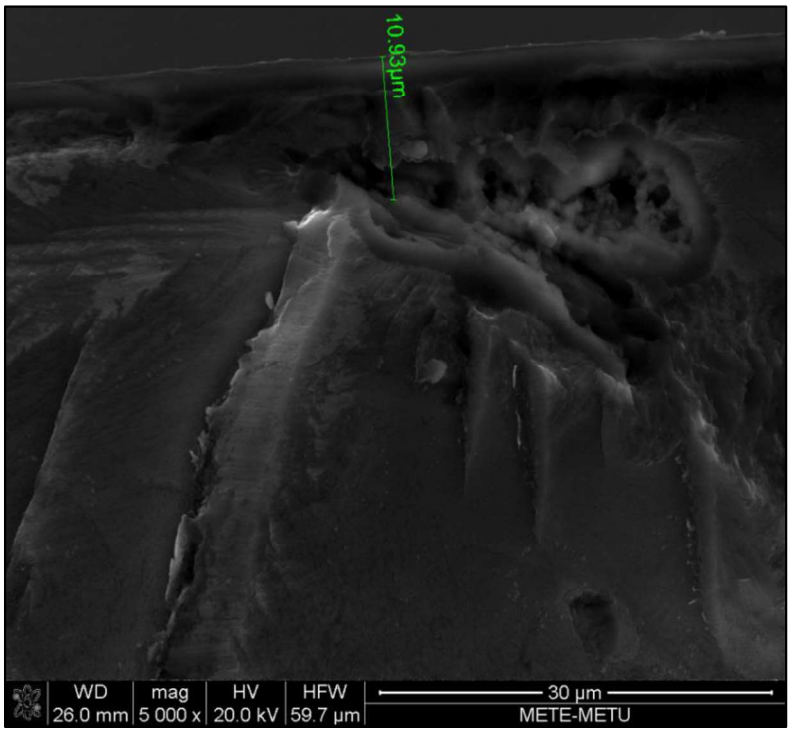

Figure 77. SEM image of CAA-1 first crack initiation site

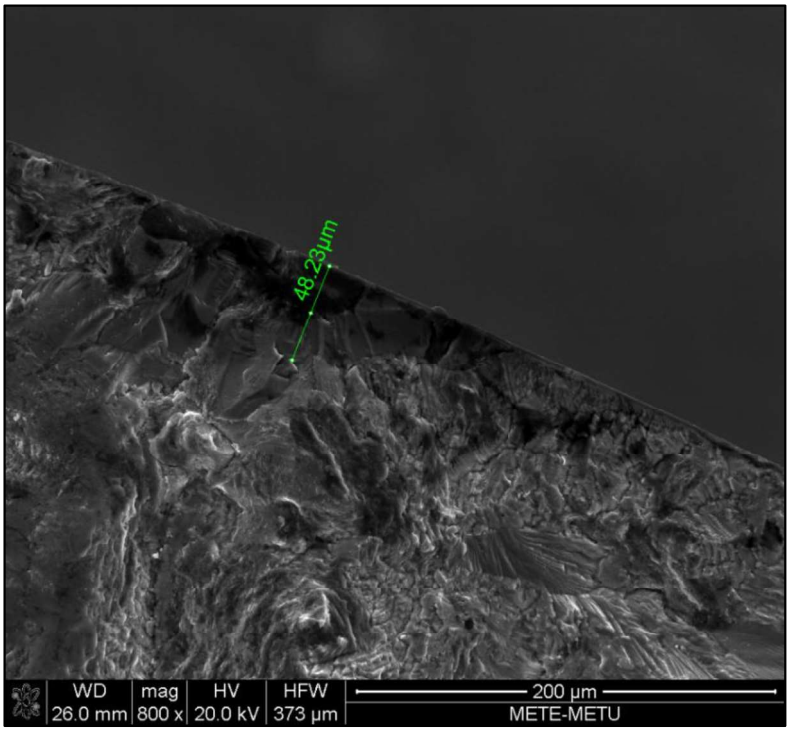

Figure 78. SEM image of CAA-1 second crack initiation site

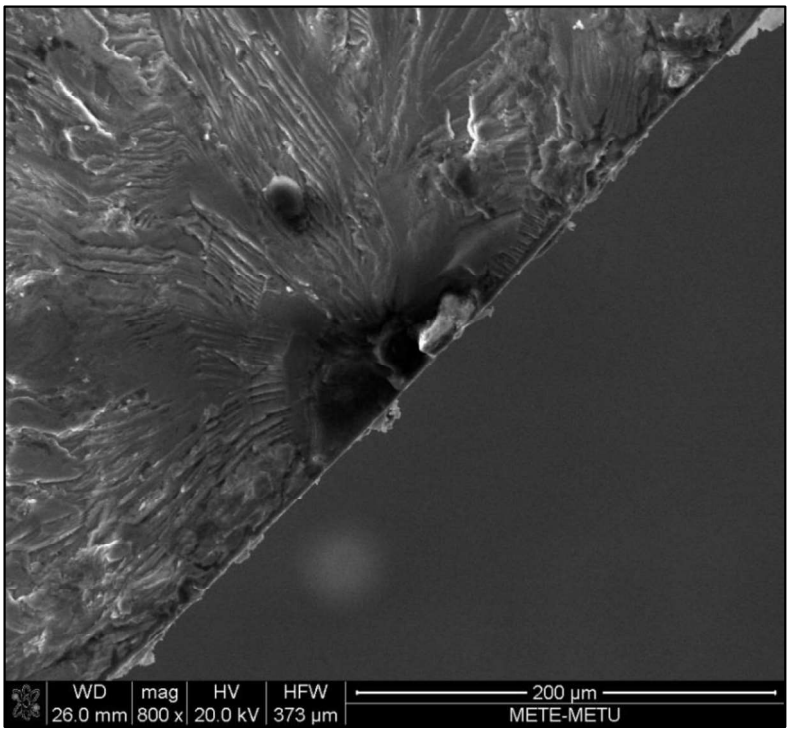

Figure 79. SEM image of CAAT-1 crack initiation site

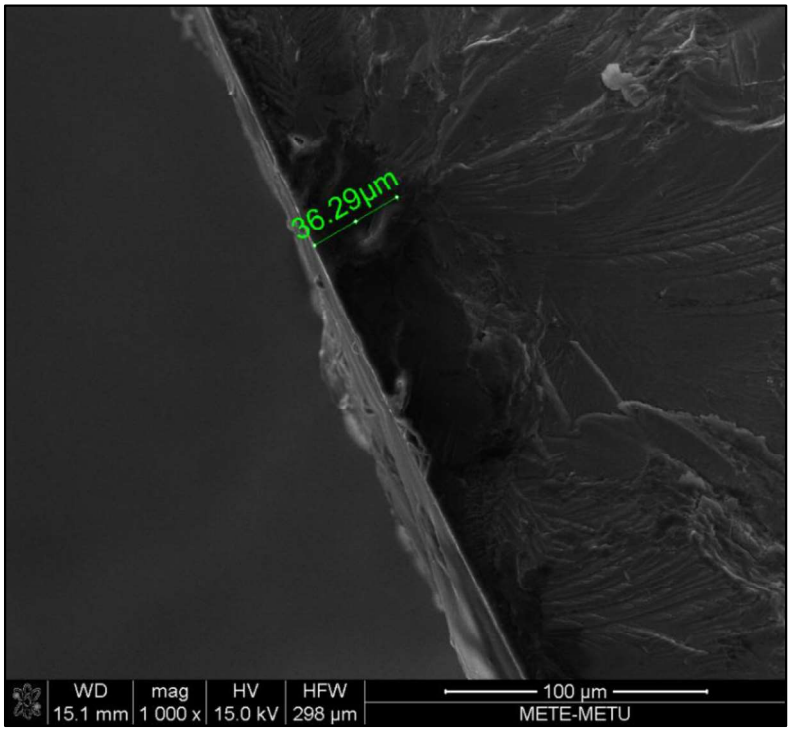

Figure 80. SEM image of CAAT-2 crack initiation site

4.4.1. Striation Counting

Finally, striation width measurement was applied to seven fatigue specimens including both of as-machined and the surface treated types in order to evaluate crack growth behavior. Distance from the crack origin was also measured to calculate stress intensity factor(ΔK) in addition to striation width. Detail of the striation counting was stated in Section 3.4 Fractographic analysis procedure. Striation width, distance from the crack origin and ΔK values were tabulated for each measurement at Table 26.

Table 26. *Sitriation Counting measurements & calculations*

Measurements		Stress (MPa)	Group	Specimen	ΔK (MPa.√m)
d (mm)	i or da/dN (μm)				
2.22	0.80	165	CAA	CAA-2	13.78
3.54	1.20	165	CAA	CAA-2	17.40
4.36	3.00	165	CAA	CAA-2	19.31
4.80	3.30	165	CAA	CAA-2	20.26
2.70	0.50	165	CAAT	CAAT-2	15.20
4.49	1.40	165	CAAT	CAAT-2	19.60
5.10	4.00	165	CAAT	CAAT-2	20.89
2.00	0.75	220	ASM	ASM-1	17.44
3.00	5.00	220	ASM	ASM-1	21.36
1.74	1.00	300	ASM	ASM-6	22.18
2.89	4.50	300	ASM	ASM-6	28.59
3.28	6.00	300	ASM	ASM-6	30.45
1.80	0.38	210	ASM	ASM-5	15.79
3.11	1.38	210	ASM	ASM-5	20.76
4.48	3.12	210	ASM	ASM-5	24.91
3.18	0.66	150	CAAT	CAAT-6	14.99
4.53	2.00	150	CAAT	CAAT-6	17.89
1.97	0.50	170	PRET	PRET-4	13.37
3.64	3.30	170	PRET	PRET-4	18.18

Crack growth rate (da/dN) with respect to stress intensity factor (ΔK) was plotted depending on the striation counting for as-machined and the surface treated groups. Plotted da/dN curve represented only linear portion which is Paris-Erdogan region since striation counting can be applied only this region. Outside of the Paris-Erdogan region, striations were invisible due to its very small width or not observable because of the crack initiation stage or the catastrophic failure. Curves for both surface treated and as-machined groups were very close to each other and compatible with the literature curves [28]. On the other hand, slope of the curves were 3.90 and 4.49 for as-machined and the surface treated curves respectively. They were acceptable results because expected value was approximately 4. However, coefficient of determinations

(R^2) for the curves were low which were 0.75 and 0.79 for as-machined and the surface treated curves respectively due to lack of striation counting data. This leads to observation of two similar but separated curves for each group. Although, striation counting data should be increased to plot one solid curve from all data points, obtained data were sufficient to evaluate that chromic acid anodizing and its pretreatments did not affect crack propagation stage of the fatigue.

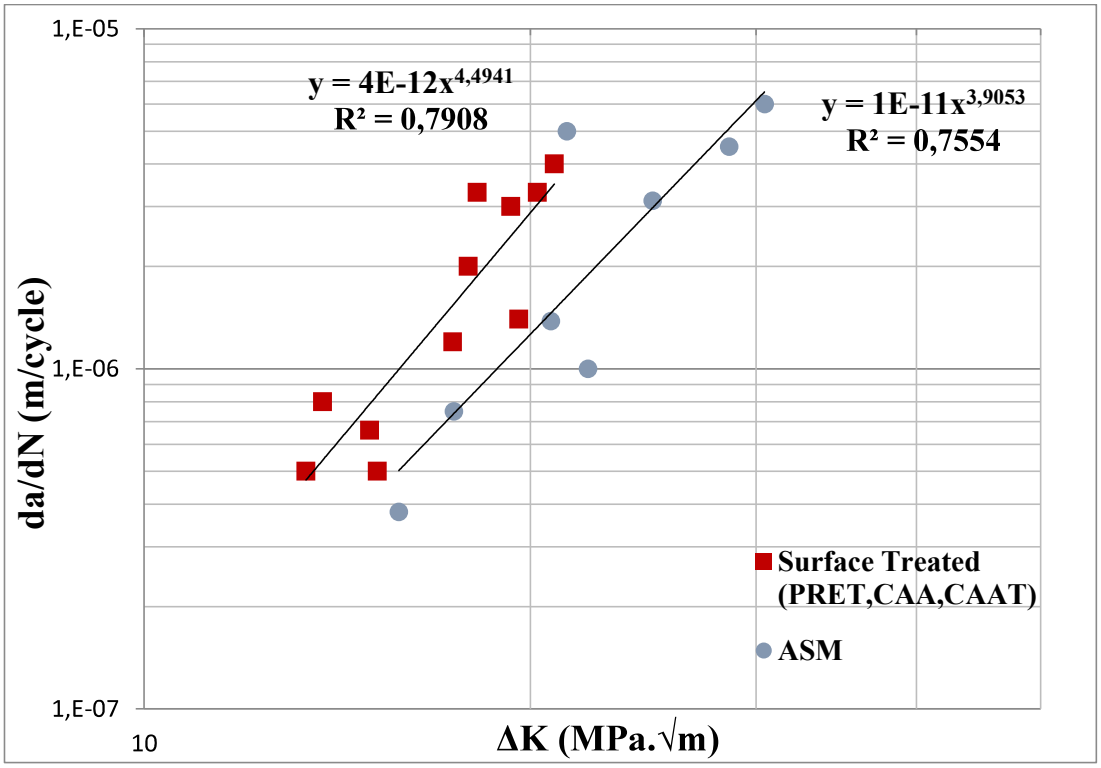

Figure 81. da/dN curves of surface treated and asmachined groups

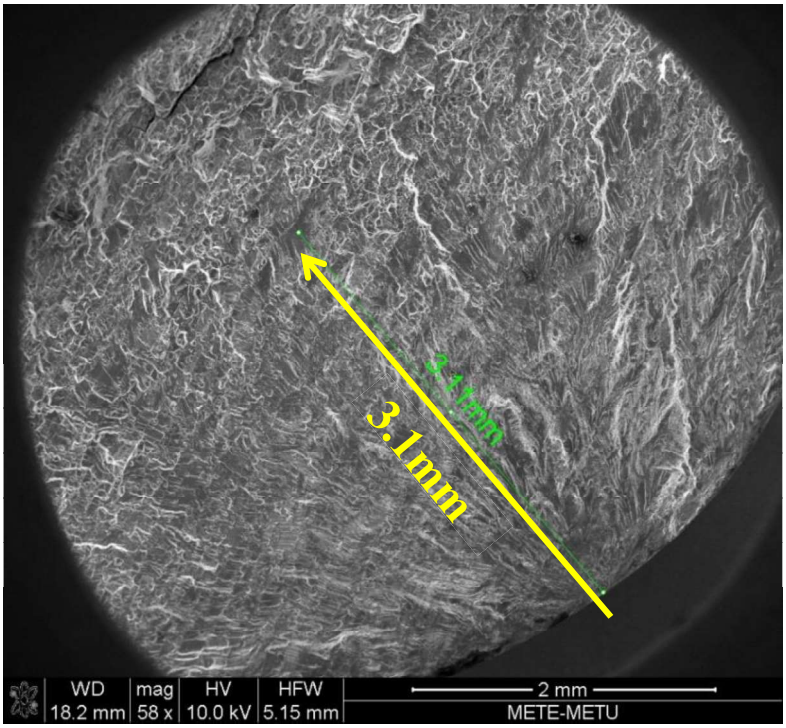

Figure 82. Striation measurement point of ASM-5

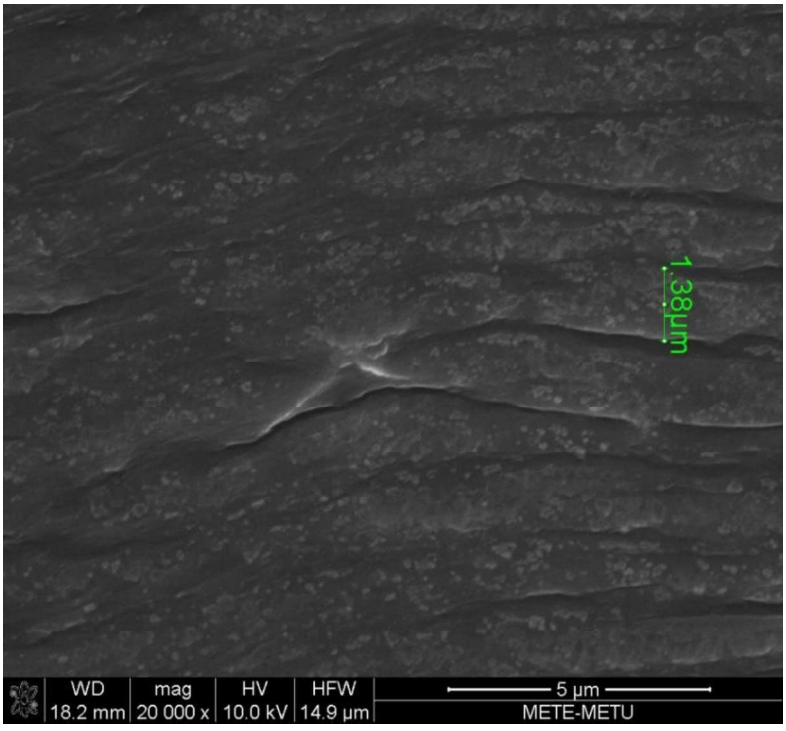

Figure 83. Striation width of ASM-5 at 3.1mm away from crack origin

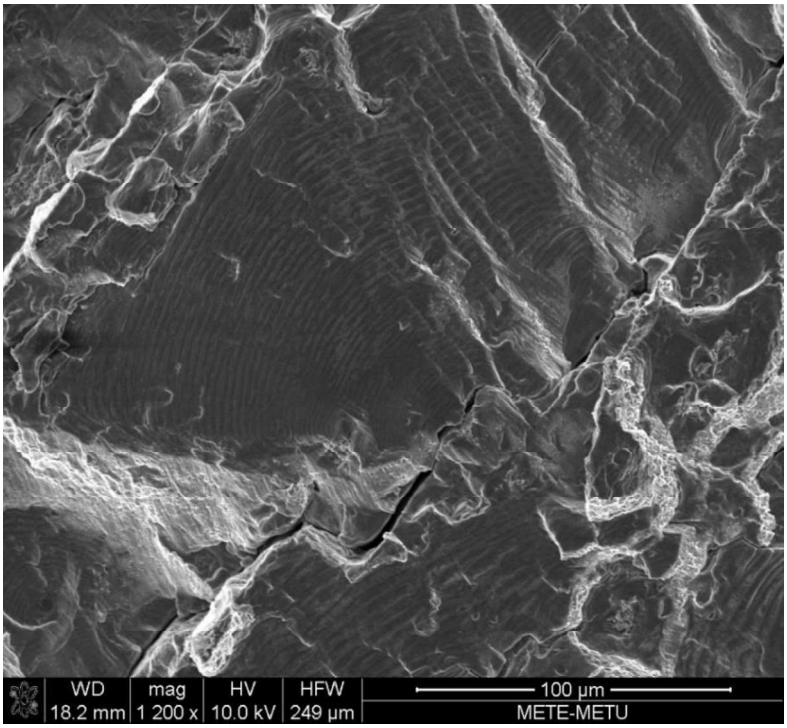

Figure 84. Striations of ASM-5 at 4.48mm away from crack origin

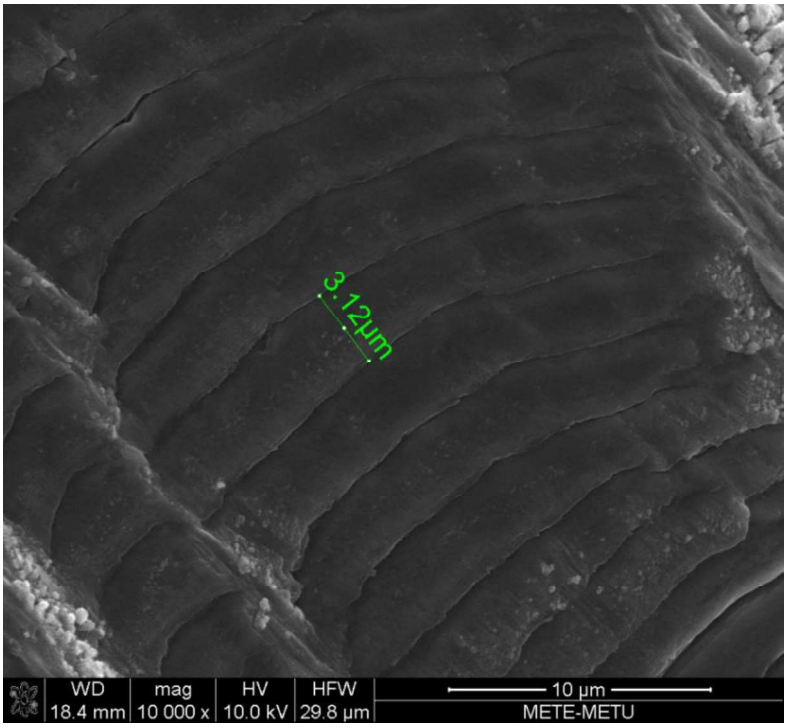

Figure 85. Striation width of ASM-5 at 4.48mm away from crack origin

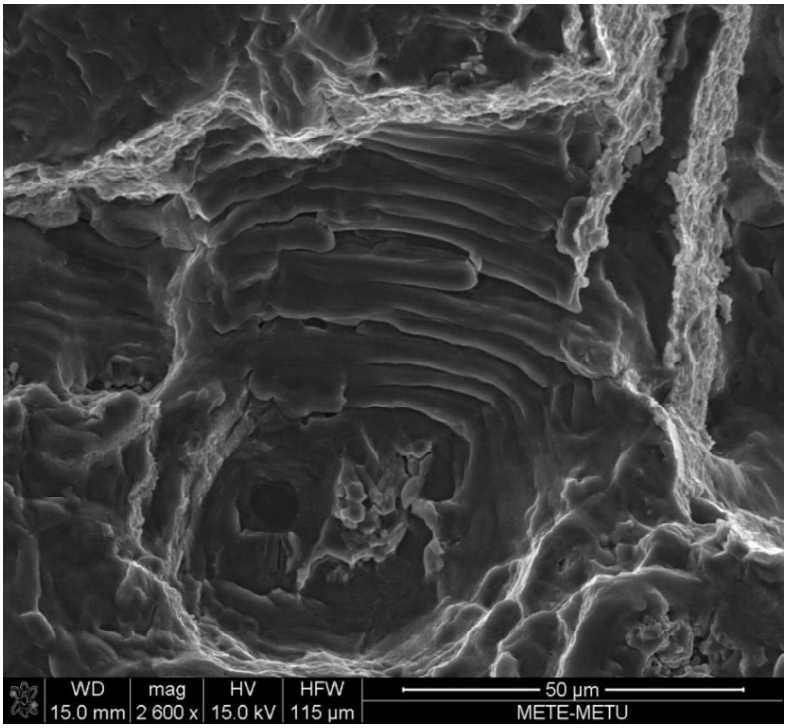

Figure 86. Striations of PRET-4 at 3.64 mm away from crack origin

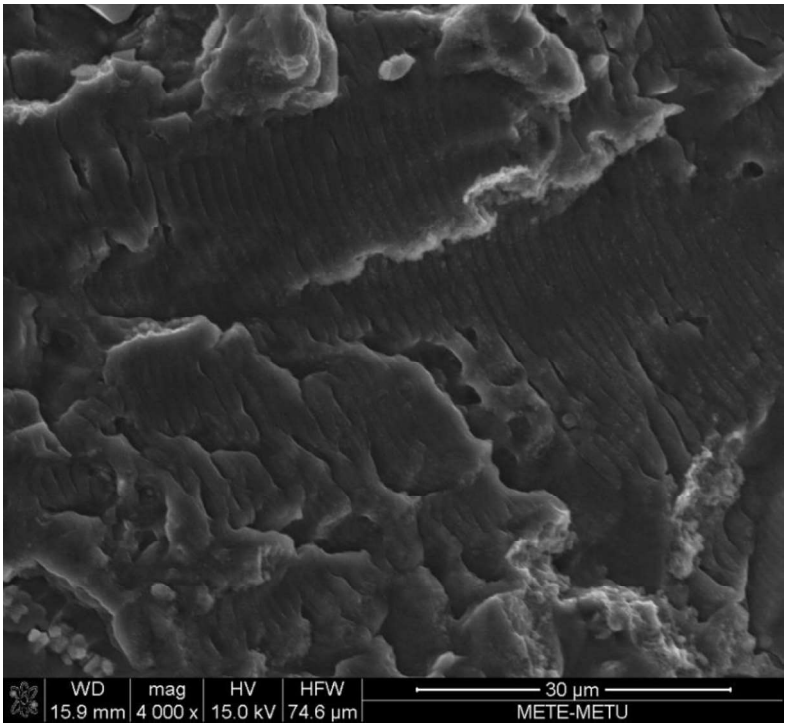

Figure 87. Striations of CAA-2 at 3.54 mm away from crack origin

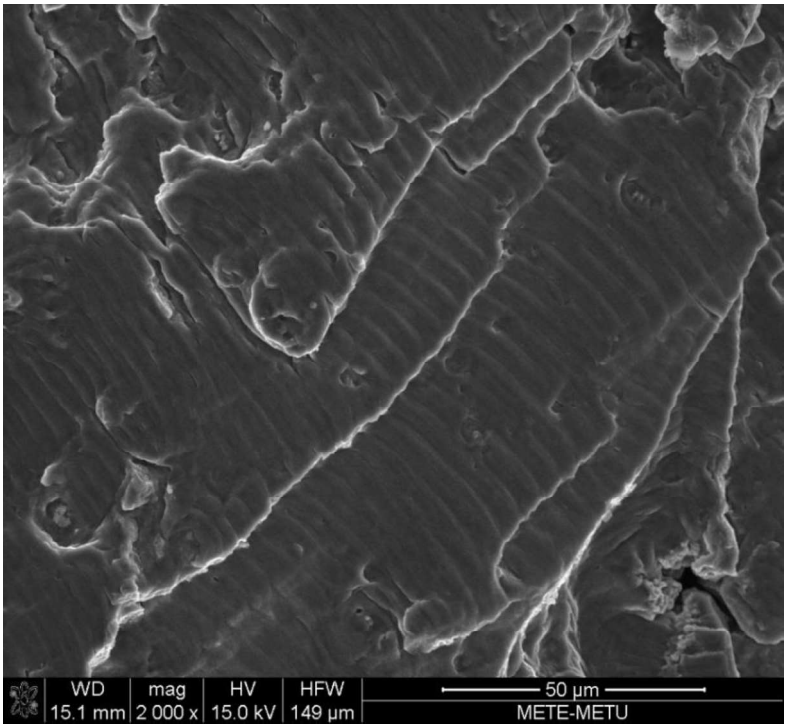

Figure 88. Striations of CAAT-2 at 5.1 mm away from crack origin

CHAPTER 5

CONCLUSION

In this study, fatigue behavior of 7050 T7451 aluminum alloy was investigated with regards to impact of chromic acid anodizing (CAA). In the light of the test results, reduced fatigue performance of 7050 T7451 due to CAA have to be considered as a design criterion. The major conclusions drawn from the results were stated below.

1. Maximum pit depth 48 μm and the highest average pit depth 15 μm were obtained as a result of Chromic acid anodizing (CAA) process which consisted of pickling with 15 % NaOH and 30% H_2SO_4 solutions as the pretreatments stages and anodizing with 5% Cr_2O_3 solution for the final stage.
2. S/N curve of the 7050 T7451 was shifted to lower stress state due to CAA surface treatment. Maximum fatigue limit reduction of 7050 T7451 was found as 31.8% at 500,000 cycles. Moreover, fatigue limit reduction had a descending trend as number of cycles decreases which was reaching 1.4% at the first cycle since crack initiation stage of fatigue failure was less dominant at low cycles region.
3. S/N curve of pretreated group was overlapped with S/N curve of the complete CAA applied group. Therefore, the source of fatigue life reduction was found as pretreatments of CAA process. Furthermore, effect of immersion time of CAA without any changes on pretreatments was examined by holding specimens in anodizing bath during different durations. Fatigue behavior of 7050 T7451 was not influenced by immersion time of CAA.
4. Crack growth behavior of 7050 T7451 showed that crack propagation was independent from CAA surface treatment. Hence, fatigue limit reduction was caused by influencing crack initiation stage due to CAA

REFERENCES

[1] M. Shahzad, M. Chaussumier, R. Chieragatti, C. Mabru, and F. Rezai-Aria, "Surface characterization and influence of anodizing process on fatigue life of Al 7050 alloy," *Mater. Des.*, vol. 32, no. 6, pp. 3328–3335, 2011.

[2] F. C. Campbell, *Manufacturing Technology for aerospace strutural materials*. 2006.

[3] H. Asoh, K. Nishio, M. Nakao, T. Tamamura, and H. Masuda, "Conditions for Fabrication of Ideally Ordered Anodic Porous Alumina Using Pretextured Al," *J. Electrochem. Soc.*, vol. 148, no. 4, p. B152, 2001.

[4] G. E. Dieter, *Mechanical Metallurgy*, vol. 273, no. 4. 1962.

[5] J. R. Davis, "ASM Specialty Handbook Aluminum and Aluminum Alloys," *ASM Int.*, pp. 3–12, 1993.

[6] R. J. H. Wanhill, *Aerospace Materials and Material Technologies*, vol. 2. 2017.

[7] SAE International Group, "Aerospace Material Specification (AMS 4050) of Aluminum Alloy," no. H, p. 10, 2016.

[8] SAE, "Aerospace Material," *AMS2772 Heat Treat. Alum. Alloy Raw Mater.*, no. F, pp. 1–11, 2011.

[9] B. R. W. Buzzard, "Anodizing of aluminum alloys in chromic acid solutions of different concentrations," *J. Res. Natl. Bur. Stand. (1934).*, vol. 18, 1937.

[10] C. A. Grubbs, "Anodizing of aluminum," *Met. Finish.*, vol. 105, no. 10, pp. 397–412, 2007.

[11] H. Takahashi, "Aluminum Anodizing," *ASM Handbook, Vol. 13A Corros. Fundam. Testing, Prot.*, vol. 13A, pp. 736–740, 2003.

[12] F. M. Stevenson, “Anodizing,” *ASM Handb.*, vol. 5.

[13] N. Alr and D. Lakehurst, “Military Specification of Anodic Coating for Aluminum and Aluminum Alloys (MIL-A-8625F),” 1993.

[14] W. T.Becker and R. J.Shipley, *Failure Analysis and Prevention Handbook*, vol. 11. 2002.

[15] W. A. Wood, “Some Basic Studies of Fatigue in Metals,” *Fracture*, 1959.

[16] J. Schjive, *Fatigue of Structures and Materials*, Second. Delft, The Netherlands: Springer Science,Business Media, B.V., 2009.

[17] R. B. Heywood, “Proc.Inst.Mech.En.,” vol. 165, pp. 11–124, 1951.

[18] AGARD, *Helicopter Fatigue Design Guide*. North Atlantic Treaty Organization, 1983.

[19] ASTM, “Standard Practice for Conducting Force Controlled Constant Amplitude Axial Fatigue Tests of Metallic Materials,” vol. E 466, no. 07, pp. 4–8, 2002.

[20] ASTM, “Standard Test Method for Measurement of Fatigue Crack Growth Rates,” vol. E647, no. 11, pp. 1–45, 2010.

[21] W. Weibull, *Fatigue Testing and Analysis of Results*. Pergamon Press, 1961.

[22] M. Shahzad, M. Chaussumier, R. Chieragatti, C. Mabru, and F. Rezai-Aria, “Influence of anodizing process on fatigue life of machined aluminium alloy,” *Procedia Eng.*, vol. 2, no. 1, pp. 1015–1024, 2010.

[23] M. Chaussumier, C. Mabru, R. Chieragatti, and M. Shahzad, “Fatigue life model for 7050 chromic anodized aluminium alloy,” *Procedia Eng.*, vol. 66, pp. 300–312, 2013.

[24] S. A. Barter, P. K. Sharp, G. Holden, and G. Clark, “Initiation and early growth of fatigue cracks in an aerospace aluminum alloy,” *Fatigue Fract. Eng. Mater.*

Struct., pp. 111–125, 2001.

[25] T.-S. Shih, T.-H. Lee, and Y.-J. Jhou, "The Effects of Anodization Treatment on the Microstructure and Fatigue Behavior of 7075-T73 Aluminum Alloy," *Mater. Trans.*, vol. 55, no. 8, pp. 1280–1285, 2014.

[26] ASTM Int., "ASTM E8-Standard Test Methods for Tension Testing of Metallic Materials," *Astm*, no. 13a, pp. 1–27, 2009.

[27] ASTM, "B244-Standard Test Method for Measurement of Thickness of Anodic Coatings on Aluminum and of Other Nonconductive Coatings on Nonmagnetic Basis Metals with Eddy-Current Instruments," pp. 1–4, 2017.

[28] S. Mechanics, L. Molent, D. Science, S. Barter, D. Science, and R. Jones, "Multiscale Fatigue Crack Initiation and Propagation of Engineering Materials: Structural Integrity and Microstructural Worthiness," *Solid Mech. its Appl.*, vol. 152, no. January, 2008.